

REPORT NO.
UCB/EERC-97/08
July 1997

EARTHQUAKE ENGINEERING RESEARCH CENTER



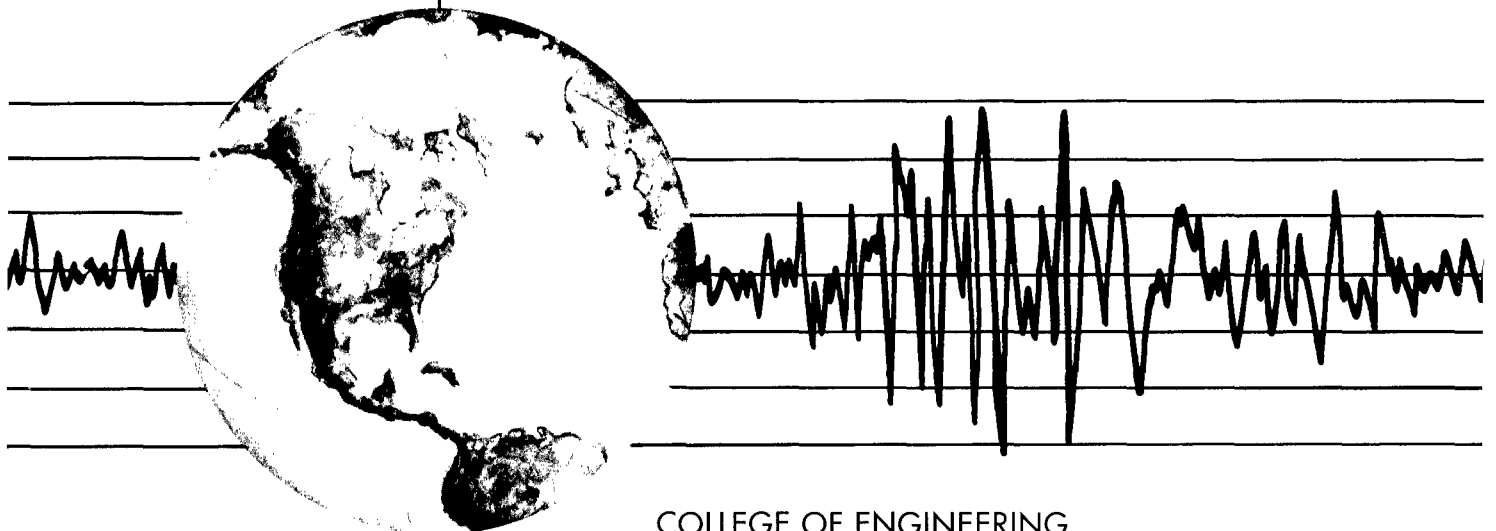
PB99-107492

**IMPLICATIONS OF THE LANDERS AND
BIG BEAR EARTHQUAKES ON
EARTHQUAKE RESISTANT DESIGN
OF STRUCTURES**

by

JAMES C. ANDERSON
VITELMO V. BERTERO

Report to the National Science Foundation



COLLEGE OF ENGINEERING
UNIVERSITY OF CALIFORNIA AT BERKELEY

For sale by the National Technical Information Service, U.S. Department of Commerce, Springfield, Virginia 22161

See back of report for up to date listing of EERC reports.

DISCLAIMER

Any opinions, findings, and conclusions or recommendations expressed in this publication are those of the authors and do not necessarily reflect the views of the National Science Foundation or the Earthquake Engineering Research Center, University of California at Berkeley.

**IMPLICATIONS OF THE LANDERS AND BIG BEAR EARTHQUAKES
ON EARTHQUAKE RESISTANT DESIGN OF STRUCTURES**

by

James C. Anderson

and

Vitelmo V. Bertero

Report to the National Science Foundation

Report No. UCB/EERC-97/08
Earthquake Engineering Research Center
College of Engineering
University of California at Berkeley

July, 1997

PROTECTED UNDER INTERNATIONAL COPYRIGHT
ALL RIGHTS RESERVED.
NATIONAL TECHNICAL INFORMATION SERVICE
U.S. DEPARTMENT OF COMMERCE

ABSTRACT

The magnitude 7.3 Landers earthquake (1992) produced two long duration records of strong ground motion and one strong record in the near fault region. Three hours later the magnitude 6.2 Big Bear earthquake (1992) occurred some twenty miles to the west. Had these ground motions occurred in a populated region rather than on the western edge of the Mojave Desert, damage to all types of civil engineering facilities would have been substantial.

Since there were no engineered structures in the region of strong ground motion for the Landers earthquake, the performances of a six story building and a seventeen story building which had been studied previously were evaluated for the recorded free field ground motions. Results show that displacement and ductility demands for the two long duration ground motions are similar to those obtained from the ground motions recorded during other strong earthquakes such as El Centro (1979) and Loma Prieta (1989). It is also shown that when multiple strong earthquakes (or aftershocks) occur and the first is strong enough to drive the structure into the inelastic range, the second can not only induce an increase in the amount of accumulated plastic energy but can also drive the structure further into the inelastic range thereby increasing the displacement and ductility demands.

The near fault record obtained from this earthquake is extremely significant because it is the first record obtained in the near fault region for an earthquake of

magnitude 7.3. The study shows that the effect of this base motion on structures, particularly those with periods of vibration above one second, is to greatly increase the displacement response and ductility demands to levels well above those considered in current code provisions and possibly above structure capacity.

The Big Bear earthquake which occurred in the San Bernardino Mountains, generated free field motions having high acceleration and high frequency content which are representative of rock motions. The most significant record from this earthquake was obtained in the free field near a two story steel frame building. The high acceleration, high frequency record combined with the relative short period of the low rise building resulted in high stresses in the structural frame with small displacements. For this reason, damage to the steel frame was not discovered until almost two years after the earthquake. Results indicate that cracking in the steel frame may have been due in part to the ground motions developed during the Big Bear earthquake.

ACKNOWLEDGMENTS

The research reported herein was part of a research project on the "Implications of Recorded Data from the 1992 Southern California Earthquakes for Earthquake-Resistant Design" supported by the National Science Foundation (NSF). The support provided by NSF is gratefully acknowledged along with the continuing support of NSF Program Manager Dr. S.C. Liu. The opinions, discussions, findings and conclusions expressed in this report are solely those of the authors and do not necessarily reflect those of the sponsor.

A corrected copy of the Lucerne Valley record was obtained from Dr. Paul Somerville of Woodward-Clyde Federal Services. Data on the building at Big Bear was obtained from Mr. Patrick Carrol of the Building Department of the City of Big Bear. Photographs of the site of the Big Bear instrument were provided by Dr. Robin Shepherd of Earthquake Damage Analysis Company. These contributions are gratefully appreciated.

TABLE OF CONTENTS

ABSTRACT	i
ACKNOWLEDGMENTS	iii
TABLE OF CONTENTS	iv
LIST OF TABLES	v
LIST OF FIGURES	vi
1. INTRODUCTION	1
2. RECORDED DATA	2
2.1 Landers Earthquake	3
2.2 Big Bear Earthquake	6
3. SIX STORY BUILDING, LANDERS	7
3.1 General	7
3.2 Building Description	7
3.3 Elastic Response Analyses.....	8
3.4 Inelastic Response Analyses	12
3.5 Multiple Event Analyses	17
4. SEVENTEEN STORY BUILDING, LANDERS	18
4.1 Building Description	18
4.2 Elastic Response Analyses	20
4.3 Inelastic Response Analyses	22
4.4 Postscript	27
5. TWO STORY BUILDING, BIG BEAR	27
5.1 General	27
5.2 Elastic Response Analyses	29
5.3 Inelastic Response Analyses	32
5.3.1 Static (Pushover) Analyses	32
5.3.2 Time History Analyses	33
6. SUMMARY AND CONCLUSIONS	35
TABLES	40
FIGURES	42
REFERENCES	88

LIST OF TABLES

Table 1	Recorded Free Field Motions, Landers Earthquake	40
Table 2	Recorded Free Field Motions, Big Bear Earthquake	41

LIST OF FIGURES

Figure 1	Map of Western Mojave Desert	42
Figure 2	Recorded Accelerations, Joshua Tree	43
	(a) East-West Time History	
	(b) North-South Time History	
	(c) Elastic Response Spectra, 5% Damping	
Figure 3	Recorded Accelerations, Yermo	44
	(a) East-West Time History	
	(b) North-South Time History	
	(c) Elastic Response Spectra, 5% Damping	
Figure 4	Recorded Accelerations, Desert Hot Springs ..	45
	(a) East-West Time History	
	(b) North-South Time History	
	(c) Elastic Response Spectra, 5% Damping	
Figure 5	Recorded Accelerations, Big Bear (Landers) ..	46
	(a) East-West Time History	
	(b) North-South Time History	
	(c) Elastic Response Spectra, 5% Damping	
Figure 6	Recorded Accelerations, Lucerne Valley	47
	(a) East-West Time History	
	(b) North-South Time History	
	(c) Elastic Response Spectra, 5% Damping	
Figure 7	Recorded Velocities, Lucerne Valley	48
	(a) East-West Time History	
	(b) North-South Time History	
Figure 8	Recorded Accelerations, Big Bear (Big Bear) .	49
	(a) East-West Time History	
	(b) North-South Time History	
	(c) Elastic Response Spectra, 5% Damping	
Figure 9	Elastic Dynamic Model, 6 Story Building	50
Figure 10	Calculated Mode Shapes, 6 Story Building	51
	(a) Mode 1	
	(b) Mode 2	
	(c) Mode 3	
Figure 11	Maximum Elastic Response, 6 Story Building ..	52
	(a) Lateral Displacement	
	(b) Interstory Drift Index	
	(c) Inertia Forces	
	(d) Story Shears	

Figure 12	Stress Ratios, LRFD, 6 Story Building	53
	(a) Joshua Tree	
	(b) Yermo	
	(c) Lucerne	
Figure 13	Nonlinear 2D Model, 6 Story Building	54
Figure 14	Maximum Inelastic Response, 6 Story Building	55
	(a) Lateral Displacement	
	(b) Interstory Drift Index	
	(c) Girder Ductility Demand	
	(d) Column Ductility Demand	
Figure 15	Plastic Hinge Locations, 6 Story Building ...	56
	(a) Joshua Tree	
	(b) Yermo	
	(c) Lucerne	
Figure 16	Hysteretic Response, 1st Story Column	57
	(a) Joshua Tree	
	(b) Yermo	
	(c) Lucerne	
Figure 17	Six Story Bldg. Response, Joshua Tree	58
	(a) Roof Displacement	
	(b) Base Shear	
Figure 18	Six Story Bldg. Response, Yermo	59
	(a) Roof Displacement	
	(b) Base Shear	
Figure 19	Six Story Bldg. Response, Lucerne	60
	(a) Roof Displacement	
	(b) Base Shear	
Figure 20	Combined Yermo Ground Motions	61
Figure 21	Inelastic Response, 6 Story Building, Yermo x 2	62
	(a) Lateral Displacement	
	(b) Interstory Drift Index	
	(c) Girder Ductility Demand	
	(d) Column Ductility Demand	
Figure 22	Hysteretic Response, 6 Story Building, Yermo x 2	63
Figure 23	Roof Displacement, 6 Story Building	64
	(a) Yermo (E-W)	
	(b) Yermo2 (E-W)	

Figure 24	Typical Floor Plan, Canoga Building	65
Figure 25	Elastic Dynamic Model, Canoga Building	66
Figure 26	Calculated Mode Shapes, Canoga Building	67
	(a) Mode 1	
	(b) Mode 2	
	(c) Mode 3	
Figure 27	Maximum Elastic Response, Canoga Building ...	68
	(a) Lateral Displacement	
	(b) Interstory Drift Index	
	(c) Inertia Forces	
	(d) Story Shears	
Figure 28	Stress Ratios, LRFD, Canoga Building	69
	(a) Joshua Tree	
	(b) Yermo	
	(c) Lucerne	
Figure 29	Nonlinear 2D Model, Canoga Building	70
Figure 30	Maximum Inelastic Response, Canoga Building .	71
	(a) Lateral Displacement	
	(b) Interstory Drift Index	
	(c) Girder Ductility Demand	
	(d) Column Ductility Demand	
Figure 31	Plastic Hinge Locations, Canoga Building	72
	(a) Joshua Tree	
	(b) Yermo	
	(c) Lucerne	
Figure 32	Canoga Bldg. Response, Joshua Tree	73
	(a) Roof Displacement	
	(b) Base Shear	
Figure 33	Canoga Bldg. Response, Yermo	74
	(a) Roof Displacement	
	(b) Base Shear	
Figure 34	Canoga Bldg. Response, Lucerne	75
	(a) Roof Displacement	
	(b) Base Shear	
Figure 35	Pushover Analysis, Canoga Building	76
Figure 36	Comparison of Lucerne Record Processing	76
Figure 37	Big Bear Civic Center, Recording Instrument .	77
Figure 38	Typical Floor Plan, Big Bear Civic Center ...	78

Figure 39	Elastic Response Model, Big Bear Civic Center	79
	(a) Isometric View	
	(b) Plan View	
Figure 40	Calculated Mode Shapes, Big Bear Civic Center	80
	(a) Mode 1	
	(b) Mode 2	
	(c) Mode 3	
Figure 41	Maximum Elastic Response, Big Bear Civic Center	81
	(a) Lateral Displacement	
	(b) Interstory Drift Index	
	(c) Inertia Forces	
	(d) Story Shears	
Figure 42	Stress Ratios, LRFD, Big Bear Civic Center ..	82
Figure 43	Nonlinear 2D Models, Big Bear Civic Center ..	83
	(a) East-West Framing	
	(b) North-South Framing	
Figure 44	Pushover Analysis, Big Bear Civic Center	84
Figure 45	Plastic Hinge Locations, Pushover	85
	(a) E-W Frames	
	(b) N-S Frames	
Figure 46	Maximum Inelastic Response, Big Bear Civic Center	86
	(a) Lateral Displacement	
	(b) Interstory Drift Index	
	(c) Girder Ductility Demand	
	(d) Column Ductility Demand	
Figure 47	Plastic Hinge Locations	87
	(a) East-West Framing	
	(b) North-South Framing	



1.0 INTRODUCTION

On June 28, 1992, a pair of strong earthquakes occurred within three hours of each other in Southern California. A map of the region of occurrence is shown in Figure 1 [1]. The first of these occurred at 5:00 a.m. and was centered near the desert community of Landers, approximately 100 miles east of Los Angeles. This earthquake which was assigned a magnitude of 7.3 on the Richter scale was the largest earthquake to occur in California since 1952 (Taft) and the second largest to occur since 1906 (San Francisco). The second earthquake occurred at approximately 8:00 a.m., was assigned a magnitude of 6.2 and was located near the city of Big Bear in the San Bernardino Mountains, about 20 miles west of the initial shock.

The two events caused an estimated damage of approximately \$100 million and injury to about 400 people with one fatality. These losses are extremely small for two back to back earthquakes of these magnitudes. The reason for the small losses is the sparse population in the area affected by the earthquakes. The Landers earthquake occurred at the western edge of the Mojave Desert and the surface fault rupture propagated in a northwesterly direction for some 43 miles, stopping just south of Barstow. Therefore, the main force of the earthquake was directed away from the desert community of Palm Springs which is located about 30 miles south of the epicenter. Displacements along the

strike-slip fault averaged about 10 feet with a maximum of 21 feet occurring near the Emerson Fault. Damaged commercial buildings in the desert communities included a bowling alley in Yucca Valley, a convenience store in Joshua Tree and a department store located between these two communities.

In the city of Big Bear, local building officials estimate that approximately 40% of local structures had some form of damage. Much of this damage was to houses which either moved off of their foundations or suffered collapsed chimneys and roof damage. However, there was one engineered building which suffered extensive damage although it was not discovered until well after the earthquake. This building is a two story, steel moment frame which experienced significant cracking in the welded moment connections. A free field recording station, maintained by the Strong Motion Instrumentation Program (SMIP) of the California Division of Mines and Geology (CDMG) is located on the building grounds and recorded peak accelerations in excess of 0.5g in both directions. The behavior of this building will be discussed in detail in a later part of this report.

2.0 RECORDED DATA

Due to the remote location of the earthquake, motions recorded in buildings were at a considerable distance from the epicenter and were not located in the direction of fault propagation. For these reasons, building response records were not particularly significant for these earthquakes [2],

[3]. Therefore, attention will be focused on recorded data obtained from free field instruments, including one located 1 1/4 mile from the surface rupture and another which was in close proximity to a damaged, low rise, engineered building.

2.1 LANDERS EARTHQUAKE

Directivity effects of the Landers earthquake have been discussed by Somerville and Graves [4]. The free field data recorded during the Landers Earthquake is summarized in Table 1. From the data presented in this table, the following observations can be made. Of these records, the lowest ground accelerations were recorded at Palm Springs which is approximately 30 miles south of the epicenter and opposite to the direction of fault propagation. This region is referred to in reference [4] as the "backward directivity region" and is characterized by long duration, low amplitude motions.

The peak responses recorded at Desert Hot Springs, 18 miles south of the epicenter, are similar to those recorded at Barstow, 50 miles north of the epicenter. This similarity in ground acceleration at different distances represents the effect of the directionality of fault propagation. Two stronger records were recorded at Joshua Tree, 8.7 miles southeast of the epicenter, and Yermo, 51 miles north of the epicenter. As before, a comparison of these recordings illustrate the effect of directionality. A maximum displacement of more than 16 inches was recorded at Yermo. This data also illustrates how the strong motions from this

earthquake occurred either near the epicenter or along the line of fault rupture toward the northwest.

An additional record was obtained from a station operated by the Southern California Edison Company at Lucerne Valley [5]. This instrument (SMA-2/EMA) was located 1.24 miles (2 km) from the fault trace and 26 miles (42 km) north of the epicenter. This region is referred to in reference [4] as the "forward directivity region" and is characterized by short duration, high amplitude long period motions. This is the first record which has been obtained in the near fault region for a magnitude 7.3 earthquake.

The time histories of the ground accelerations recorded at the Joshua Tree Fire Station are shown in Figure 2 along with the response spectra for elastic systems with 5% of damping. It can be seen that this record has a duration of thirty seconds of strong motion which is relatively long. The spectra for the two components are about the same for periods less than one second. Beyond this point the E-W component becomes dominant. Similar data for the ground accelerations recorded at the Yermo Fire Station are shown in Figure 3. The spectrum of the E-W component is similar to that of E-W component of Joshua Tree and has a stronger response in the long period region. However, the duration of strong shaking is considerably less (10 sec.).

Time histories and spectra for the ground motions recorded at Desert Hot Springs are shown in Figure 4. Here it can be seen that while the duration of strong motion is

similar to Joshua, the amplitude of the ground accelerations is considerably less. The response spectra indicate that the N-S component is stronger for periods up to 0.7 second, however, for longer periods the E-W component becomes dominant. The time histories and spectra for the ground motions recorded at the Big Bear Civic Center during the Landers Earthquake are shown in Figure 5. Here it can be seen that the duration of strong ground motion is approximately 20 seconds, however, the accelerations are all less than 0.20g. The spectra for the two components, shown in Figure 5c, have similar shapes to those shown in Figure 4 for Desert Hot Springs with the exception that the N-S component becomes dominate in the long period region.

Time histories and spectra for the ground motions recorded at Lucerne Valley are shown in Figure 6. Time histories for the two horizontal components, shown in Figures 6a and 6b, indicate peak accelerations in excess of 0.7g and duration of strong shaking of approximately 15 seconds for both components. The response spectra for the two components, shown in Figure 6c indicates that the characteristics of the two components are quite similar up to a period of one second. Beyond one second, the E-W component (normal to fault) becomes strongly dominate. The spectrum for this component indicates that it will have a significant effect on longer period structures, particularly structures having a period of approximately four seconds.

Time histories of the velocities of the two horizontal components are shown in Figure 7. The time history for the E-W component, shown in Figure 7a, indicates that this component contains a strong velocity pulse which occurs at approximately ten seconds. The peak velocity is 53 inches/second and the incremental velocity (peak to peak) is 78 inches/second. This is a characteristic forward rupture directivity effect which produces a large pulse of long period motion normal to the fault. In the N-S direction, shown in Figure 7b, the velocity pulse is much less pronounced (28 inches/second).

2.2 BIG BEAR EARTHQUAKE

In general, both free field and building responses recorded during the Big Bear Earthquake were less than those recorded during the Landers Earthquake. One exception was the accelerations recorded at the Big Bear Civic Center which was approximately 6.8 miles from the epicenter. The peak responses for the two horizontal components of this record are summarized in Table 2.

This data indicates that the peak accelerations in both horizontal directions are near or above 0.5g. Time histories and the 5% damped spectra of the recorded ground accelerations are shown in Figure 8. The spectra for the two components are quite similar, Figure 8c, and contain strong spectral accelerations greater than 1.0 g for periods up to 0.4 seconds. These records are of particular interest because the free field instrument is located at the Big Bear

Civic Center which suffered extensive damage to the welded connections in the steel moment frame.

3.0 SIX STORY BUILDING, LANDERS

3.1 General

Since the Landers earthquake did not produce any significant building response records, a representative low rise building, six stories in height, was selected as an initial case study building. The six story building selected was also used in an earlier study of the effects of the Whittier Narrows earthquake on building response [6]. The structure is a steel frame building with lateral resistance provided by a perimeter moment frame. The building has been instrumented as part of the SMIP, however, the peak acceleration recorded at the base of the building during the Landers earthquake was only 0.05 g (epicentral distance = 107 miles) and only 0.04 g during the Big Bear earthquake (epicentral distance = 85 miles). These values compare with 0.22 g during the Whittier Narrows earthquake (epicentral distance = 16 miles). Therefore, free field records obtained during the Landers earthquake from recording stations in the Mojave Desert region are used as input to study the building response.

3.2 Building Description

The building is 82.5 feet high with a 120 foot by 120 foot square plan. The continuity of the perimeter frame is broken at the corners by shear connections to the weak axes

of the corner columns. Gravity loads are carried by an interior framing system consisting of much lighter sections with simple, non-moment connections. The columns of the perimeter frames are supported on two, 30 inch diameter reinforced concrete piles which are 32 feet long. At the second floor level and at the roof, the deck extends a distance of 6 1/2 feet beyond the perimeter moment frame giving these two levels plan dimensions of 132 feet by 132 feet.

The building was designed in 1976 to the requirements of the 1973 Uniform Building Code (UBC)[7]. The required lateral forces are expressed in terms of the base shear, V , which is given by the formula,

$$V = (ZKCIS)W$$

which can be represented as

$$V = C_S W$$

where C_S is the design seismic resistance coefficient. The seismic dead load, W , is estimated to be 7,785 kips and Z , S , and I are taken as unity. The coefficient $C = 1/(15 \cdot T)$ or $C = 1/(15 \cdot 0.1N) = 0.086$ and $K = 0.67$. Using these values results in a design seismic resistance coefficient, C_S , of 0.058 (5.8%) and a base shear of 449 kips.

3.3 Elastic Response Analyses

A three dimensional model of the building was developed for elastic response analyses using the ETABS Plus [8] computer program. An isometric view of the perimeter moment

frame showing the girder releases at the corner columns is shown in Figure 9.

The calculated periods of the first two modes of vibration are both equal to 1.45 seconds due to the symmetry of the building. The deflected shapes, shown in Figures 10a and 10b indicate that these modes are translational modes in the two principal directions. The deflected shape of the third mode, shown in Figure 10c, is a torsional mode which has a period of 0.83 seconds. The fourth and fifth modes are translational modes in the two principal directions, both having a period of 0.52 seconds. The sixth mode is the second torsional mode having a period of 0.31 seconds. Nine modes of vibration were used to represent the response of the three dimensional system. These modes represented 98.8% of the effective mass in the X direction and 99.2% in the Y direction.

The response of the building is evaluated for the three stronger ground motions recorded during the Landers earthquake; Joshua Tree Fire Station and Yermo Fire Station and Lucerne Valley. From the elastic response spectra shown in Figures 2c, 3c and 6c it can be seen that the fundamental periods of this building in both principal directions (1.45 seconds) place the building in the region of strong response for all of these earthquake ground motions.

The maximum elastic response is summarized in Figure 11 in terms of the lateral displacement, interstory drift index (IDI), inertia force distribution and story shear

distribution. The maximum lateral displacement, shown in Figure 11a, indicates that the near fault, Lucerne record produces a displacement of 16.5 inches at the roof compared to 12.5 inches for Yermo and 11.0 inches for Joshua Tree. These are relatively large displacements, resulting in an average drift of 1.7% based on the building height of 82.5 feet. In a previous study [9] the authors have shown that the elastic roof displacement of this building reaches 15.0 inches under the Hollister (1989) motion and 8.5 inches under the James Road (1979) motion.

The maximum values of interstory drift index (maximum relative story displacement/story height) are shown in Figure 11b. This data indicates that the interstory drift index (IDI) under the Lucerne motion approaches 2% at the third story level compared to 1.5% for the Yermo motion. The IDI for the Joshua Tree motion is slightly less at 1.35%.

The distribution of the inertia forces over the height of the building is shown in Figure 11c, where it can be seen that the maximum inertia force at the roof reaches 1,300 kips under the Lucerne motion and 1,000 kips under the Yermo motion. The inertia force at the roof due to the Joshua Tree motion is 836 kips.

The distribution of the story shears over the height of the structure are shown in Figure 11d. The maximum base shear is due to the Lucerne motion and reaches a value of 4,500 kips. The next largest, due to the Yermo motion, is 3,238 kips and the base shear due to the Joshua Tree motion

is 2,500 kips. All of these values are significantly higher than the code design value of 449 kips with the base shear due to the Lucerne motion being more than ten times larger. The smaller base shear due to the Joshua Tree motion is still more than 5.5 times larger than the code design value. These values for base shear can also be compared with the results of the previous study which obtained base shears of 2,500 kips for James Road (1979) and 3,200 kips for Hollister (1989).

The members of the steel frame are stress checked using the STEELER postprocessor program [10] and the AISC-LRFD86 Specifications [11] for these three ground motions with the material yield stress taken as the nominal value. The results are summarized in Figure 12. The stress ratios for the frame under the Joshua Tree ground motion are shown in Figure 12a. This data indicates that with the exception of the roof beams, almost all members of the frame are overstressed under this ground motion. The stress ratios further indicate that the critical members are the columns of the first floor level with stress ratios reaching 2.89. A similar result was obtained in the previous study for other ground motions [6]. Under the Yermo ground motion, the stress ratios, shown in Figure 12b, are even higher, reaching a maximum value of 3.71 in the first story columns. The largest stress ratios are obtained under the Lucerne motion and are shown in Figure 12c where values as high as 5.47 are obtained in the columns of the first story level.

These results indicate that this frame will experience inelastic behavior in a substantial number of structural members under these three ground motions. This implies that nonlinear dynamic analyses should be conducted to evaluate the effect of inelastic behavior on the structural response. This will be done in the following section. Comparing the elastic response results from this study with those obtained from a previous study [9], indicates that the three ground motions recorded during the Landers earthquake are among the more critical ground motions for this structure.

3.4 Inelastic Response Analyses

Due to the symmetry of the building, the nonlinear dynamic analyses are conducted on a two dimensional model of one of the exterior frames, shown in Figure 13. The nonlinear dynamic analysis is done using an in-house analysis program which uses a two-component beam element to represent the inelastic behavior. Ductility demands of all elements are given in terms of curvature ductility which is defined as the maximum curvature divided by the curvature at yield.

Results of the inelastic, time-history analysis are shown in Figure 14 in terms of lateral displacement, IDI, girder ductility demand and column ductility demand. The plot of maximum lateral displacements, shown in Figure 14a, indicates that the Lucerne motion produces the largest displacement response although the envelope for the upper floors is less than for the elastic response with a maximum

roof displacement of 12.2 inches compared with 16.5 inches elastic. However, at the second floor level, the inelastic lateral displacement reaches 6 inches compared with an elastic displacement of 4 inches. The IDI results, shown in Figure 14b, also indicate that the relative displacements due to Lucerne are larger than those due to Joshua Tree or Yermo. The difference is particularly significant at the first floor level where the drift due to Lucerne reaches 3.4% compared to 2.3% for Yermo and 1.2% for Joshua Tree. These values are significantly larger than those obtained in the elastic analyses and indicate that much of the earthquake input is being dissipated in the first story which is acting as a "soft story".

Girder ductility demands for the three ground motions are shown in Figure 14c. The maximum demand is due to the Lucerne motion and occurs at both the first story level and the third story level, having a value of 2.5. A similar pattern develops under the Joshua Tree motion, however, the maximum demand is only 1.5. Under the Yermo motion, the maximum girder ductility demand is in the first story and reaches a value of 2.0. Results of the previous study [6] indicated the maximum girder ductility demand was 1.5 under both James Road and Hollister.

The maximum column ductility demand is shown in Figure 14d. As before, the maximum demand is due to the Lucerne motion and reaches a value of more than 5 in the first story level. The maximum demands for all three earthquakes occur

in the first story with Yermo producing a demand of 3.5 and Joshua Tree 1.9. These values compare to 2.4 under the James Road motion and 3.0 under the Hollister motion.

The locations of plastic hinges and their corresponding ductility demands are shown graphically in Figure 15 for the three ground motions. Under the Joshua Tree motion, shown in Figure 15a, all ductility demands are less than three. There is considerable hinging in the columns of the first, third, fourth and fifth story levels with no column hinging in the second and sixth story levels. For the Yermo ground motion, shown in Figure 15b, the ductility demands in the first story columns increase such that most are in the range of 3 to 6. This figure indicates that the critical members for this building are the columns of the first story level and that this story level tends to act like a soft story. Under the Lucerne motion, shown in Figure 15c, it can be seen that a sway mechanism has formed in the first story level and that hinging has spread throughout most of the frame.

The hysteresis curves of moment versus rotation for the critical first story column under the three ground motions are shown in Figure 16. The one for the Joshua Tree ground motion, shown in Figure 16a, indicates that although the ductility demand is less, there are approximately nine yield reversals. The one for the Yermo motion, shown in Figure 16b, indicates a larger ductility, however, there are only seven yield reversals. A similar curve for Lucerne is shown in Figure 16c, indicating only one main yield reversal with

a large ductility. This response is representative of the effect of near fault ground motion having just one large velocity pulse.

Time history responses for the roof displacement and the base shear are shown in Figure 17 for the Joshua Tree ground motion. The time history of the roof displacement is shown in Figure 17a which indicates a long duration, harmonic type of input motion resulting in the three "beats". These occur because there is significant frequency content in the input ground motion which is near the natural frequency of the structure. A similar time history variation is shown in Figure 17b which presents the time history of the base shear. Note that the maximum base shear for the single frame is approximately 850 kips (1,700 kips for both frames). This is much less than the 2,500 kips predicted from the elastic analysis, however, it is about 3.8 times the value of the UBC design base shear (449 kips). It can also be seen that there is practically no residual displacement at the end of the time history.

The time history results under the Yermo ground motion are shown in Figure 18. In this case, the time history of the roof displacement, Figure 18a, tends to be more characteristic of a pulse type of input motion. The main pulse appears to occur at about 16 seconds at which time the displacement starts to increase, rises very rapidly to a maximum of approximately 9 inches and then decays exponentially. Note the residual displacement of

approximately two inches at the end of the time history. A similar behavior is shown in the time history of the base shear, Figure 18b, where the shear rises very rapidly to the maximum of 900 kips for the single frame (1,800 kips for both). This is also well below the 3,100 kips predicted from the elastic dynamic analysis but is 4 times the value of the UBC design base shear (449 kips).

The behavior of the roof displacement under the near fault, Lucerne ground motion is shown in Figure 19a. From this figure it can be seen that at about 10.5 seconds, there is an extremely sudden jump to a displacement of twelve inches followed by an exponential decay which drops the displacement to the residual value of approximately seven inches. The behavior of the base shear, shown in Figure 19b has a spike which reaches a maximum of 950 kips (1,900 kips for both), which is also well below the value of 4,500 kips predicted by the elastic analysis but more than 4.2 times the value of the UBC design base shear. The reduction in the base shear obtained by the nonlinear analysis is due to the force-limiting effect of the sway mechanism that forms in the first (soft) story.

A static nonlinear (pushover) conducted on this building in an earlier study [6] resulted in an estimate of 800 kips for the ultimate load for a single frame. The values obtained from the three ground motions used in this study range from 850 kips to 950 kips. The higher values obtained for the dynamic analyses are due to the effect of

the actual dynamic distribution of the inertia forces over the height of the frame, including the effect of the higher modes of vibration, and the effect of the damping forces both of which are neglected in the static pushover analysis.

3.5 Multiple Event Analyses

The occurrence of these two major earthquakes within only three hours of each other raises the question of the effect of multiple earthquakes or strong aftershocks on the behavior of a structure. This effect is investigated in this study by considering the effect of two consecutive earthquakes represented by the Yermo record (Yermo 2). The time history accelerations of the two Yermo records are shown in Figure 20. The total duration of the Yermo 2 record is 160 seconds. The figure indicates that the time between the end of strong ground motion from the first shock and the occurrence of strong ground motion from the second shock is more than 40 seconds. This time span allows the building to almost come to rest in a deformed position before the occurrence of the second shock.

The effect of the multiple event on the performance of the structure is shown in Figure 21 by comparing the nonlinear response parameters of the single event to those of the double event. It can be seen that the multiple event increases the envelopes of maximum values for all response parameters. Of particular interest is the increase in the ductility demand for the critical first story column, shown

in Figure 21d. For this member, the ductility demand increases from 3.5 to 4.5, a 28% increase.

The hysteresis curve for the critical column under the multiple event earthquakes is shown in Figure 22. Of particular interest in addition to the increased inelastic deformation, is the number of yield reversals which has almost doubled compared to the single event. This significant increase in the demanded energy dissipation due to plastic deformation is of great importance because it can lead to low cycle fatigue failure. The time histories of the displacements at the roof level are shown in Figure 23 for the single and multiple event conditions. For the single event, shown in Figure 23a, the maximum displacement is less than ten inches, however, there is a residual displacement at the end of the time history of about 2 inches. For the multiple event, shown in Figure 23b, the maximum displacement increases to 12 inches and the residual displacement at the roof increases to 3 inches.

4.0 SEVENTEEN STORY BUILDING, LANDERS

4.1 Building Description

In order to further investigate the effects of the Landers earthquake ground motions on building structures, a second case study building having a longer period of vibration was considered. The building is a seventeen story steel structure with a penthouse at the eighteenth story level. It has an overall height of 248' and was studied in

detail following the Northridge earthquake [12]. A typical floor has a rectangular plan which is 116'-8" by 154'-8", as shown in Figure 24. In general, lateral resistance is provided by four, two-bay moment resisting frames, the exception being the two frames in the north-south direction which have three moment resistant bays in the first two story levels creating a setback. Three of these frames are located on the perimeter of the structure, however, one is located one bay, 30'-4", from the north face of the building.

Although the building is assumed to be fixed at the base, it is supported on a pile foundation in which 12" x 12" prestressed piles extend a minimum of 48' below the pile cap. Typical floor construction is 3 1/2" light weight concrete fill over a 20 gage metal deck with A-36 steel beams framing into A572-50 steel columns. For purposes of identification, this building will be referred to as the "Canoga" building in the remainder of this study.

The building was designed in 1984 for the lateral force requirements of the 1982 Uniform Building Code. The lateral force requirements are similar to those presented previously for the six story building (1973 code). The design seismic resistance coefficient is expressed as

$$C_s = ZKCIS$$

where $Z = 1$, $K = 0.67$, $T = 0.1N = 1.7$ seconds, $C = 1/15^T = 0.51$, $I = 1.0$ and $S = 1.5$. These values result in a design

seismic resistance coefficient of 0.051. The base shear is then 5.1% of the effective dead load, W , which is estimated to be 27,155 kips. Hence, the design base shear is estimated to be 1,395 kips.

4.2 Elastic Response Analyses

The three dimensional model of the building used for the elastic dynamic analyses is shown in an isometric view in Figure 25. Deflected shapes for the first three modes of vibration are shown in Figure 26. The first mode, shown in Figure 26a, is a translational mode in the X direction which has a period of 4.12 seconds. The second mode, shown in Figure 26b, is a translational mode in the Y direction having a period of 3.85 seconds. The third mode, shown in Figure 26c is a torsional mode having a period of 2.17 seconds. The periods for 4th and 5th translational modes of vibration are 1.8 sec. N-S and 1.4 sec. E-W. From the response spectra for the Lucerne motion (Figure 6c) it can be seen that all of these periods are in the region of amplified long period response for the E-W component of this ground motion.

Envelopes of maximum elastic dynamic response are shown in Figure 27. The envelope of maximum story displacement is shown in Figure 27a. The impact of the near fault, Lucerne motion is readily apparent as it causes a roof displacement of 75 inches which is almost four times larger than the displacement demanded by the other two ground motions (20 inches for Yermo and 16.5 inches for Joshua). A similar

effect can be seen in the envelope of maximum interstory drift indices (Figure 27b). The Lucerne motion causes a severe IDI demand of approximately 3% from the 4th story level to the 13th story level. There is also a very sharp gradient between the 2nd story level and the 4th story level which will create high stresses in members of these story levels. The IDI for the other two ground motions is approximately 1%.

The envelopes of maximum inertia force are shown in Figure 27c. The forces developed by the Joshua Tree and Yermo records are similar, however, the Lucerne record generates inertia forces in the upper half of the building that are substantially higher. The envelopes of maximum story shear, shown in Figure 27d, indicate that the Lucerne ground motion is capable of generating a base shear of 7,000 kips which is more than twice as large as the other two records (3,100 kips for Yermo and 2,900 kips for Joshua) and more than five times the UBC base shear. It is of interest to note that in a previous study [12] the maximum base shear developed under the Sylmar record (Northridge, 1994) was 5,250 kips. This indicates that the Lucerne record demands an elastic base shear that is 1.3 times higher than that of the Sylmar record.

Members of the frame were stress checked for the three ground motions using the AISC-LRFD86 Specifications and nominal yield stresses (36 ksi for A36 and 50 ksi for A572

Grade 50). Results of these three analyses are summarized in Figure 28. for a typical (N-S) moment frame.

The stress ratios for the Joshua Tree motion are shown in Figure 28a. Under this motion, the columns remain within the elastic limits, with the exception of three columns in the third and fourth story levels where the stress ratios exceed unity by 1 to 5%. However, there are regions in the lower third and the upper third of the frame where the stress ratios in the girders exceed unity by approximately 30%. Stress ratios under the Yermo ground motion, shown in Figure 28b, have a similar pattern. However, stress ratios in the critical columns at the third floor setback now exceed unity by as much as 15% and those in critical girders exceed unity by as much as 37%.

Under the Lucerne motion, Figure 28c indicates that the stress ratios in both beams and columns increase significantly and stress ratios in most members exceed unity. In the critical columns at the third story setback, the stress ratios reach 3.37, whereas, in the critical beams in the fifth floor level, they reach 3.44. These values are indicative of significant inelastic behavior for this ground motion.

4.3 Inelastic Response Analyses

As in the previous case, the nonlinear dynamic analyses are conducted on a two dimensional model of one of the exterior frames, Frame B shown in Figure 29. Yield strengths of the members are determined using the nominal yield stress

of the material. Results of the inelastic, time-history analyses are shown in Figure 30 in terms of lateral displacement, IDI, girder ductility demand and column ductility demand.

The plot of maximum lateral displacements, shown in Figure 30a, indicates the significant effect of the Lucerne motion on this building. The maximum displacement of more than 60 inches, which occurs at the roof, is less than the 75 inches predicted by the elastic response analysis. The maximum displacement under the Yermo record decreases to 16 inches from 20 inches obtained from the elastic analysis and the inelastic displacement under the Joshua Tree motion increases to 18 inches compared to 16 inches estimated from the elastic response. Hence, the inelastic analysis has increased the displacement response to the Joshua Tree motion and decreased it for the Lucerne and Yermo motions.

There is a significant change in the interstory drift indices for the inelastic responses as shown in Figure 30b. Under the Lucerne motion, the IDI in the lower third of the tower increases significantly, reaching a maximum value of 4.2% at the fifth story level. This is a large drift demand and it is questionable if current welded moment connections can sustain this demanded member rotation, particularly if several reversals of significant inelastic deformation occur. The inelastic IDI demands for the other two ground motions are between 0.5% and 1.3%.

A similar situation can be seen in the envelope of the girder ductility demands, shown in Figure 30c. Curvature ductility demands in the critical fifth story girders under the Lucerne motion reach a value of 8.5 which is not thought to be sustainable with current fabrication and design details if the member experiences significant plastic hinge reversals. For the other two ground motions, the response to the Yermo ground motion is almost elastic and the curvature ductility demands under the Joshua ground motion are less than 2.25.

The envelopes of column ductility demands, shown in Figure 30d, indicate that for the Lucerne motion there is a high demand in the columns at the third story level where the setback of the tower from the lower two stories occurs. Under this ground motion, column ductility demands in excess of unity occur over most of the lower ten stories. Under the other two motions, the column behavior is elastic.

The locations of plastic hinges in this building and their corresponding ductility demands are shown graphically in Figure 31 for the three ground motions. The progressive amount of hinging that occurs under Yermo, Joshua and Lucerne is readily apparent. Under the Joshua Tree motion, shown in Figure 31a, all hinges are in the girders and are either in the upper third of the building or in the lower third with elastic behavior in the middle. Note that the maximum ductility demand is less than three (2.2 max.). For the Yermo motion, shown in Figure 31b, hinging of the

girders is just beginning to form in the upper and lower third of the frame. For this ground motion, maximum ductility demand is only 1.2.

Under the Lucerne ground motion, the amount of hinging increases significantly as shown in Figure 31c. Hinging occurs in all girders with a potential sway mechanism in the tower above the second story level. In the lower third of the building, ductility demands between 6 and 9 are required (8.5 max.). Hinges have also formed in the columns including the base of the structure. The critical columns are the ones in the bottom of the third story level at the setback from the second story level. All three columns form hinges which have ductility demands between three and six (3.6 max.).

Time history responses for the roof displacement and the base shear are shown in Figure 32 for the Joshua Tree ground motion. The displacement time history, shown in Figure 32a indicates several cycles near the maximum displacement amplitude of 18 inches. However, there does not appear to be any permanent displacement at the end of the time history. The time history of the base shear, shown in Figure 32b, indicates a maximum value of 1,500 kips (3,000 kips for two frames) which is similar to the 2,900 kips obtained from the elastic dynamic analysis.

Under the Yermo ground motion, the time history of the roof displacement, shown in Figure 33a, reaches a maximum amplitude of approximately 16 inches. The results presented in Figure 31 indicated that the building response for this

ground motion was almost elastic and hence, there is no permanent displacement at the end of the time history. The time history of the base shear, shown in Figure 33b indicates a maximum value of 1,400 kips (2,800 for both frames) which is similar to that calculated using the ETABS elastic model (3,100 kips). Although the 2,800 kips base shear is twice the UBC design base shear (1,395 kips) the response is almost linear elastic due to the overstrength of the structure.

The pulse effect of the Lucerne ground motion is apparent in the displacement time history shown in Figure 34a, where the maximum amplitude reaches 62 inches on one cycle. A permanent displacement of more than 22 inches is also indicated. The time history of the base shear (Figure 34b) indicates a maximum value of 2,000 kips. While the total base shear of 4,000 kips for two frames is less than that of the elastic dynamic analysis (7,000 kips) it is almost three times higher than the UBC design base shear of 1,395 kips.

Results of a static pushover analysis using the nominal yield stresses for the materials is shown in Figure 35. This figure indicates initial yield at a lateral load of 1,200 kips (2,400 kips for both frames) and roof displacement of 17 inches. At a roof displacement of 60 inches, a lateral load capacity of approximately 4,000 kips for the two frames is indicated. This is less than the 4,400 kips developed from the nonlinear dynamic analyses and represents the

combined effects of neglecting the actual variation of the inertia forces over the height of the structure as well as neglecting the damping forces in the static analysis. The pushover results also indicate that the frame under the Joshua Tree and Yermo ground motions, should be close to the initial yield level. This is also indicated by the results of the nonlinear dynamic analyses.

4.4 Postscript

More recently, a digitized and corrected record of the Lucerne ground motion has been released by CDMG. The elastic response spectra for this record with 5% damping is compared with the similar spectra for the original record in Figure 36. It can be seen that the spectra for the two records are quite similar up to a period of 2 seconds. In the longer period range from 2 to 10 seconds, the spectra for the CDMG record tends to indicate much lower response parameters than those given by the original processing done by Iwan. This illustrates the problems that can be experienced in digitizing and correcting recorded ground motions in the long period range.

5.0 TWO STORY BUILDING, BIG BEAR

5.1 General

One of the more interesting records obtained from the Big Bear earthquake was the one recorded at the Big Bear Civic Center. The instrument is located in the free field on shallow alluvium over granite bedrock. It is in an open area

to the west of the Big Bear Civic Center as shown in Figure 37. A peak acceleration of 0.48g was recorded in the east-west direction and 0.54g in the north-south direction.

The Big Bear Civic Center is a two story structure with lateral resistance provided by a three dimensional steel moment frame. Damage to the steel frame was not recognized immediately after the earthquake. However, after the problems with steel moment frame were identified following the Northridge earthquake (1994) a close inspection of the steel frames indicated severe cracking in the welded moment connections. The cracking was so severe, it was decided to retrofit the structure using a braced frame system to resist lateral loads.

The building was designed in 1986 and dedicated in October of 1987. Lateral force requirements were most likely based on those of the 1985 edition of the Uniform Building Code. A typical floor plan is shown in Figure 38. It can be seen that the floor system consists of wooden floor joists with a plywood cover. This results in a relatively light, yet rigid structural system. The floor weight of the second floor is estimated as follows:

2x14 floor joists @ 16" with 3/4 plywood	8.0 psf
Floor finish	4.0 psf
Hung Ceiling	8.0 psf
Partition Load	15.0 psf

Total floor dead load	35.0 psf
Wall Load	15.0 psf
Structural Steel	7.2 psf

This results in a total floor weight of 292 kips for the second floor. In a similar manner, the weight at the roof level is estimated to be 163 kips and the total building dead weight becomes 455 kips.

The lateral seismic forces specified in the 1985 edition of the UBC are expressed in terms of the base shear, V , as

$$V = (ZKCI)W = C_s W$$

The seismic dead load, W , is estimated to be 455 kips and Z , S , and I are taken as unity. The coefficient $C = 1/(15\sqrt{T})$ or $C = 1/(15\sqrt{0.1N}) = 0.149 > 0.12$. Therefore, $C = 0.12$ and $K = 0.67$. Using these values in the above equation results in a design seismic resistance coefficient, C_s , of 0.08 (8.0%) and a base shear of 36.4 kips.

5.2 Elastic Analyses

As for the previous buildings, a three dimensional, analytical model was developed for elastic response analyses using the ETABS Plus [8] computer program. An isometric view of the model is shown in Figure 39a and the plan of the structural framing is shown in Figure 39b. It can be seen that there are numerous releases in the three dimensional framing system where the moment connection is replaced by a simple shear connection. In most cases this occurs where the beam frames into the weak axis of the column. The orientation of the columns and the location of the shear connections can be seen in Figure 39b.

The deflected shapes of the first three modes of vibration are shown in Figure 40. The first mode, shown in Figure 40a is a translational mode in the N-S direction which has a period of 0.45 seconds. The second mode has a period of 0.40 seconds and is a translational mode in the E-W direction, Figure 40b. The deflected shape of the third mode, shown in Figure 40c, is a torsional mode which has a period of 0.34 seconds. The fourth mode is the second translational mode in the N-S direction and has a period of 0.14 seconds. The fifth mode represents the second translational mode in the E-W direction having a period of 0.13 seconds and the sixth mode is the second torsional mode. These modes represented 100% of the effective mass in both the X direction and the Y direction.

The elastic dynamic response of the building is evaluated by applying both components of the recorded free field motion to the base of the building simultaneously. The envelopes of maximum dynamic response in the two principal directions are shown in Figure 41. The displacement responses (Figure 41a) are approximately the same in both directions with the E-W displacement envelope being slightly larger. Note that the maximum displacement at the roof level is 2 inches which results in an average overall drift of 0.8% based on a building height of 21 feet. The IDI envelopes, shown in Figure 41b, indicate that the E-W direction has a larger response with a maximum IDI of 1% in the first story level.

The distribution of the inertia forces (Figure 41c) indicates that forces in the E-W direction are clearly predominate. Of particular interest is the distribution of the story shears which are shown in Figure 41d. The maximum shear in the first story level reaches 459 kips in the E-W direction and 351 kips in the N-S direction. Both of these values are well above the UBC design value of 36 kips and should indicate inelastic behavior in critical members.

In a similar manner to the previous two structures, the members of the steel frame are stress checked for the response to the recorded free field ground motions using the STEELER [8] postprocessor program and the AISC-LRFD86 Specifications [10]. The yield strength of the members is estimated using the nominal yield stress (36 ksi.) for the material. The results are summarized in Figure 42. These data indicate that several members have stress ratios which exceed unity. This is particularly true for the first story level where the maximum stress ratios exceed 2.0.

These results also indicate that this frame will experience inelastic behavior in a substantial number of structural members and implies that a nonlinear dynamic analysis should be conducted to evaluate the effect of inelastic behavior on the structural response. This will be done in the following section. The elastic response results also indicate that the cracking discovered in the welded steel connections may have been effected significantly by the high stress levels in the critical members.

5.3 Inelastic Analyses

In order to model the inelastic, nonlinear response of this structure to static and dynamic loads using the same two dimensional program as for the previous two structures, it was necessary to develop two dimensional, linked frame models as shown in Figure 43 where pinned connections are shown by open circles. In this model, the three moment frames in the E-W direction are connected together with pin ended rigid links as shown in Figure 43a. A similar model for the four frames in the N-S direction is shown in Figure 43b. In this direction, symmetry is used to reduce the number of frames to only two which represent only half of the building and react only half of the total mass.

5.3.1 Static (Pushover) Analyses.

In order to estimate the lateral resistance of the building at ultimate load, a static, nonlinear analysis (pushover) was conducted for proportional loading. The reference lateral load distribution is that specified in the 1985 edition of the Uniform Building Code which results in a load of 10.7 kips at the second story level and 25.7 kips at the first story level. This load distribution is multiplied by a load factor and then divided into a large number of load increments which are applied sequentially to the structure. As yielding of the members occurs, the incremental stiffness of the structure is modified for the next load increment. The magnitude of the load factor is determined by a limit condition such as overall frame

stability or by excessive rotation and ductility demands on critical frame members.

Results of the pushover analyses are summarized in Figure 44 where the roof displacement is plotted versus the base shear. These results indicate that the E-W frames have an ultimate capacity of 420 kips whereas the N-S frames reach 285 kips. Recall that symmetry was used in the N-S direction so that the total lateral resistance in this direction is actually 570 kips. Both frames have a smooth transition from purely elastic behavior to failure mechanism (sway mechanism in the columns of the first floor). The smooth transition is a result of the high redundancy and many plastic hinges in the first floor level. When these values are compared with the UBC design base shear (36.4 kips) it is clear that the designed structure has a very high overstrength of more than ten times.

The locations and curvature ductility demands in the hinges of the frames in the E-W direction are shown in Figure 45a. A sway mechanism can be seen in the first story level with ductility requirements in the beams and columns approaching 9. In the frames in the N-S direction, shown in Figure 45b, the ductility demands in many of the members exceed 9 and may be excessive.

5.3.2 Time History Analyses.

Results of the inelastic, time-history analysis are shown in Figure 46 in terms of lateral displacement, IDI, girder ductility demand and column ductility demand. The

inelastic dynamic response increases the maximum roof displacement from 2.0 inches (elastic) to almost 2.5 inches in the N-S direction. In the E-W direction, the inelastic behavior actually reduces the maximum roof displacement from 2.1 inches (elastic) to 1.9 inches. Note that for the inelastic response, the maximum displacement occurs in the N-S direction rather than in the E-W direction as predicted by the elastic response. It should also be noted that the displacement of 2.5 inches N-S places the frame in the transition region on the pushover curve. In the E-W direction, the displacement of 1.9 inches places the structure at the onset of inelastic behavior. The maximum IDI, shown in Figure 46b, also occurs in the N-S direction and has a value of 1.1% which is not considered very high although it is about 1.3 times the elastic value.

Girder ductility demands, shown in Figure 46c, are just above unity in the second floor level and at unity in the roof level. Ductility demands in the columns, shown in Figure 46d, are above unity in both directions in the first story level, reaching a maximum value of 1.4 which is considered moderate. When these maximum ductility ratios are compared with the stress ratios of Figure 42, it is apparent that they are not as severe as the stress ratios would indicate.

The distribution of plastic hinges and their corresponding curvature ductility demands are shown in Figure 47. For the frames in the E-W direction (Figure 47a)

most hinges are located in the columns of the first story level, however, four beams at this level developed hinges at both ends. All ductility demands are in the range of 1 to 3 (1.3 max.). For the members of the N-S frames, shown in Figure 47b, most of the hinging is in one of the frames which is on the left side of the figure with hinges developed in most of the first story columns and one of the second story columns. As before, the ductility demands are not large, being in the range of 1 to 3 (1.4 max.). This data gives further indication that the cracking of the welded moment connections may have occurred near the plastic moment capacity of the structural members but with low ductility demands.

6.0 SUMMARY AND CONCLUSIONS

The magnitude 7.3 Landers earthquake (1992) is the second largest earthquake to occur in California since 1906. It has received limited attention to date due to its location in the western Mojave Desert and the fact that its date of occurrence was between two major earthquakes which were much closer to major population centers (Loma Prieta (1989) and Northridge (1994)). Three of the free field records obtained from this earthquake are significant for their effect on engineered structures. One of these, located in the near fault region, is particularly significant for its potential damaging effect on structures having periods in the range of one to five seconds.

The effect of these three free field ground motions was investigated by considering the behavior of two case study buildings which had been investigated previously for the Whittier Narrows (1987) and the Northridge (1994) earthquakes. Both are steel structures with lateral resistance provided by perimeter moment frames. One is a six story building and the other is a seventeen story building with a penthouse. Studies of the behavior of these two buildings considered both elastic dynamic analyses and inelastic dynamic analyses for the recorded ground motions. Correlations are made with inelastic static analyses conducted as part of the previous investigations.

One record from the magnitude 6.2 Big Bear earthquake, which occurred three hours after the Landers earthquake, was obtained near a low rise office building which experienced severe cracking in the welded moment connections of a steel space frame. This building was studied in detail to determine if the cracking may have been due to this earthquake although it was not discovered until after the Northridge earthquake. Studies on this building considered elastic dynamic analyses, inelastic static analyses (pushover) and inelastic dynamic analyses.

The main observations from the results obtained in the studies of the ground motions and the response of these three buildings are summarized as follows:

1. The recorded Landers earthquake ground motions, with recorded data in the backward directivity region, the forward directivity region and the near fault region emphasize the previously observed importance of the directionality of fault rupture.

2. Comparison of the results obtained using linear elastic analyses with those obtained using nonlinear (inelastic) analyses point out that while linear elastic analyses may give a good estimate of the maximum lateral displacement (usually at the roof), they do not give a reliable estimation of the maximum interstory drift index which is a better indicator of damage potential.

3. The base shear strength demanded by the recorded ground motions was more than ten times that required by the lateral force provisions in the UBC. However, the estimation of the maximum lateral resistance using nonlinear analyses shows clearly that the actual lateral resistance of buildings designed according to UBC is higher than that required by the code. The taller the building, the lower is the overstrength. For the two story, Big Bear Civic Center, the actual lateral strength was estimated to be more than ten times the UBC required strength. This significant overstrength has prevented the collapse of low rise buildings during severe earthquakes.

4. Elastic dynamic analyses combined with the calculation of member stress ratios can give a broad indication of critical regions and member overstress.

However, they do not necessarily give good estimates of inelastic behavior including displacement responses and ductility demands.

5. The inelastic static analyses can provide estimates of the amount of inelastic behavior for a given displacement level. However, the lateral forces determined from the inelastic static analyses will be less than those determined from the inelastic dynamic analyses since the effects of the distribution of inertia forces and the inclusion of damping forces are neglected.

6. The near field velocity pulse, normal to the direction of fault propagation, can have a severe effect on structures having periods of vibration in the range of one to five seconds. This type of motion tends to dislocate the base of the structure, causing very high drift and ductility requirements over the lower third of the building height.

7. The effect of two successive strong motion earthquakes or a strong earthquake followed by a strong aftershock is to increase the displacement and ductility demands, provided the initial ground motion is capable of driving the structure into the inelastic region. Successive earthquakes can also result in a significant increase in the number of yield reversals and, therefore, in the cumulative ductility demand. Many of the structures shaken by the San Fernando (1971) and Northridge (1994) earthquakes have permanent deflections. With the next strong earthquake, the

ductility demands and particularly the cumulative ductility demands will increase and may reach the limit value.

8. The high frequency, high amplitude accelerations recorded during the Big Bear earthquake may have been responsible for initiating cracks in the welded moment connections of a two story space frame. The low period of the light-weight building placed its fundamental period close to the period range of high acceleration on the response spectrum. Due to the high frequency content of the ground motion and the high predominant frequencies of the building, the deflection and story drifts were low causing little damage and causing the damage to the connections to go unnoticed for more than 1 1/2 years under the fireproofing and partitions. It is estimated that the recorded ground motions were sufficient to drive many of the structural members to their plastic moment capacity.

The results of this study indicate the need for additional studies on the directivity effects of near fault ground motions and their effect on the built environment. It also emphasizes the need for additional studies on the effect of successive strong motion earthquakes and the effect of the later ground shaking on buildings that have sustained inelastic deformations during the initial shaking.

TABLE 1. Recorded Free Field Motions, Landers Earthquake

Location	Acceleration	Velocity	Displacement
Barstow			
E-W	132.6 cm/sec ² (0.135g)	25.1 cm/sec (9.9 in/sec)	16.9 cm (6.7 in)
N-S	129.0 cm/sec ² (0.131g)	21.9 cm/sec (8.6 in/sec)	19.0 cm (7.5 in)
Desert Hot Springs			
E-W	151.0 cm/sec ² (0.154g)	20.8 cm/sec (8.2 in/sec)	7.0 cm (2.7 in)
N-S	167.4 cm/sec ² (0.171g)	19.0 cm/sec (7.5 in/sec)	7.5 cm (3.0 in)
Joshua Tree			
E-W	278.4 cm/sec ² (0.283g)	42.7 cm/sec (16.8 in/sec)	15.7 cm (6.2 in)
N-S	268.3 cm/sec ² (0.273g)	27.1 cm/sec (10.7 in/sec)	7.9 cm (3.1 in)
Palm Springs			
E-W	87.2 cm/sec ² (0.089g)	13.9 cm/sec (5.5 in/sec)	5.0 cm (2.0 in)
N-S	74.2 cm/sec ² (0.076g)	10.8 cm/sec (4.3 in/sec)	6.8 cm (2.7 in)
Yermo			
E-W	240.0 cm/sec ² (0.244g)	50.8 cm/sec (20.0 in/sec)	41.3 cm (16.3 in)
N-S	148.5 cm/sec ² (0.151g)	29.0 cm/sec (11.4 in/sec)	22.8 cm (9.0 in)
Big Bear			
E-W	161.6 cm/sec ² (0.165g)	7.5 cm/sec (3.0 in/sec)	3.0 cm (1.2 in)
N-S	188.1 cm/sec ² (0.192g)	13.6 cm/sec (5.4 in/sec)	8.3 cm (3.3 in)

TABLE 1. Continued

Lucerne Valley

E-W	699.6 cm/sec ² (0.713g)	136.0 cm/sec (53.5 in/sec)	229.8 cm (90.5 in)
N-S	783.9 cm/sec ² (0.799g)	70.3 cm/sec (27.7 in/sec)	183.8 cm (72.4 in)

TABLE 2. Recorded Free Field Motion, Big Bear Earthquake

Location	Acceleration	Velocity	Displacement
E-W	472.2 cm/sec ² (0.481g)	28.2 cm/sec (11.1 in/sec)	4.6 cm (1.8 in)
N-S	534.2 cm/sec ² (0.544g)	34.4 cm/sec (13.5 in/sec)	4.3 cm (1.7 in)

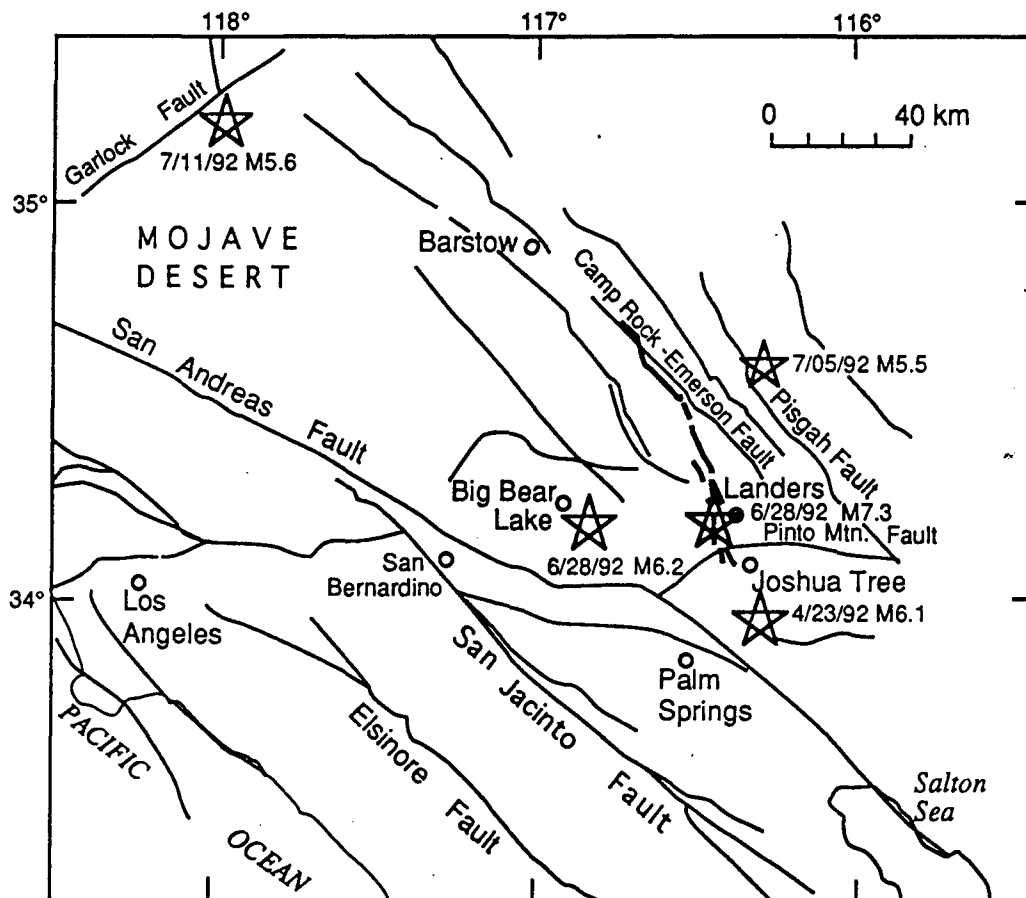
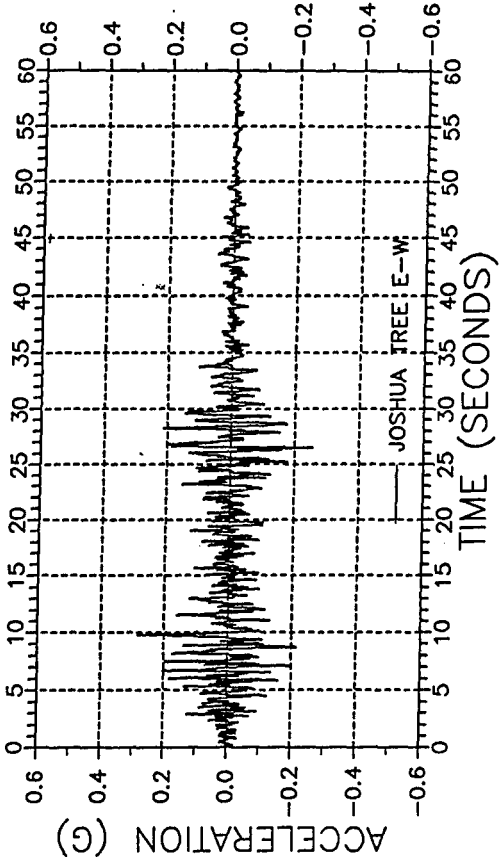
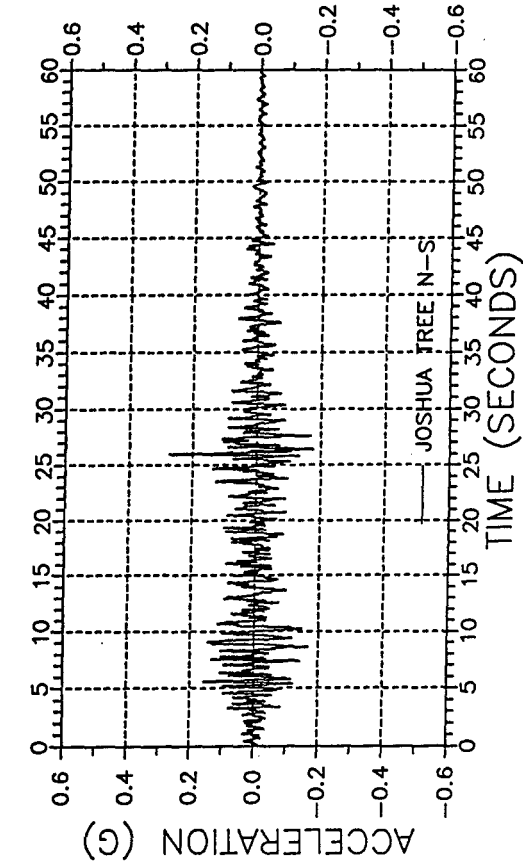


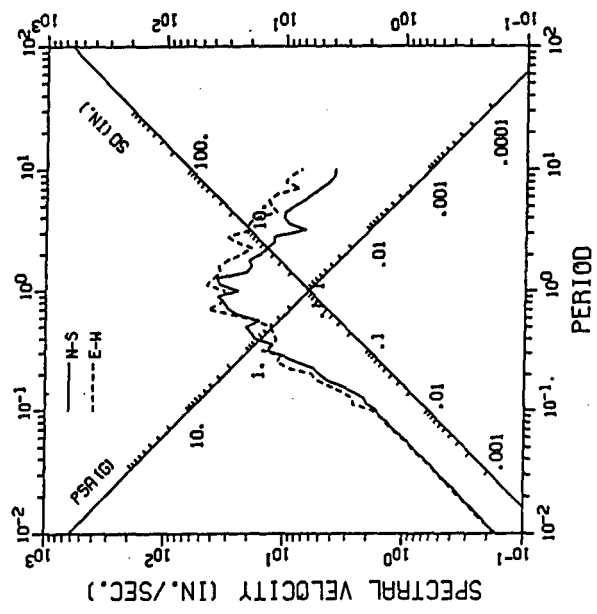
Figure 1 Map of Western Mojave Desert



(a) East-west Time History



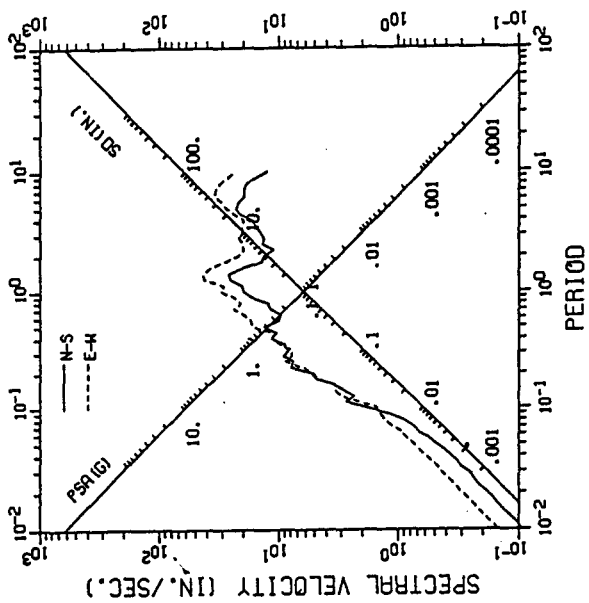
(b) North-South Time History



(c) Elastic Response Spectra, 5% Damping 43

Figure 2 Recorded Accelerations,

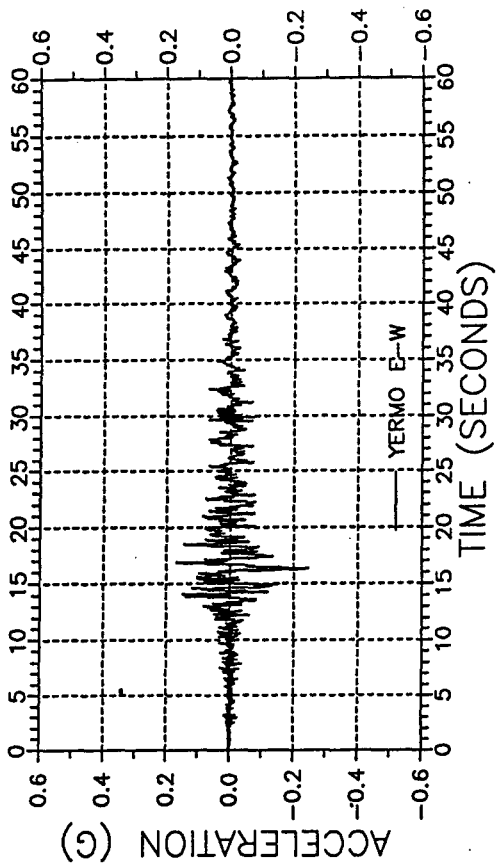
Joshua Tree



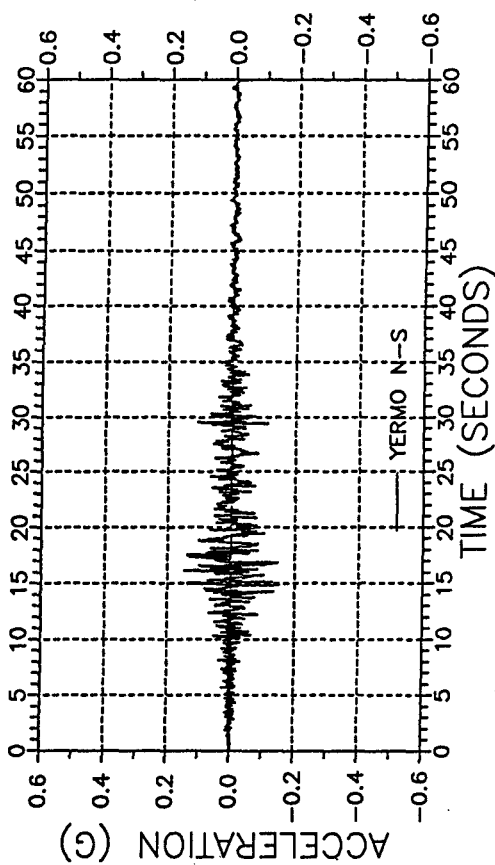
(c) Elastic Response Spectra, 5% Damping

Figure 3 Recorded Accelerations,

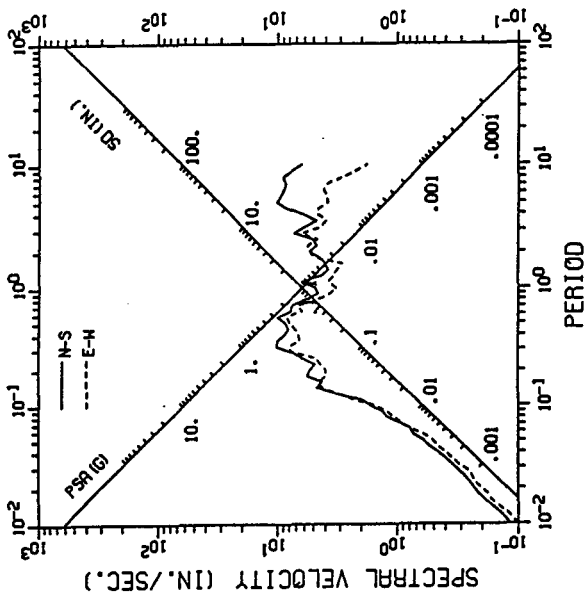
Yermo



(a) East-West Time History

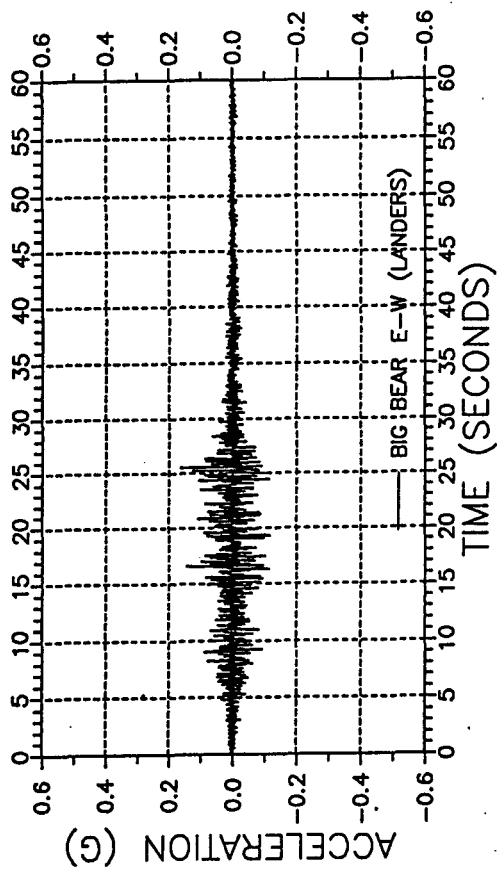


(b) North-South Time History

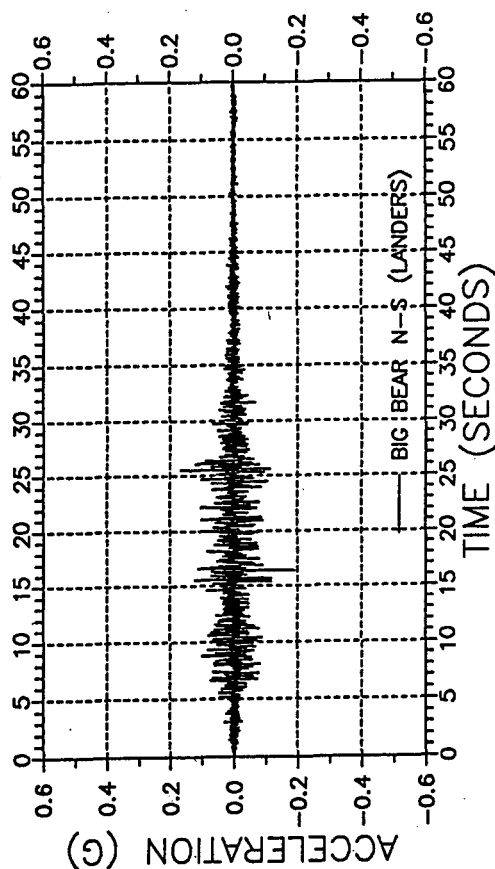


(c) Elastic Response Spectra, 5% Damping

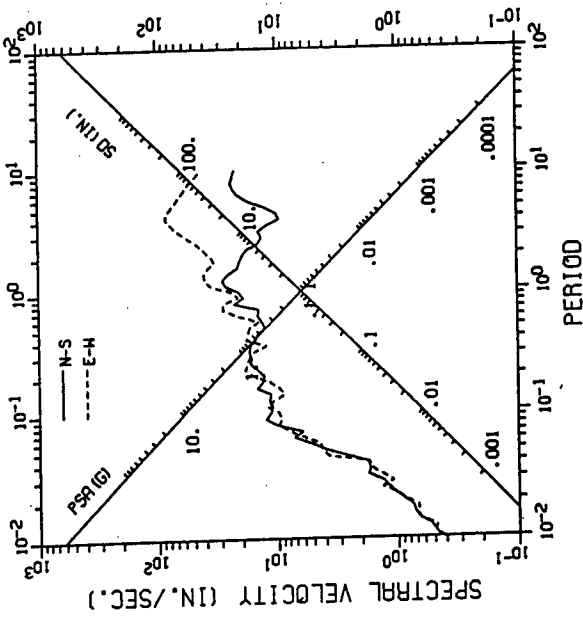
Figure 5 Recorded Accelerations,
Big Bear (Landers)



(a) East-West Time History



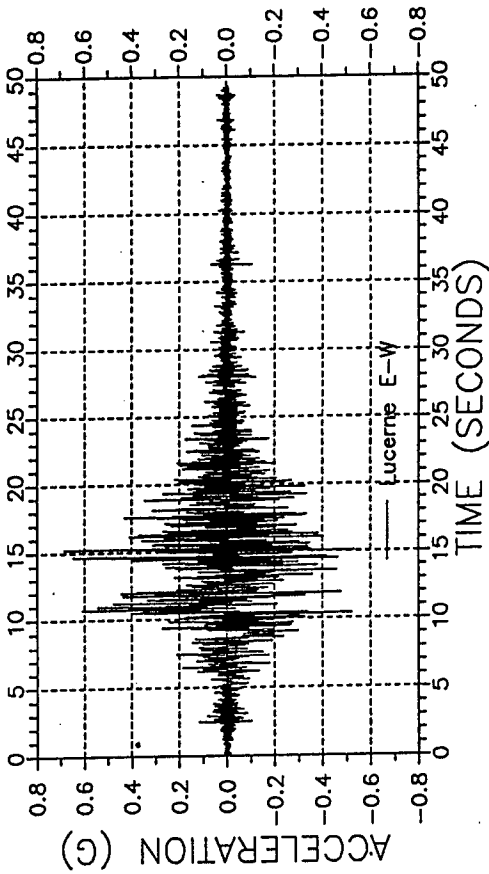
(b) North-South Time History



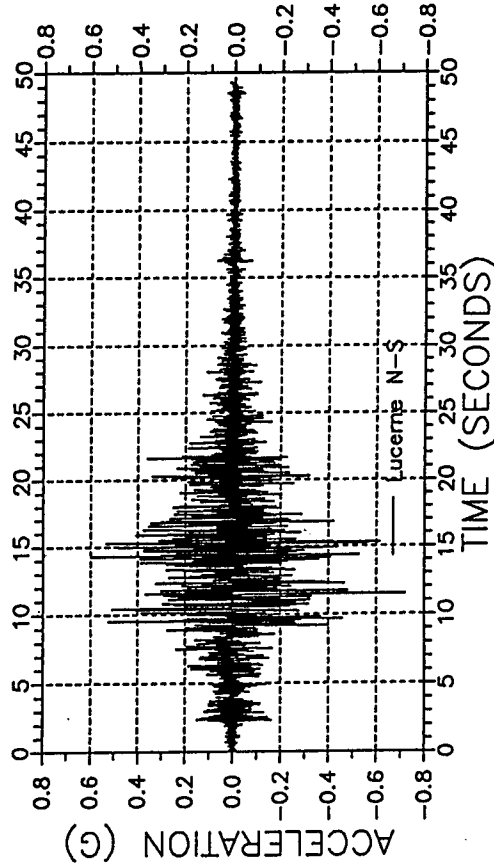
(c) Elastic Response Spectra, 5% Damping

Figure 6 Recorded Accelerations,

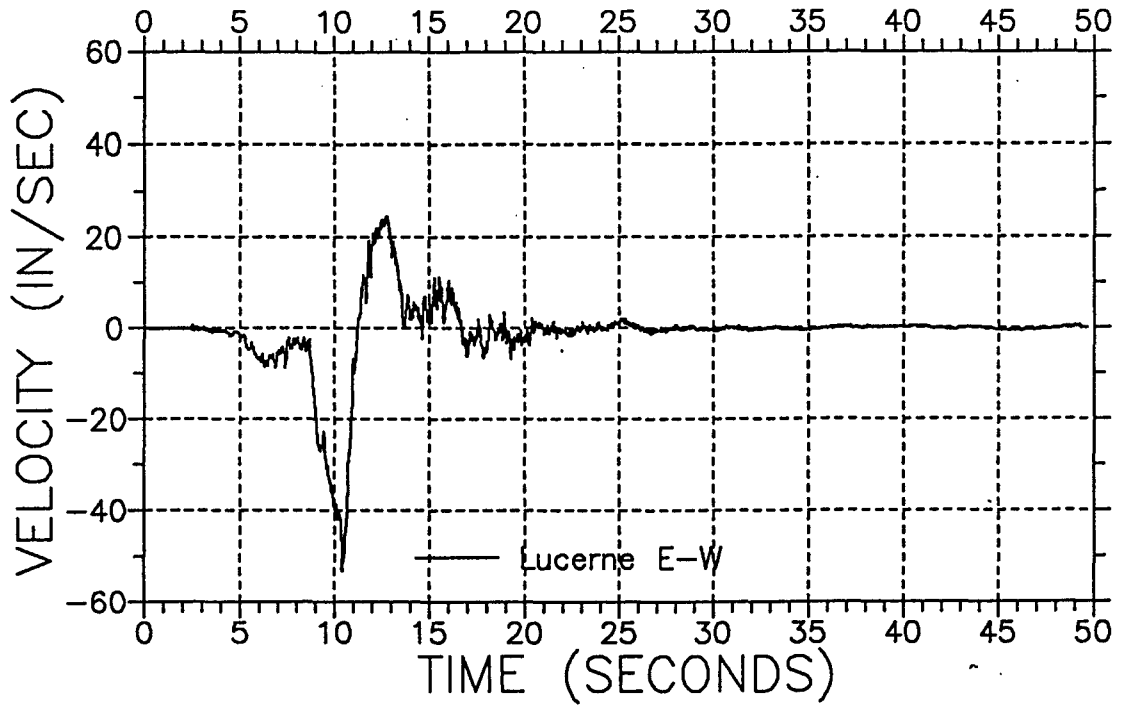
Lucerne Valley



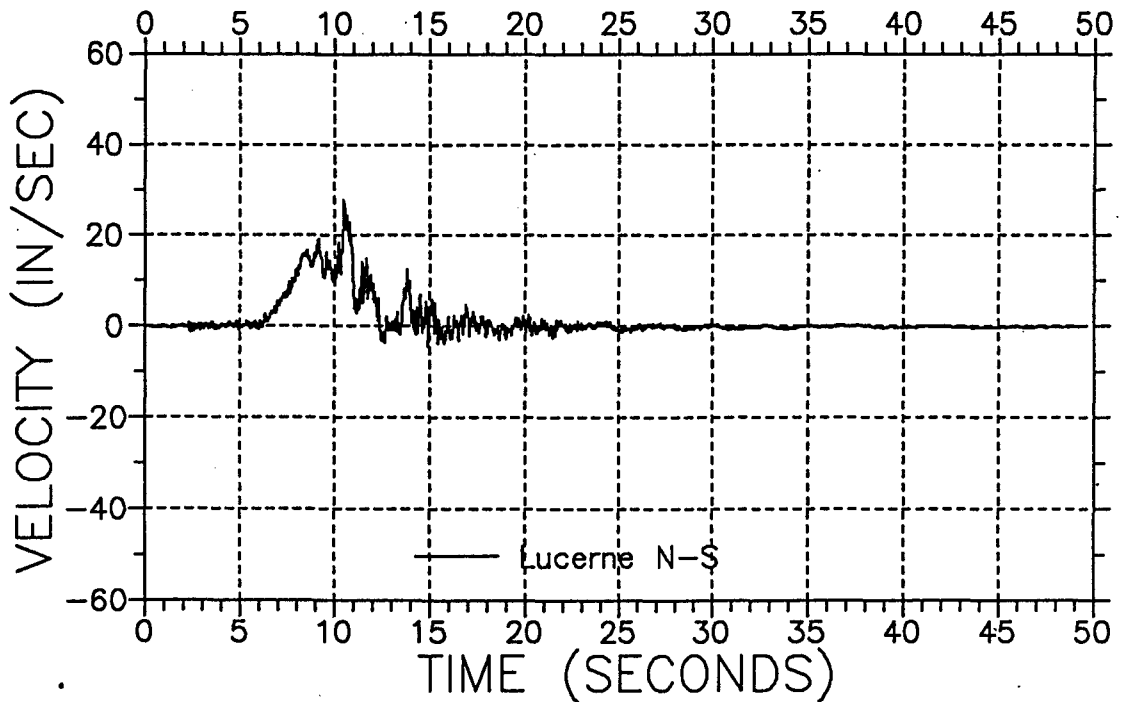
(a) East-West Time History



(b) North-South Time History

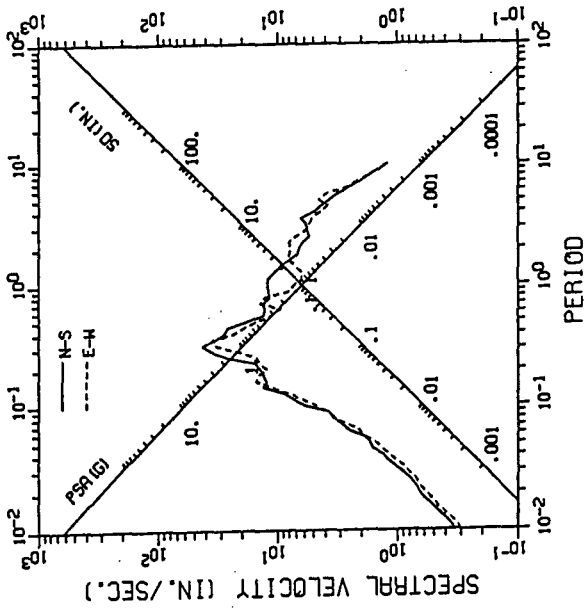


(a) East-West Time History



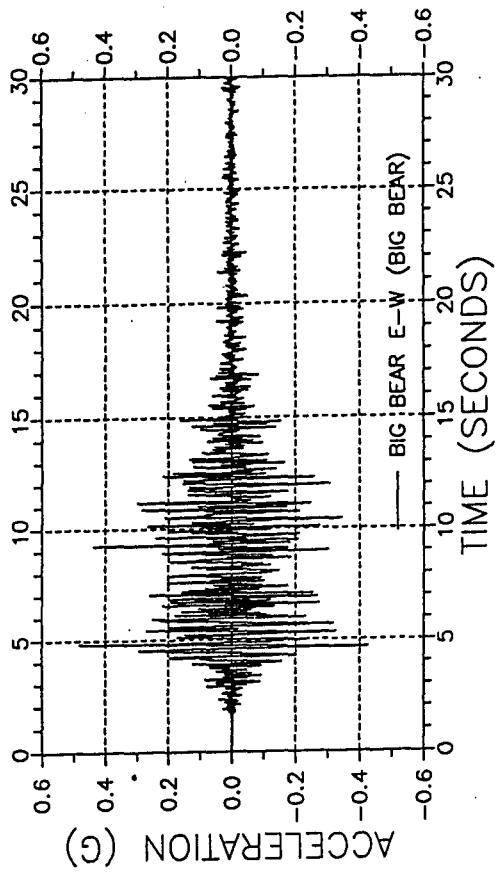
(b) North-South Time History

Figure 7 Recorded Velocities, Lucerne Valley

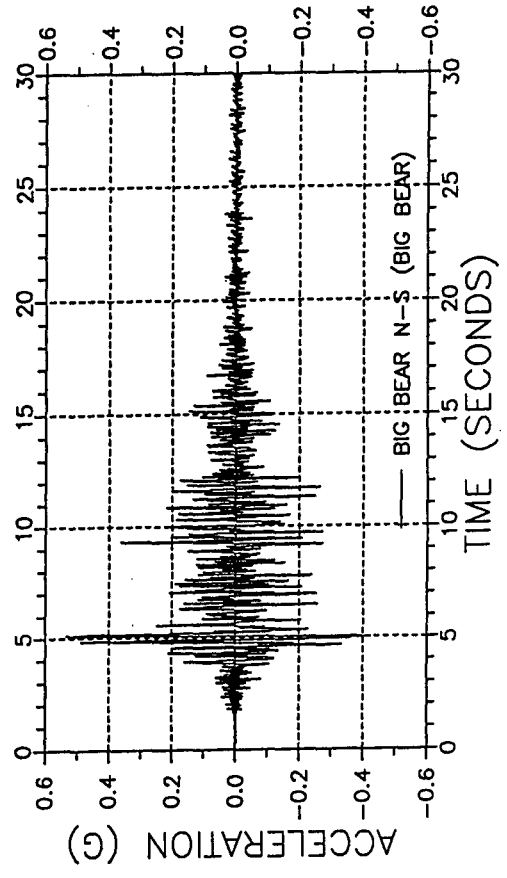


(c) Elastic Response Spectra, 5% Damping

Figure 8 Recorded Accelerations,
Big Bear (Big Bear)



(a) East-West Time History



(b) North-South Time History

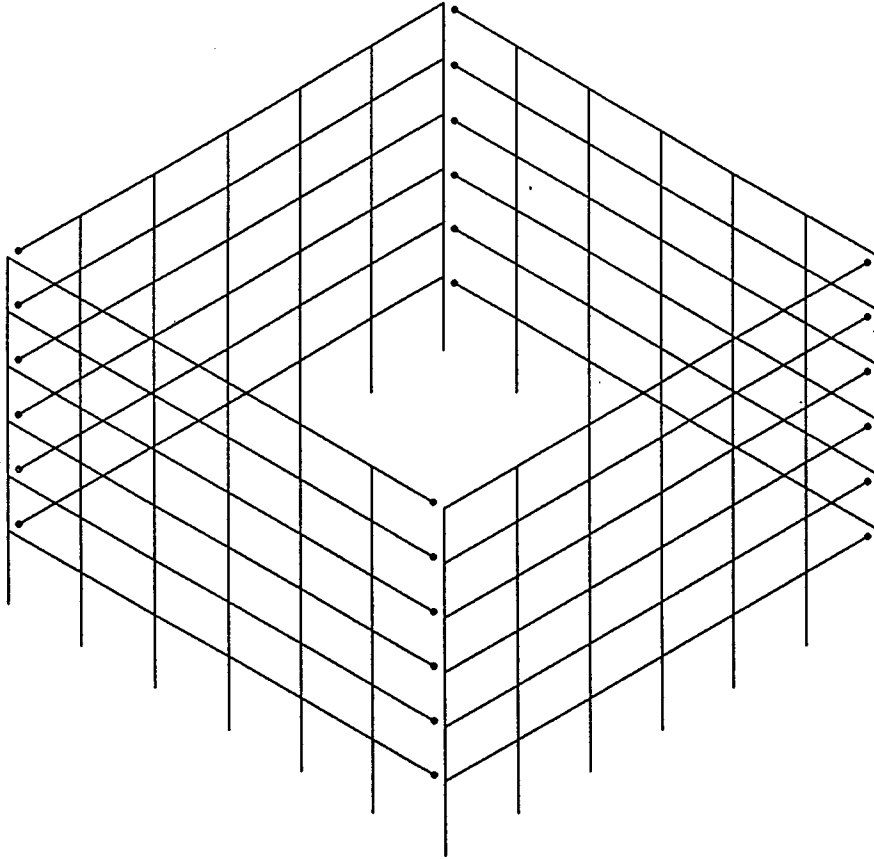
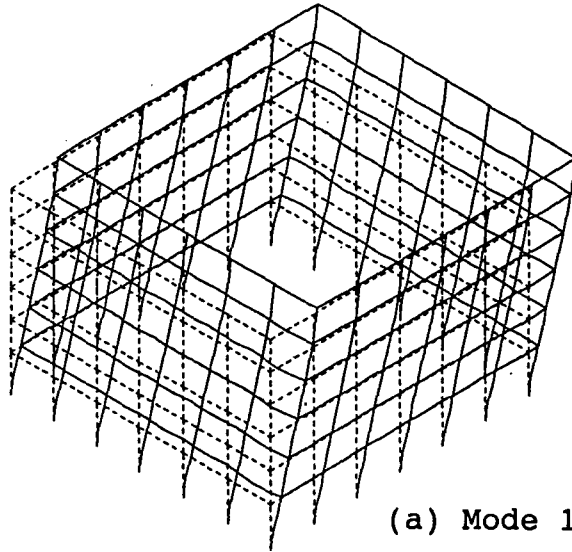
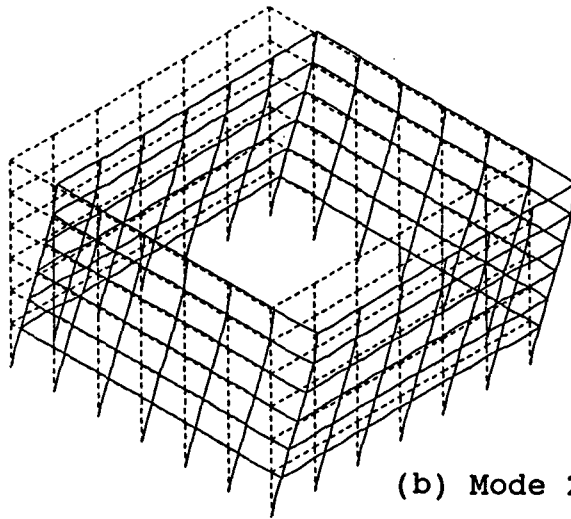


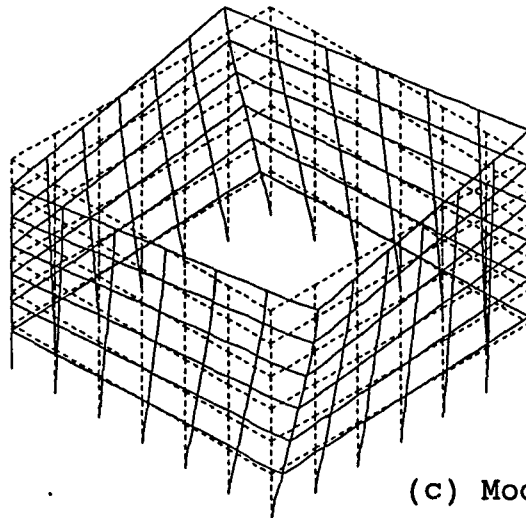
Figure 9 Elastic Dynamic Model, Six Story Building



(a) Mode 1, $T = 1.45$ Sec

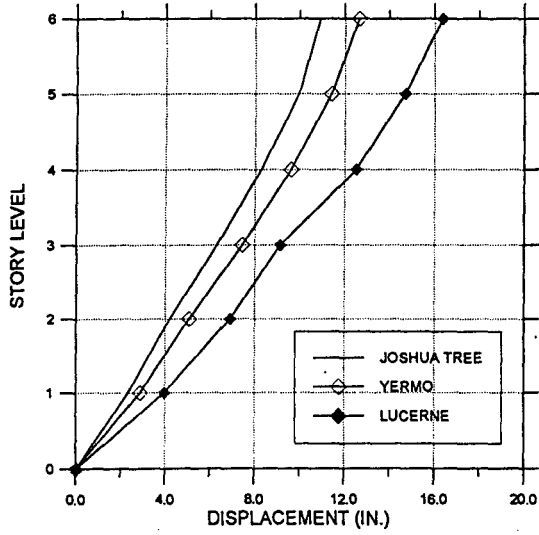


(b) Mode 2, $T = 1.45$ Sec

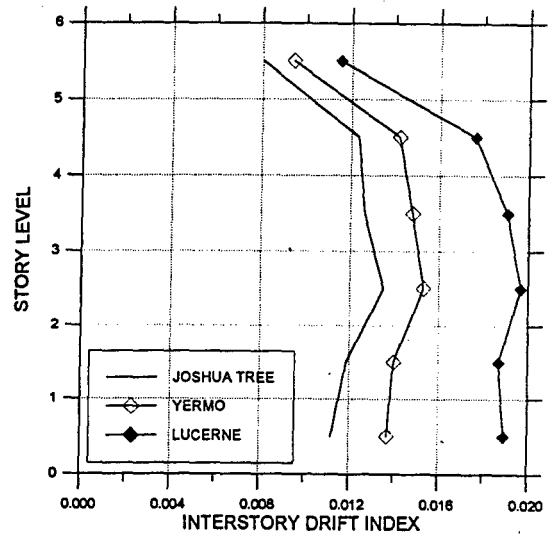


(c) Mode 3, $T = 0.83$ Sec

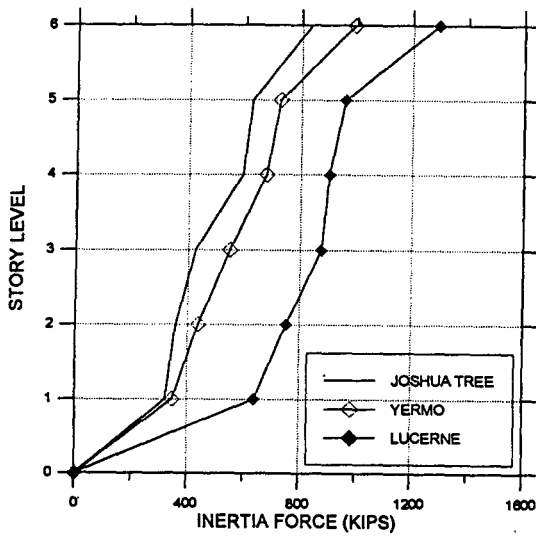
Figure 10 Calculated Mode Shapes, Six Story Building



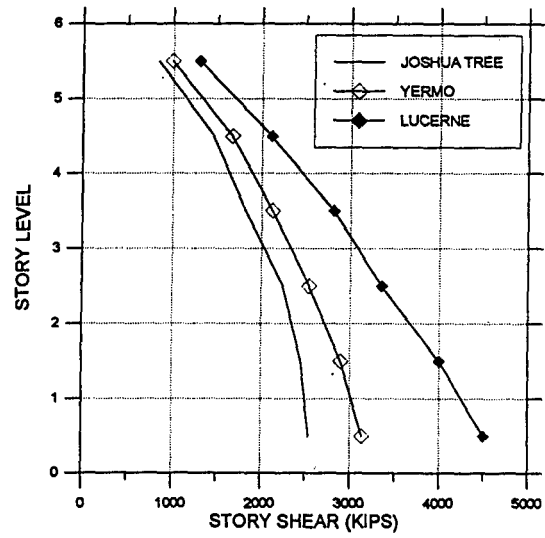
(a) Lateral Displacement



(b) Interstory Drift Index

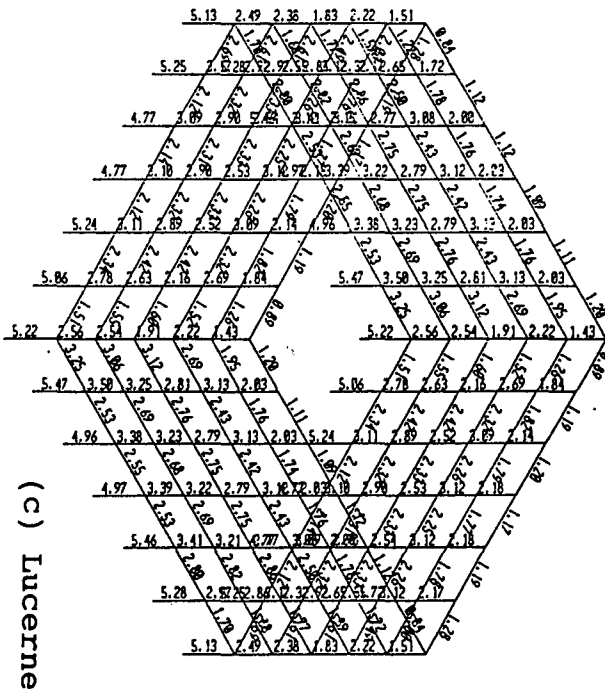


(c) Inertia Forces

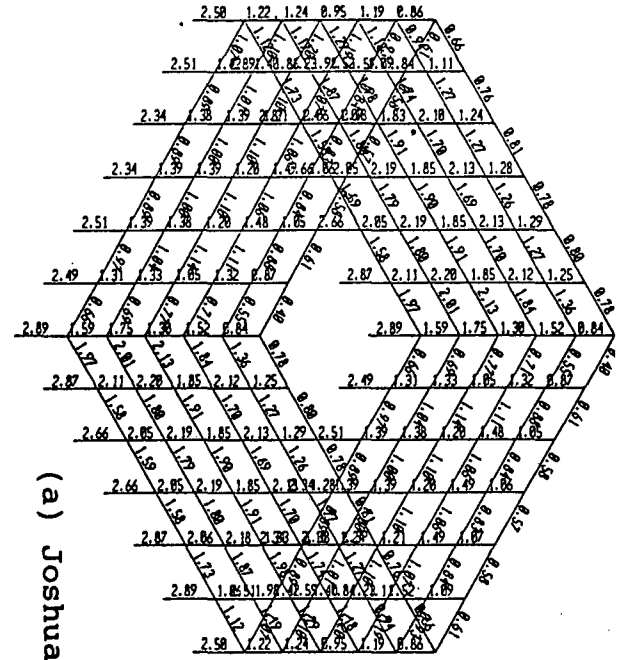


(d) Story Shears

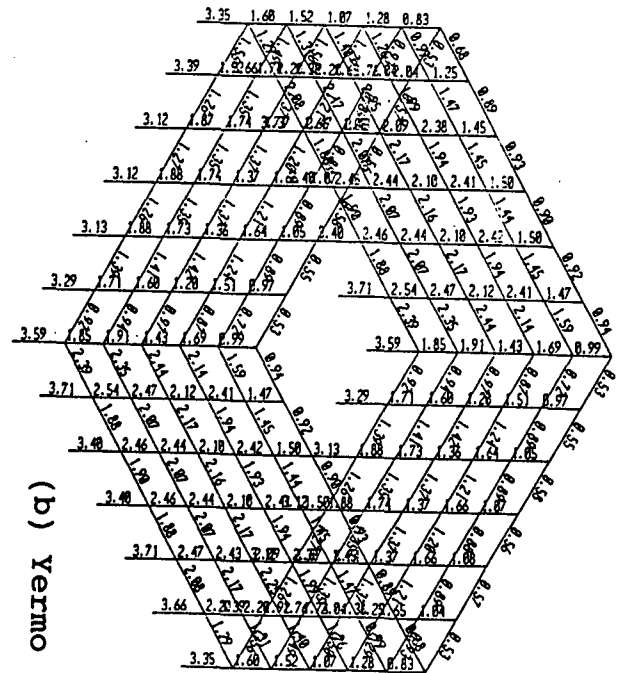
Figure 11 Maximum Elastic Response, Six Story Building



(c) Lucerne

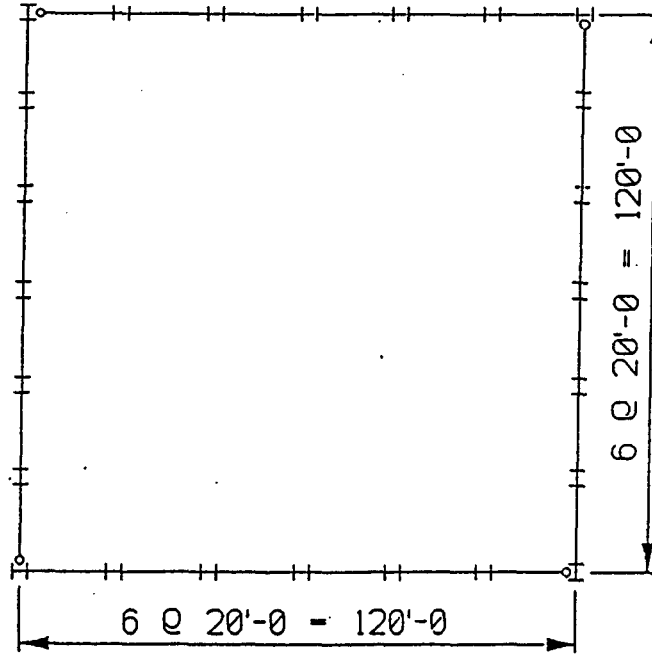


(a) Joshua Tree

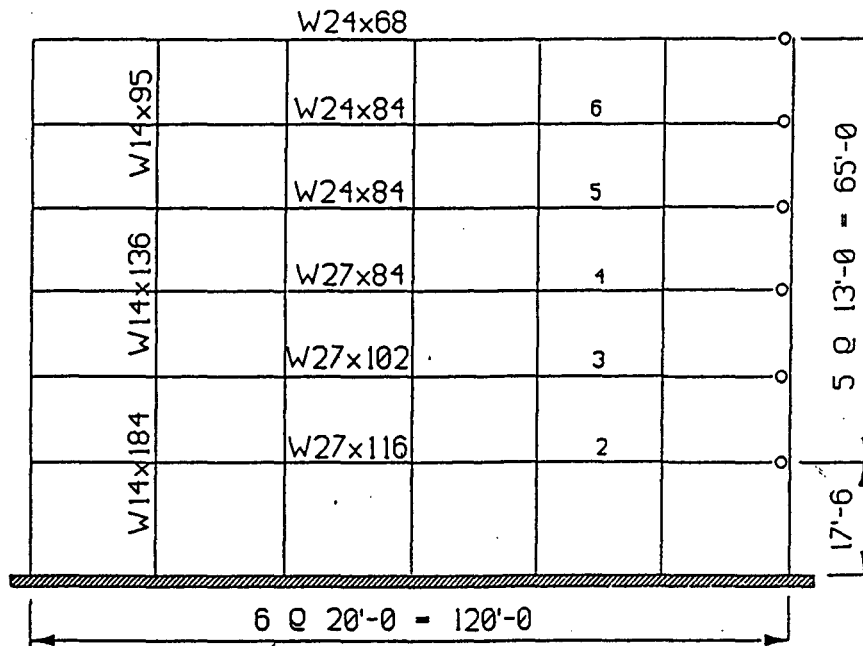


(b) Yermo

Figure 12 Stress Ratios, LFRD,
Six Story Building

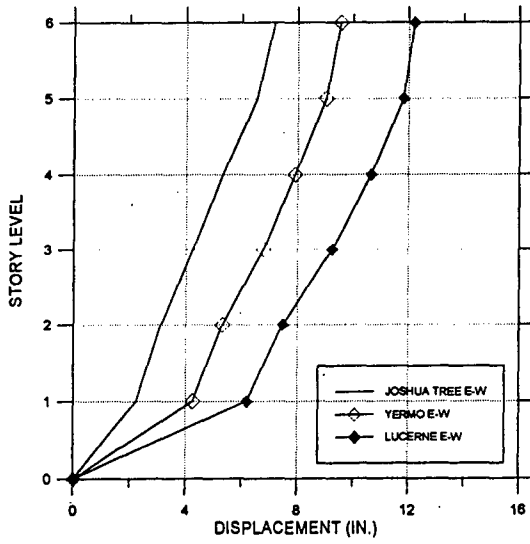


(a) Perimeter Frame Plan

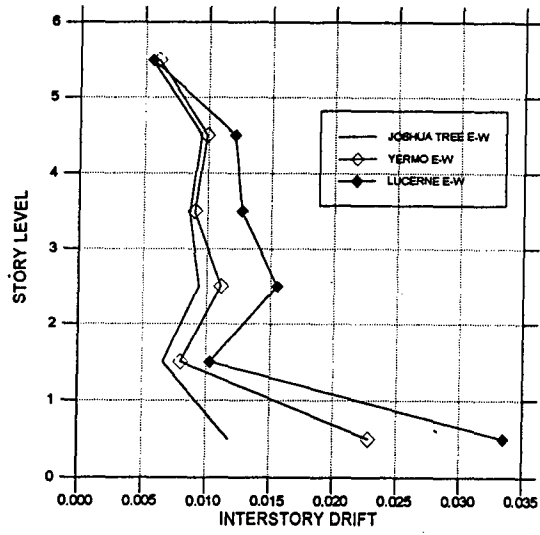


(b) Nonlinear 2D Model

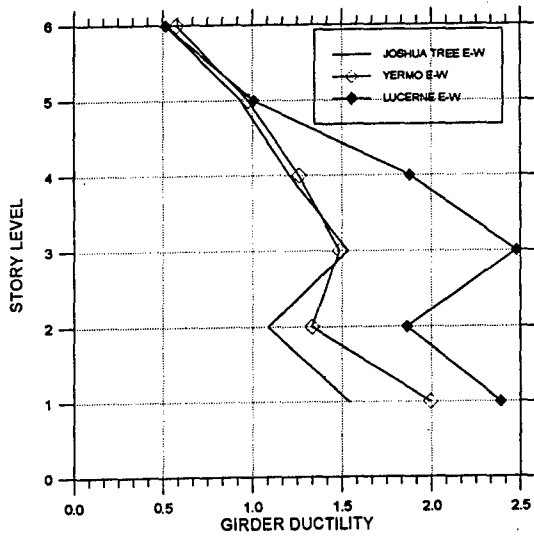
Figure 13 Nonlinear Model, Six Story Building



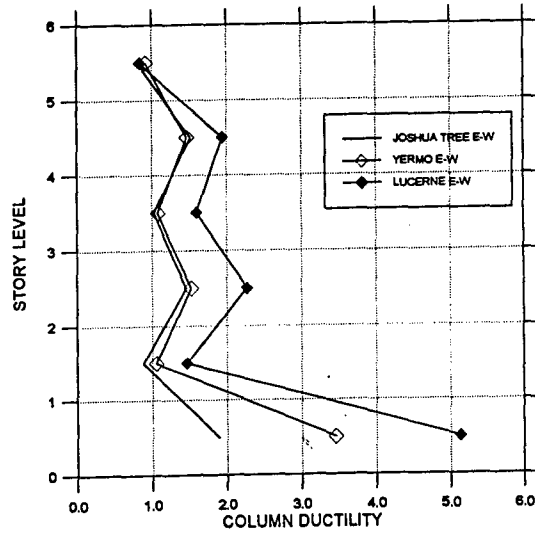
(a) Lateral Displacement



(b) Interstory Drift-Index

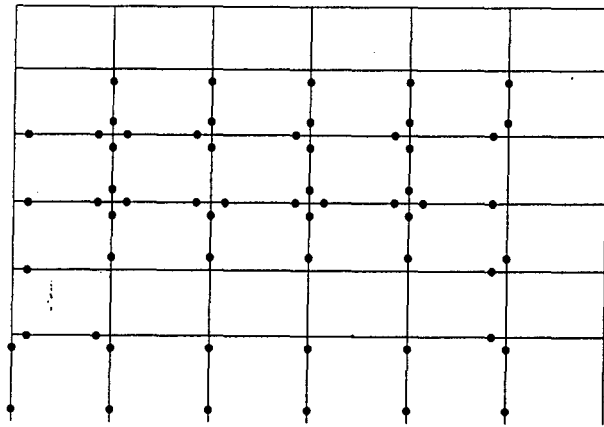


(c) Girder Ductility Demand

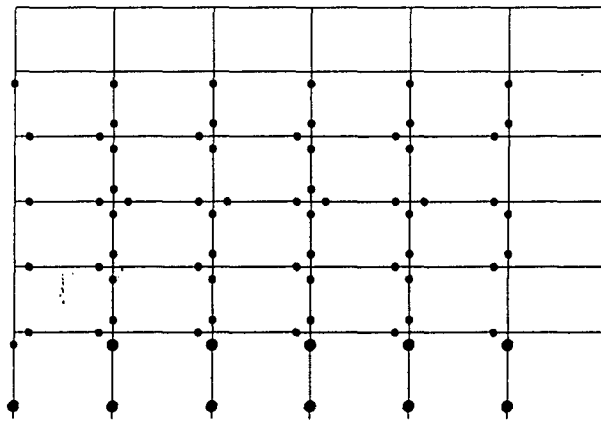


(d) Column Ductility Demand

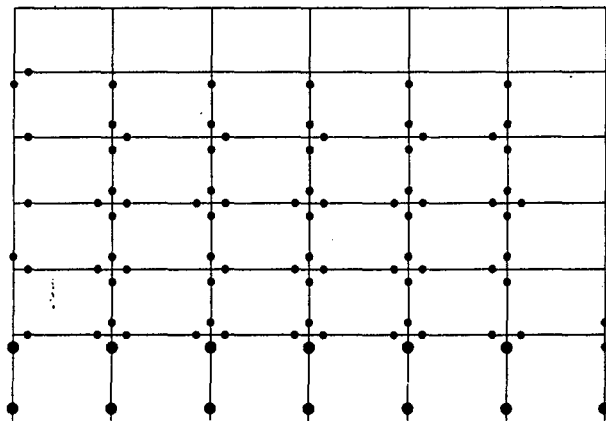
Figure 14 Maximum Inelastic Response, Six Story Building



(a) Joshua Tree

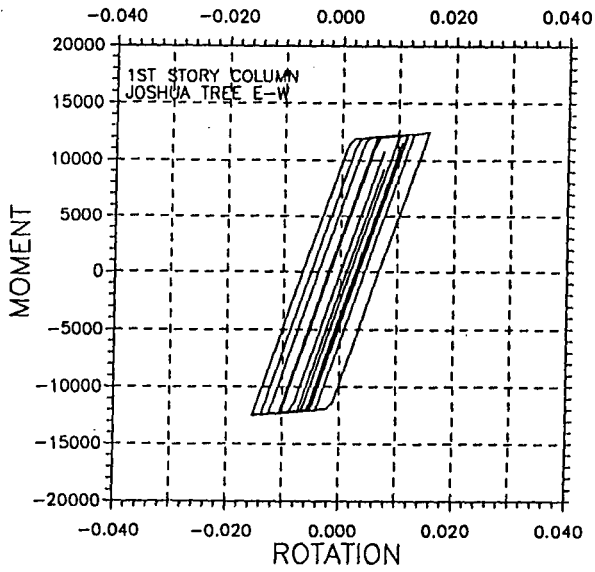


(b) Yermo

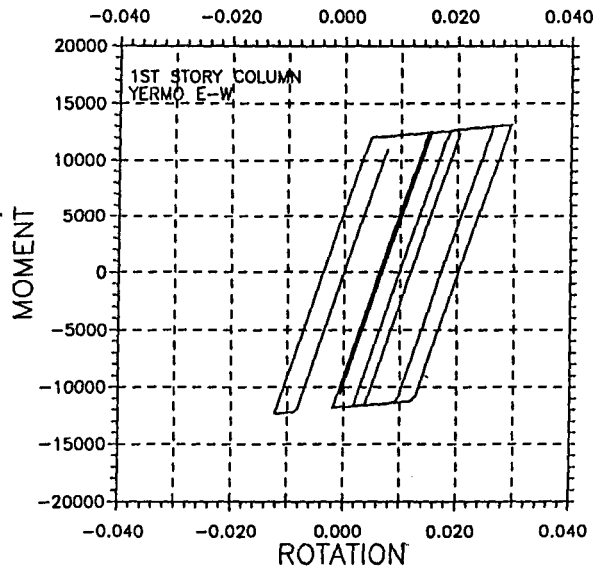


(c) Lucerne

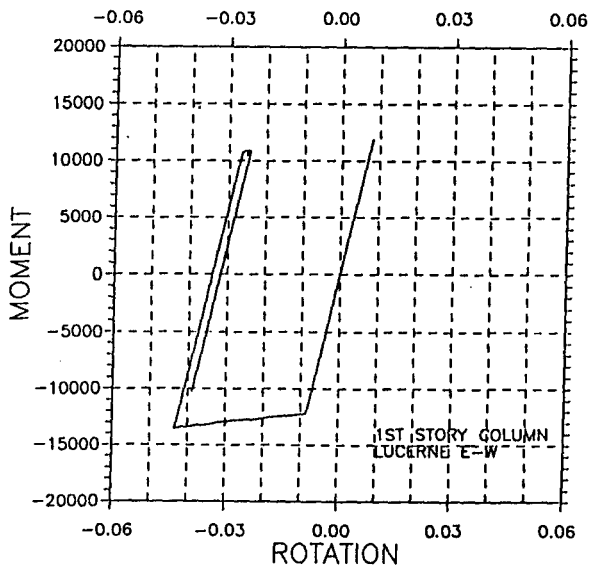
Figure 15 Plastic Hinge Locations, Six Story Building



(a) Joshua Tree

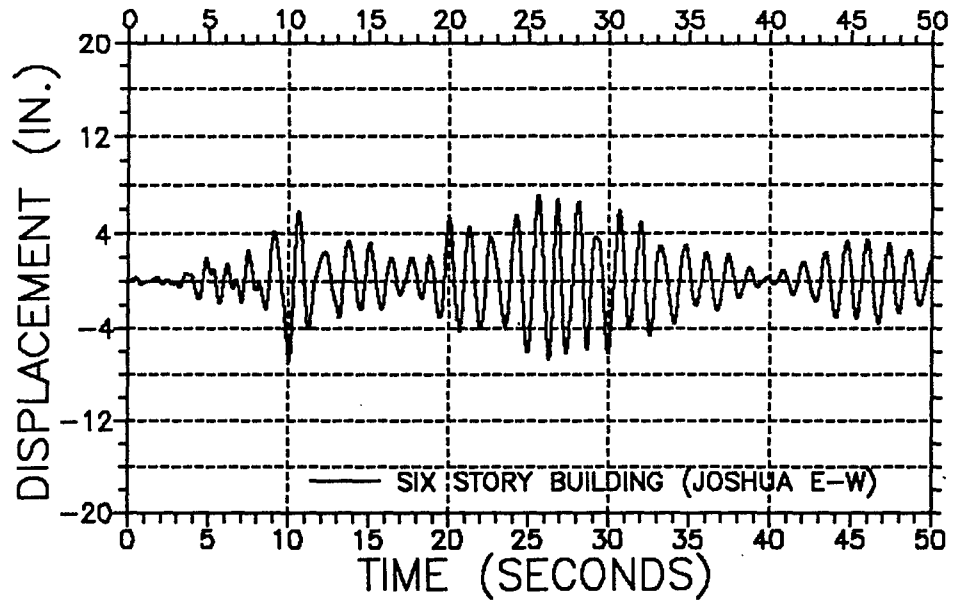


(b) Yermo

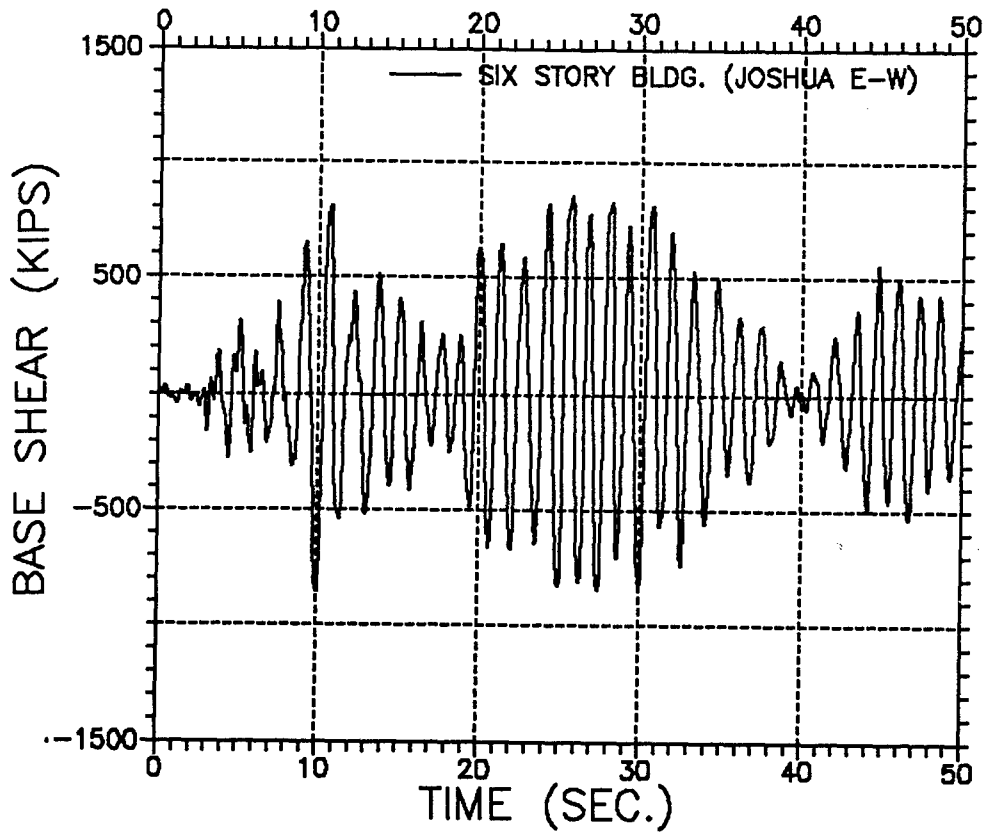


(c) Lucerne

Figure 16 Hysteretic Response, 1st Story Column

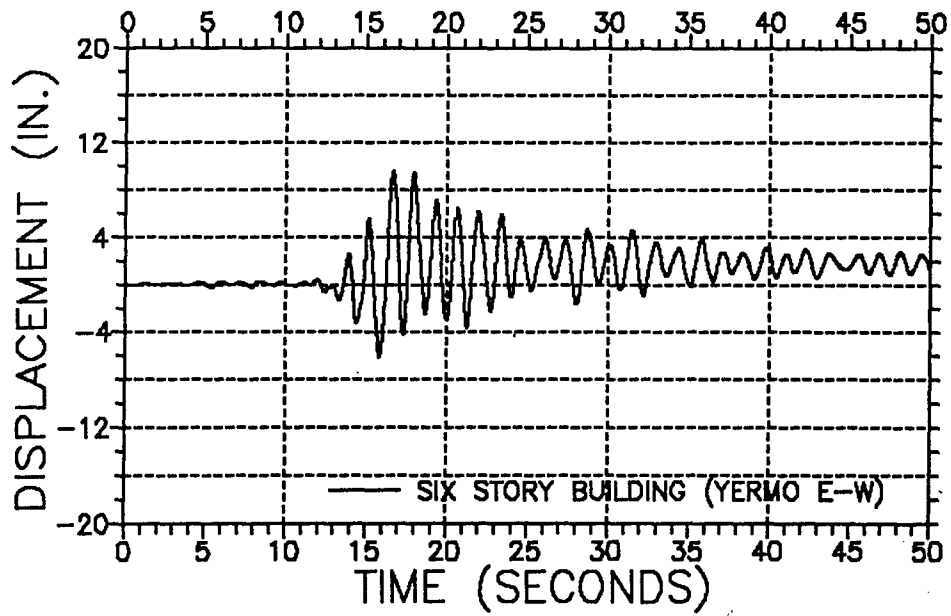


(a) Roof Displacement

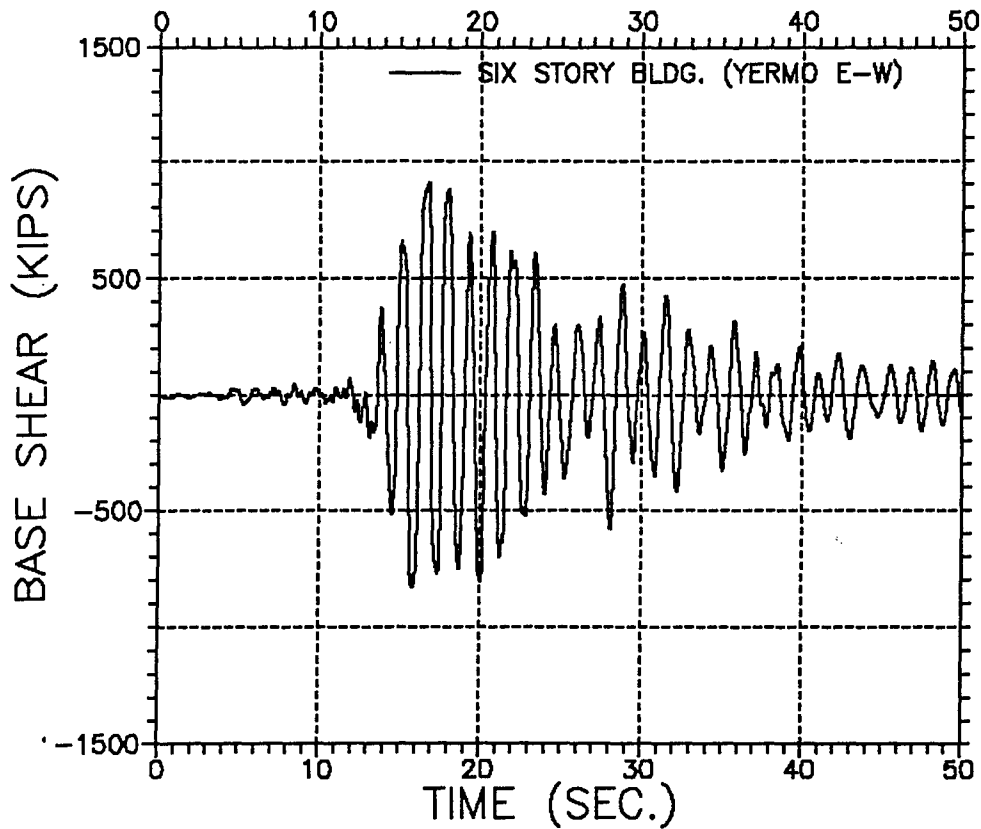


(b) Base Shear

Figure 17 Six Story Bldg. Response, Joshua Tree

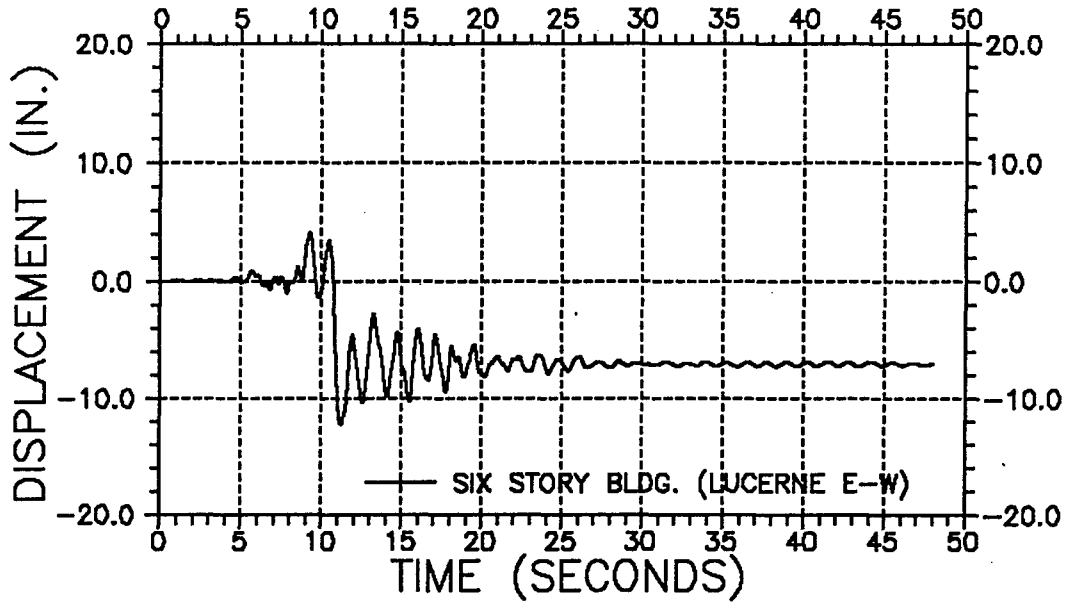


(a) Roof Displacement

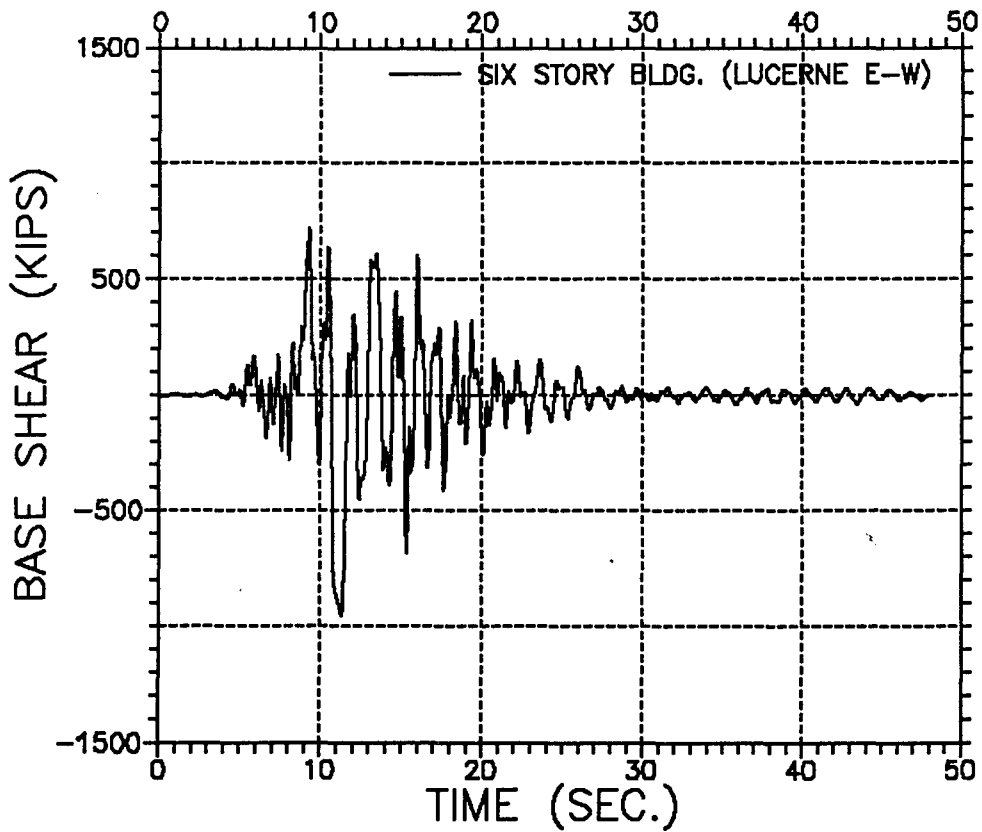


(b) Base Shear

Figure 18 Six Story Bldg. Response, Yermo



(a) Roof Displacement



(b) Base Shear

Figure 19 Six Story Bldg. Response, Lucerne

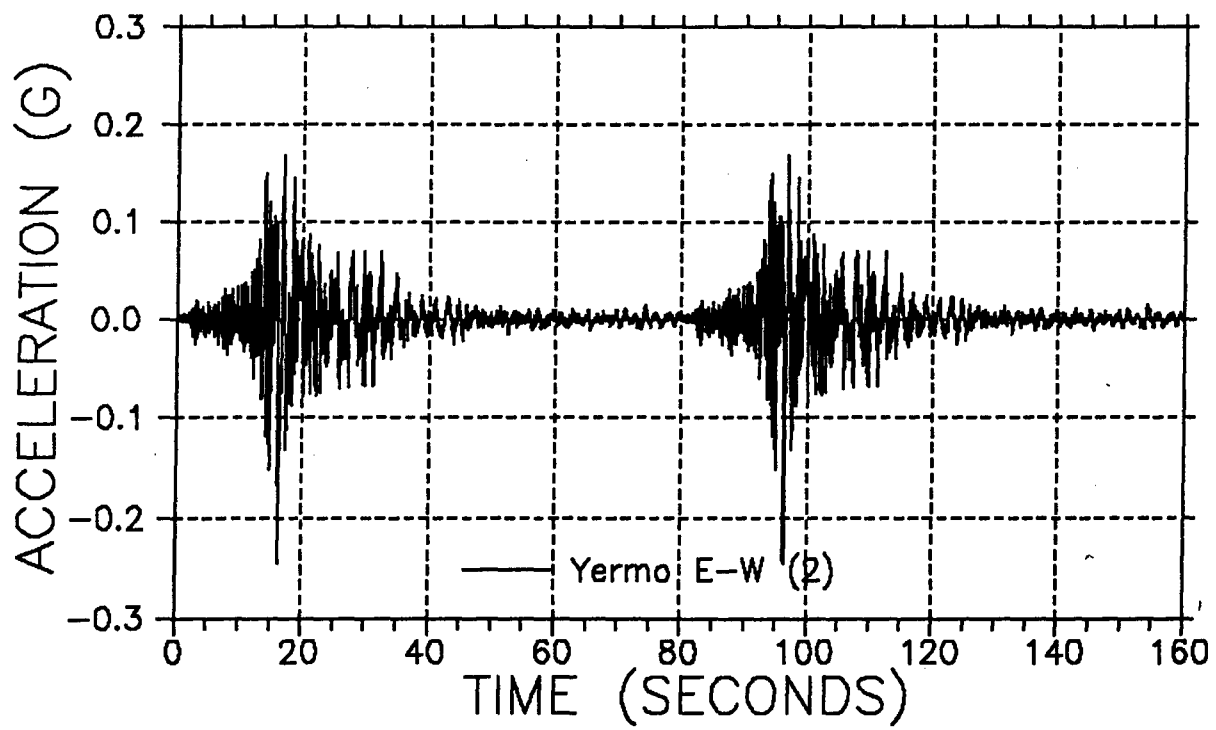
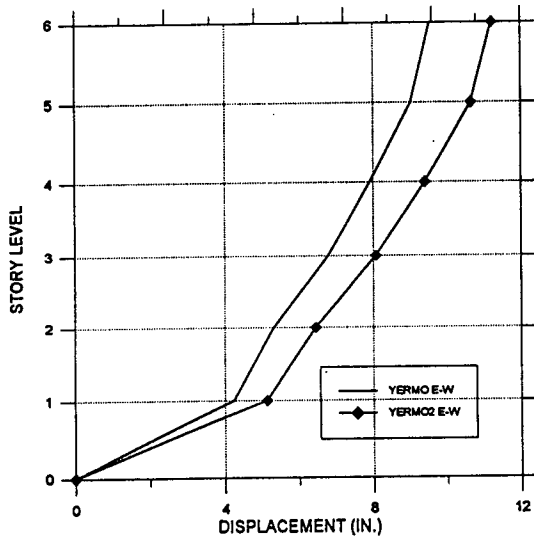
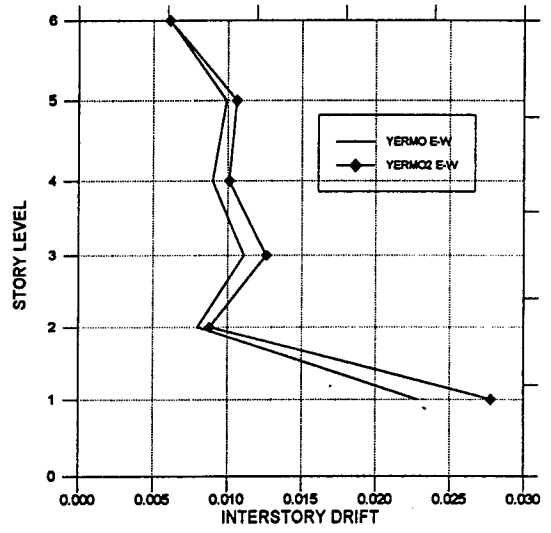


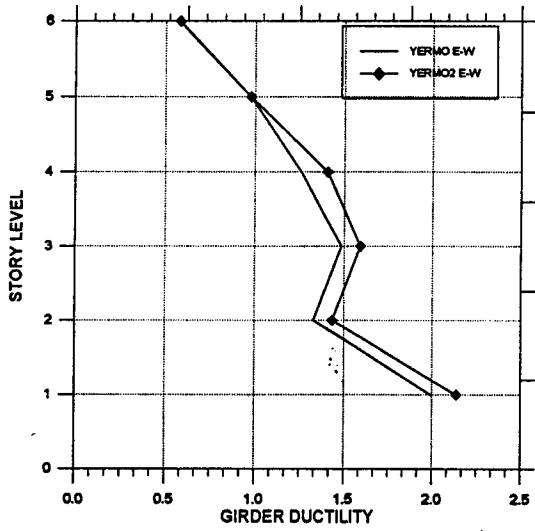
Figure 20 Combined Yermo Ground Motions



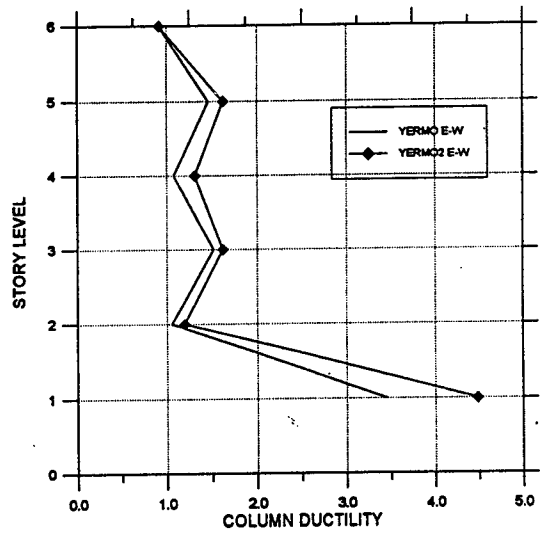
(a) Lateral Displacement



(b) Interstory Drift Index



(c) Girder Ductility Demand



(d) Column Ductility Demand

Figure 21 Inelastic Response, Six Story Building, Yermo x 2

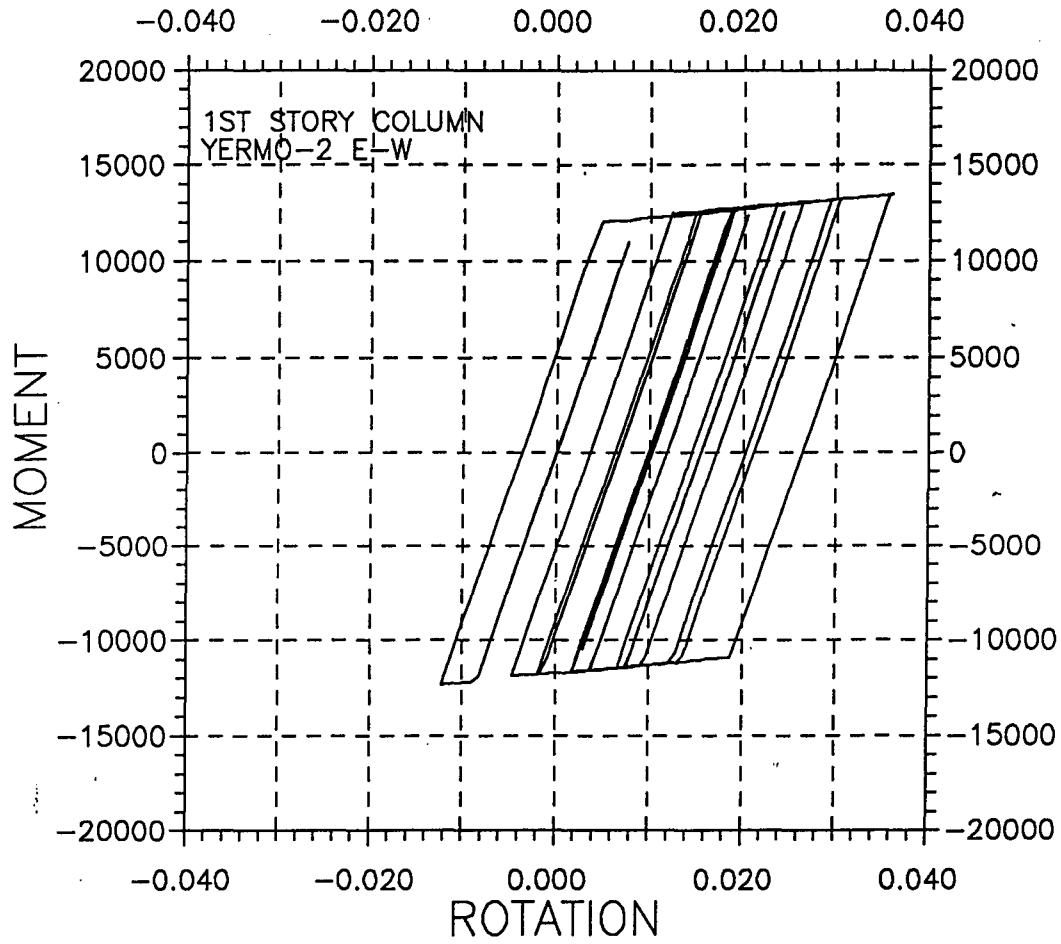
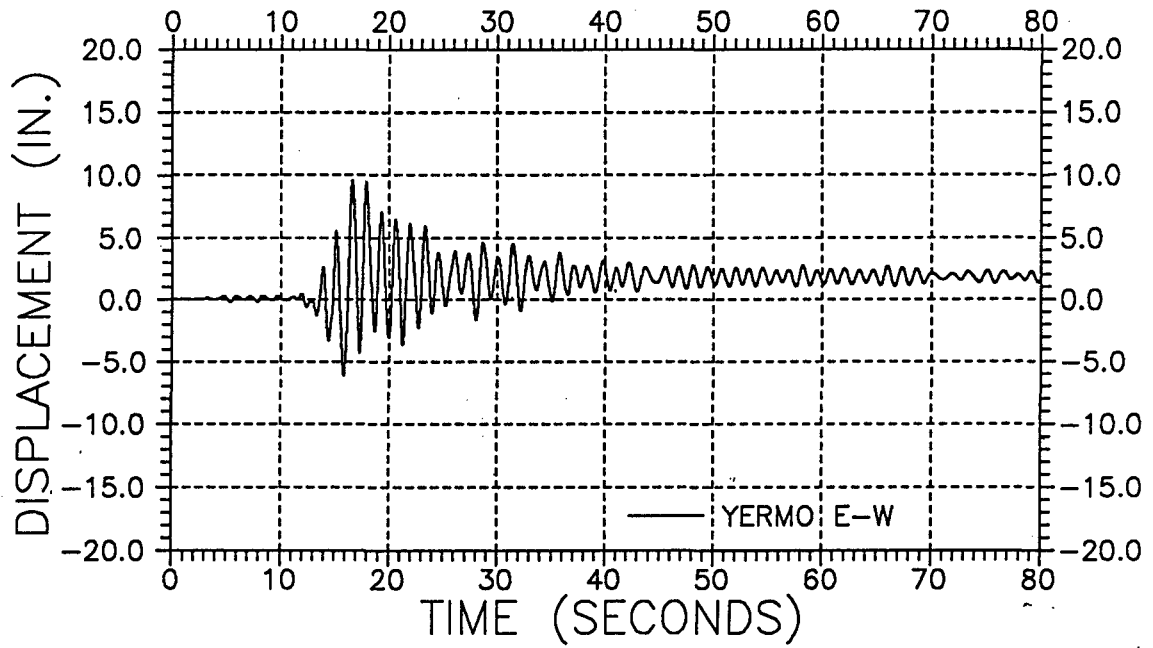
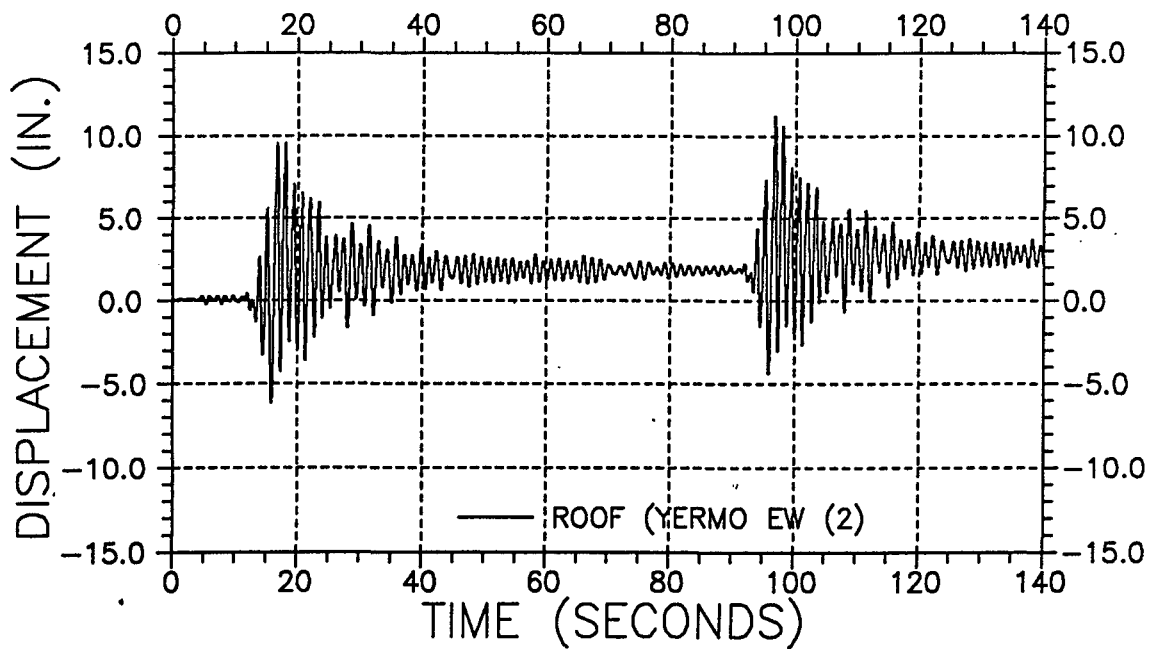


Figure 22 Hysteretic Response,
Six Story Building, Yermo x2

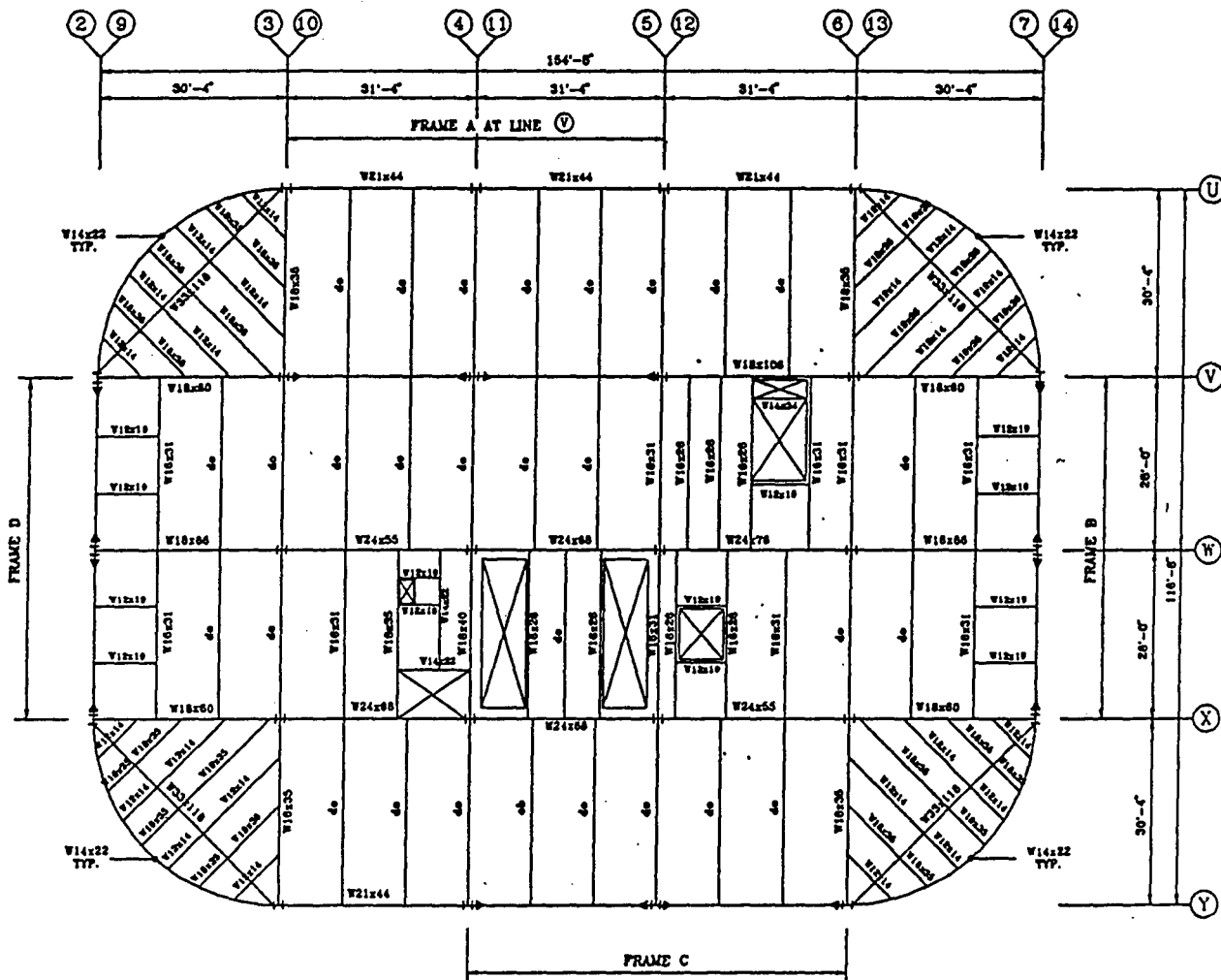


(a) Yermo (E-W)



(b) Yermo2 (E-W)

Figure 23 Roof Displacement, Six Story Building



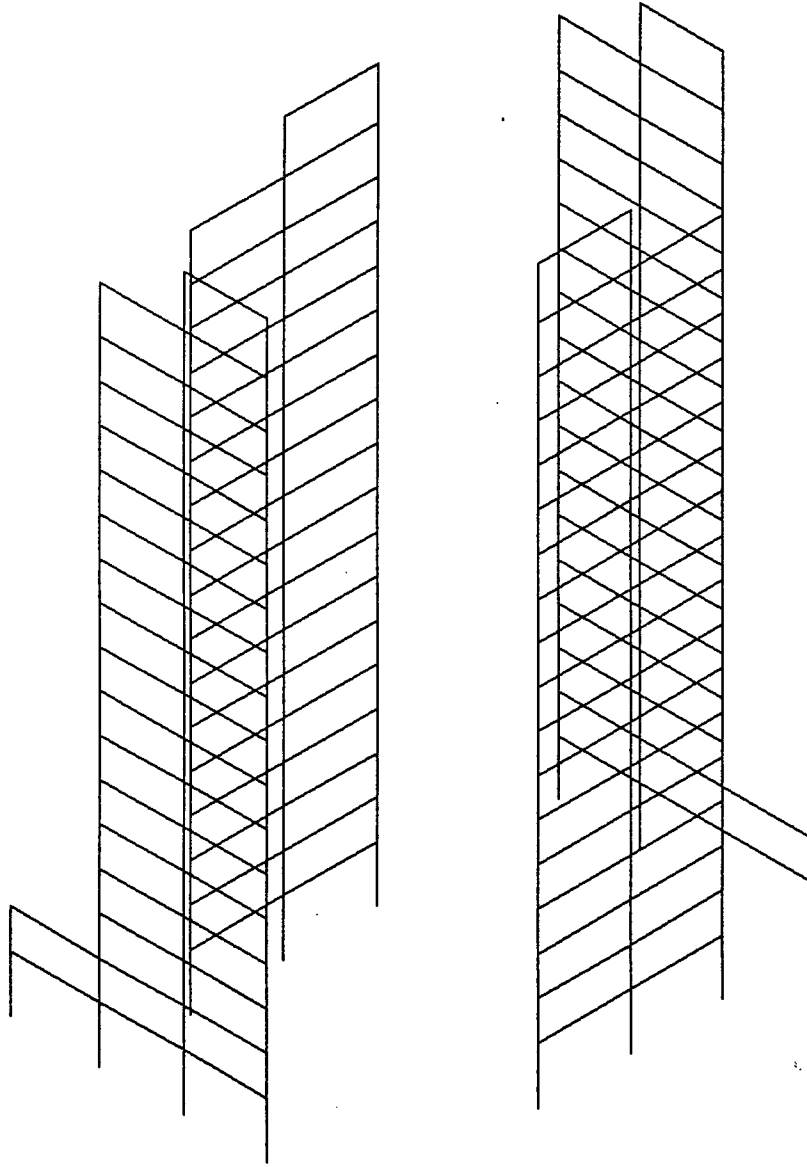
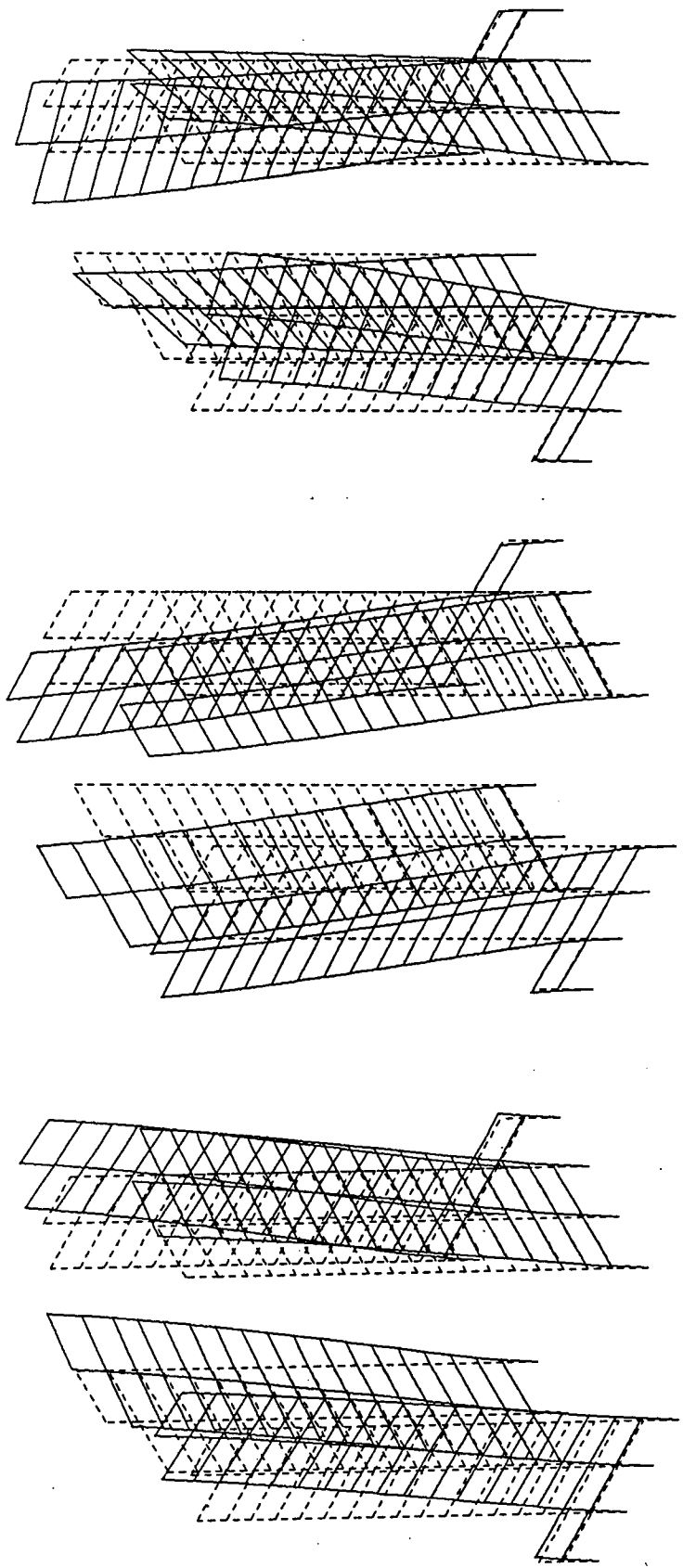
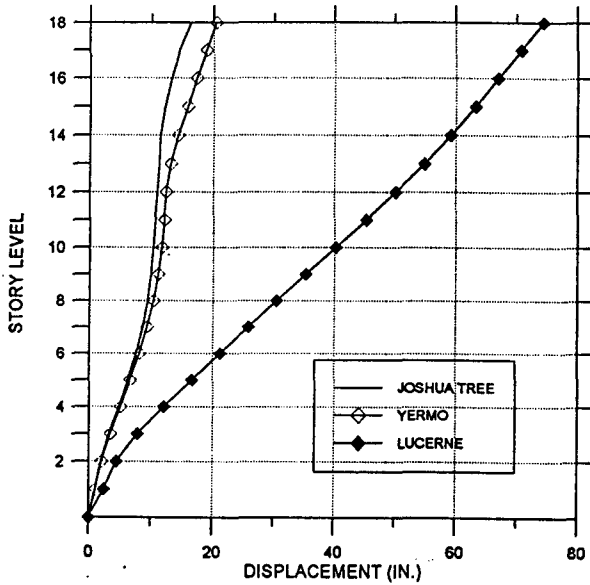


Figure 25 Elastic Dynamic Model, Canoga Building

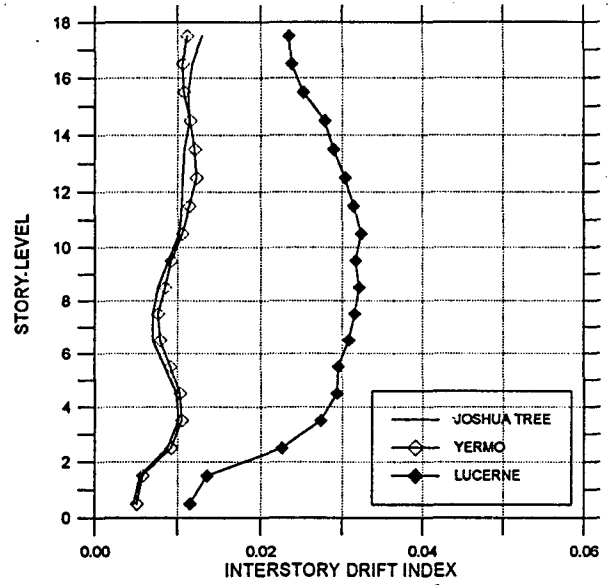


(a) Mode 1, $T = 4.12$ Sec (b) Mode 2, $T = 3.85$ Sec (c) Mode 3, $T = 2.17$ Sec

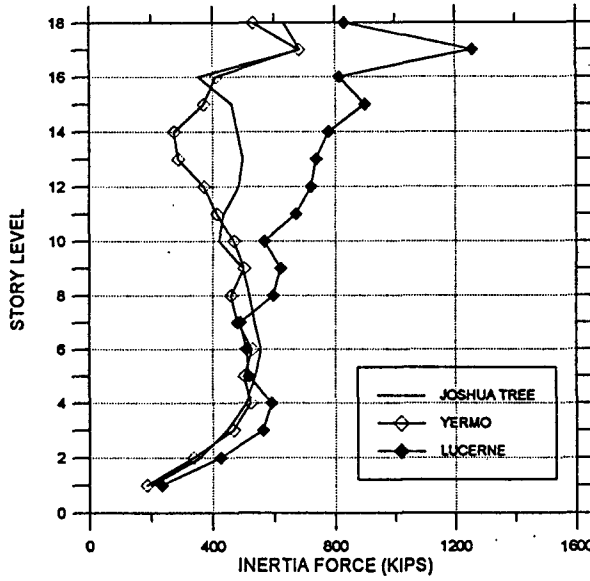
Figure 26 Calculated Mode Shapes, Canoga Building



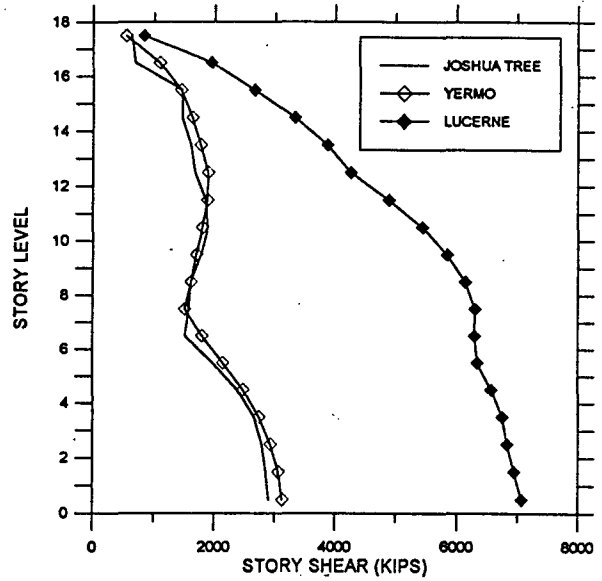
(a) Lateral Displacement



(b) Interstory Drift Index

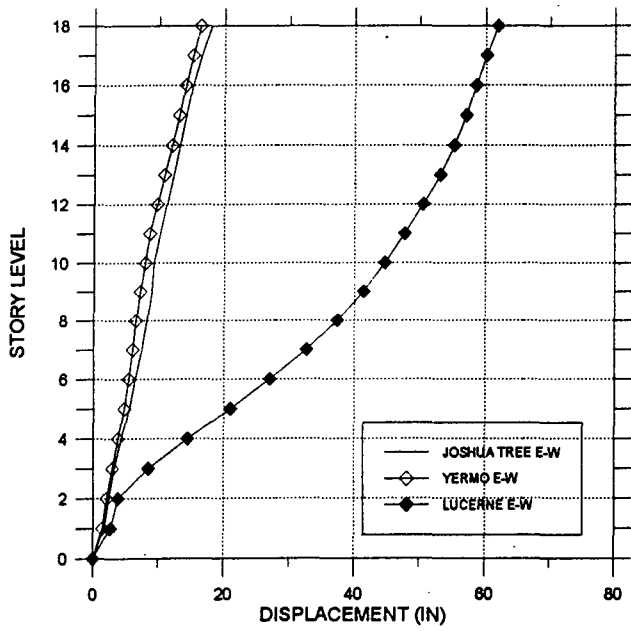


(c) Inertia Forces

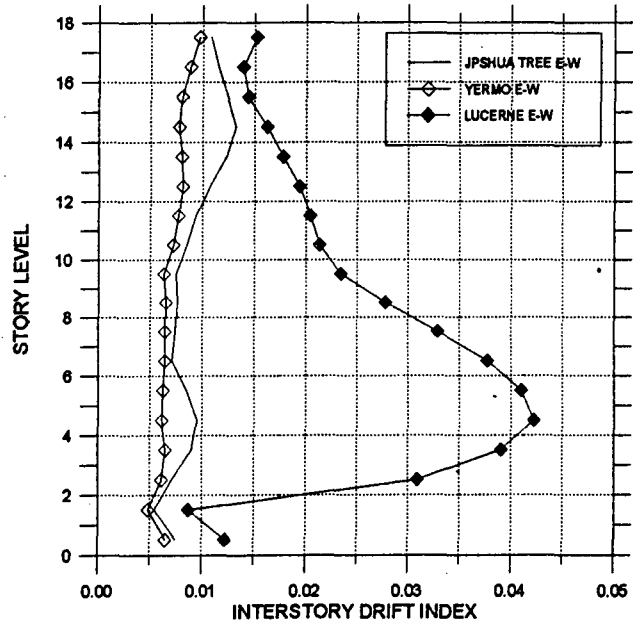


(d) Story Shears

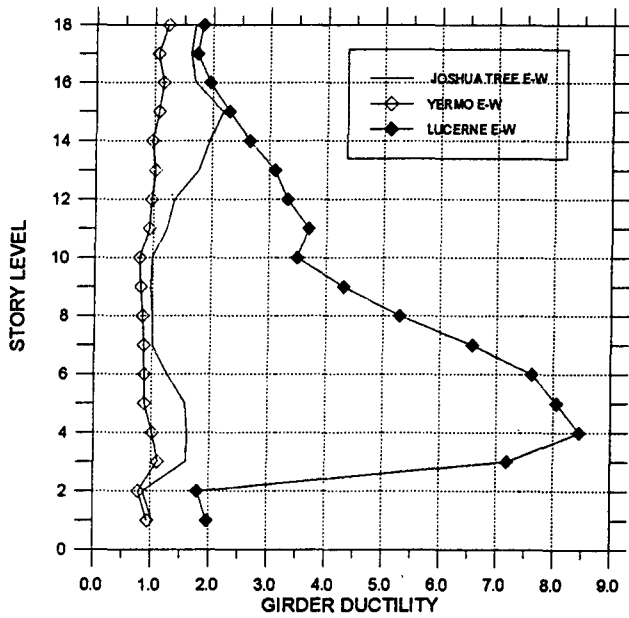
Figure 27 Maximum Elastic Response, Canoga Building



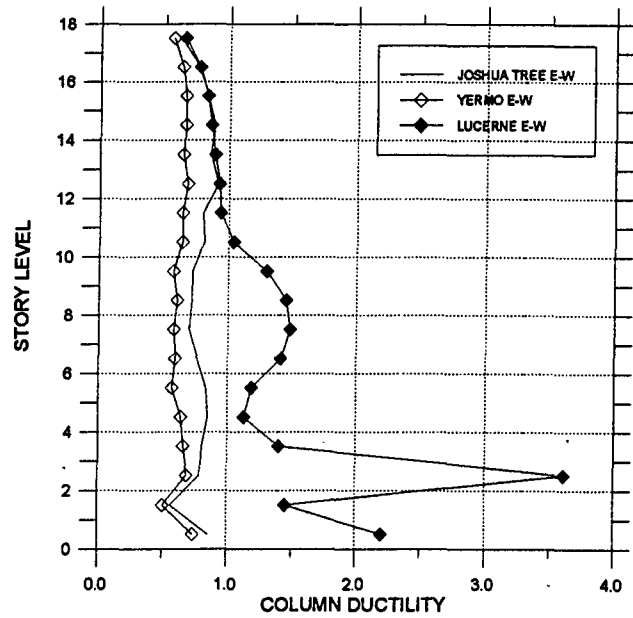
(a) Lateral Displacement



(b) Interstory Drift Index

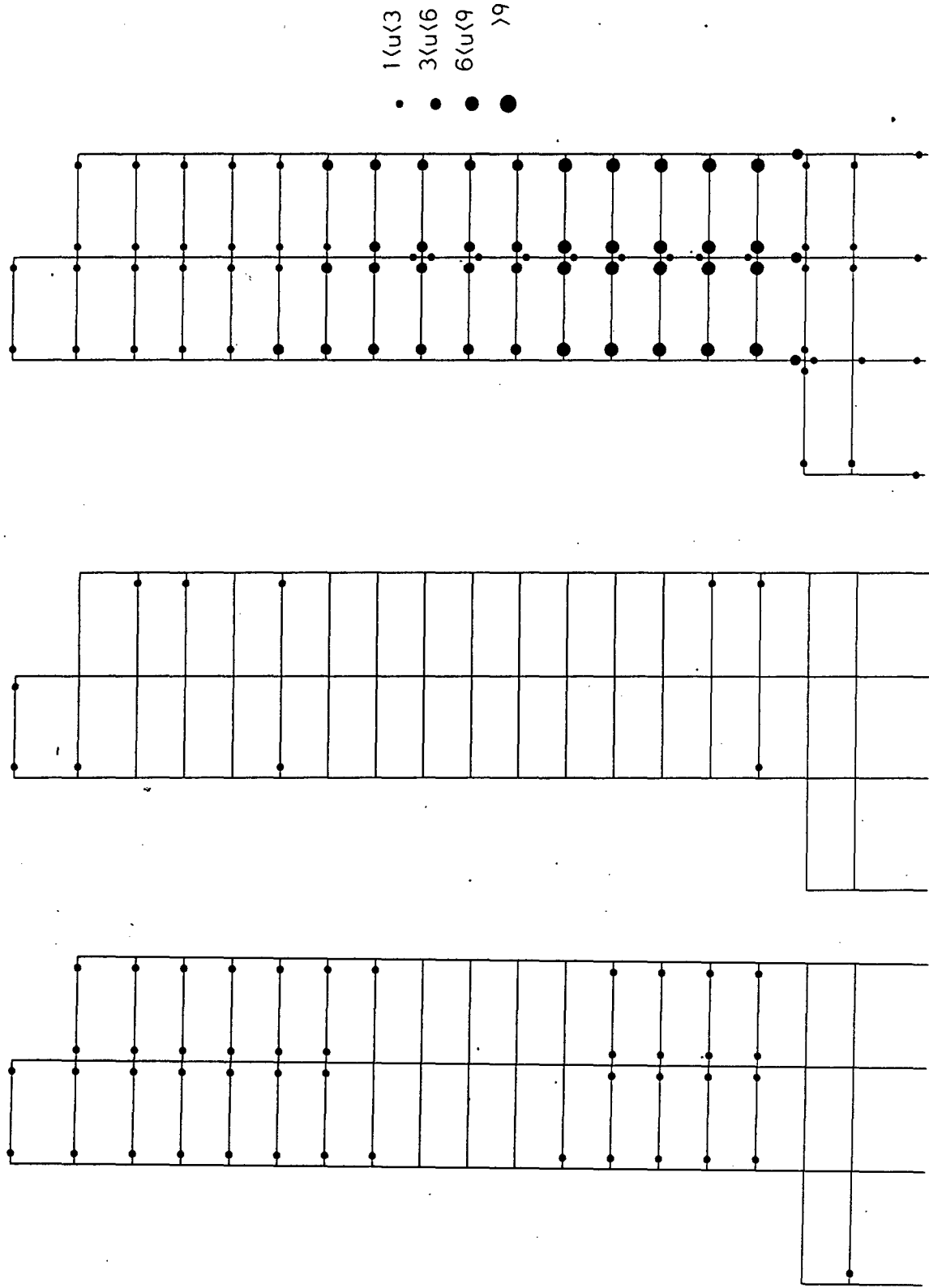


(c) Girder Ductility Demand



(d) Column Ductility Demand

Figure 30 Maximum Inelastic Response, Canoga Building

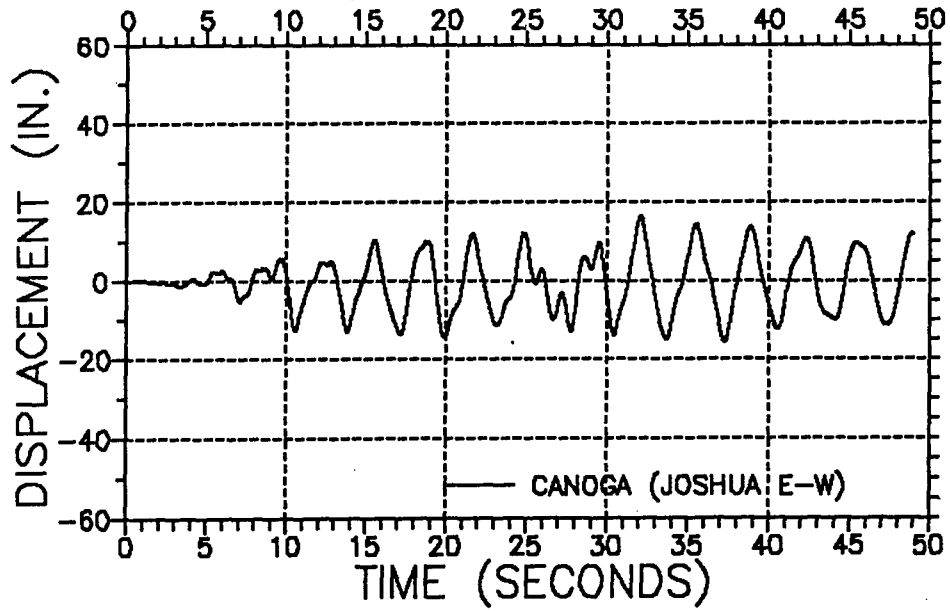


(a) Joshua Tree

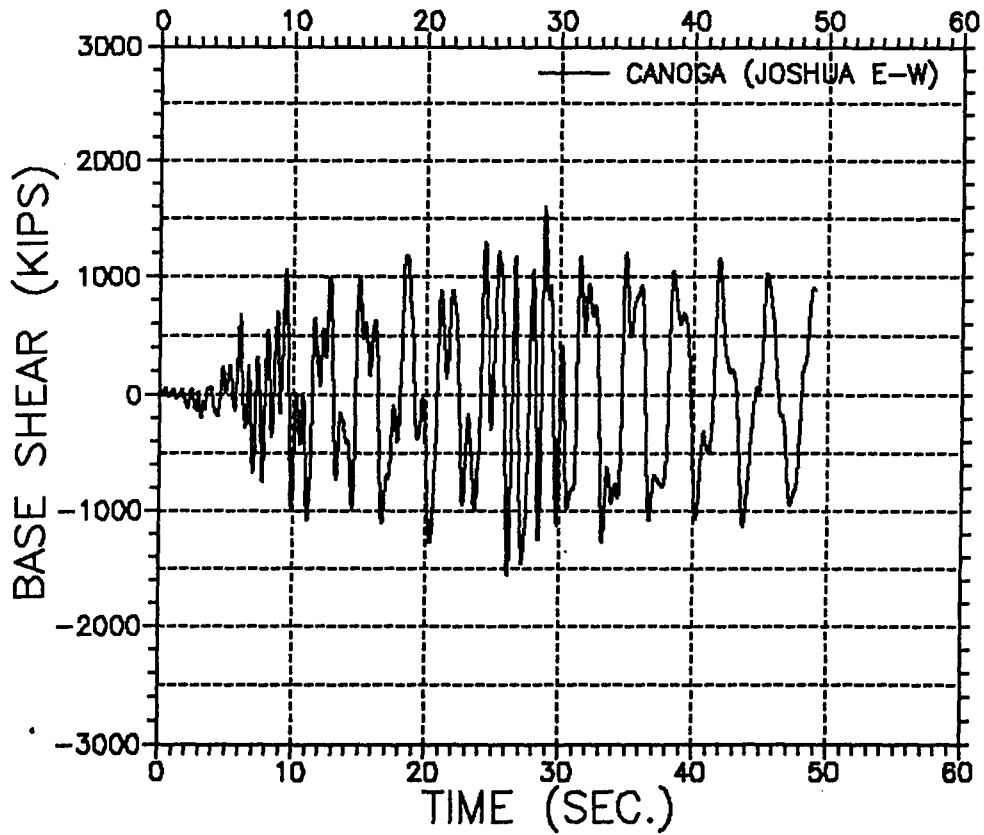
(b) Yermo

(c) Lucerne

Figure 31 Plastic Hinge Locations, Canoga Building

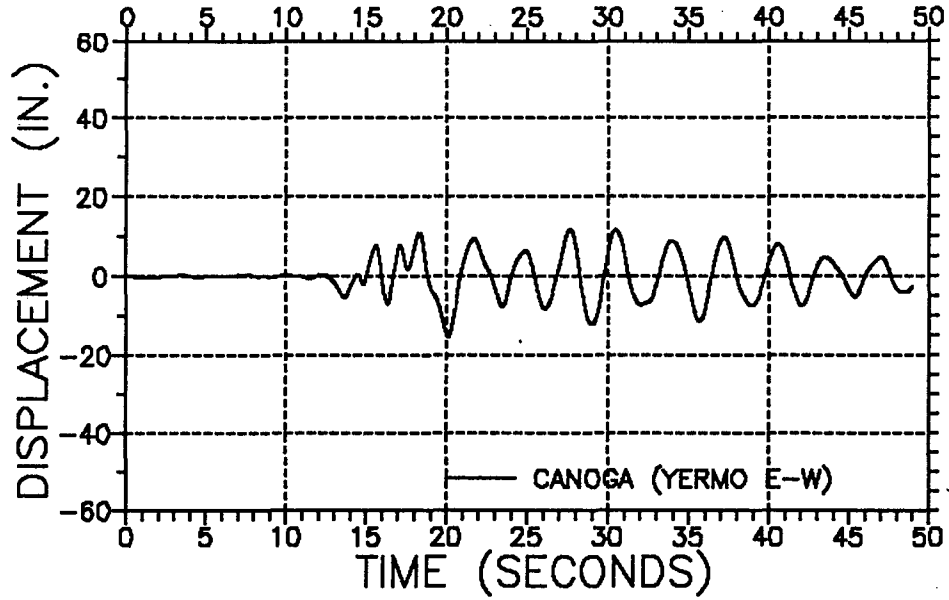


(a) Roof Displacement

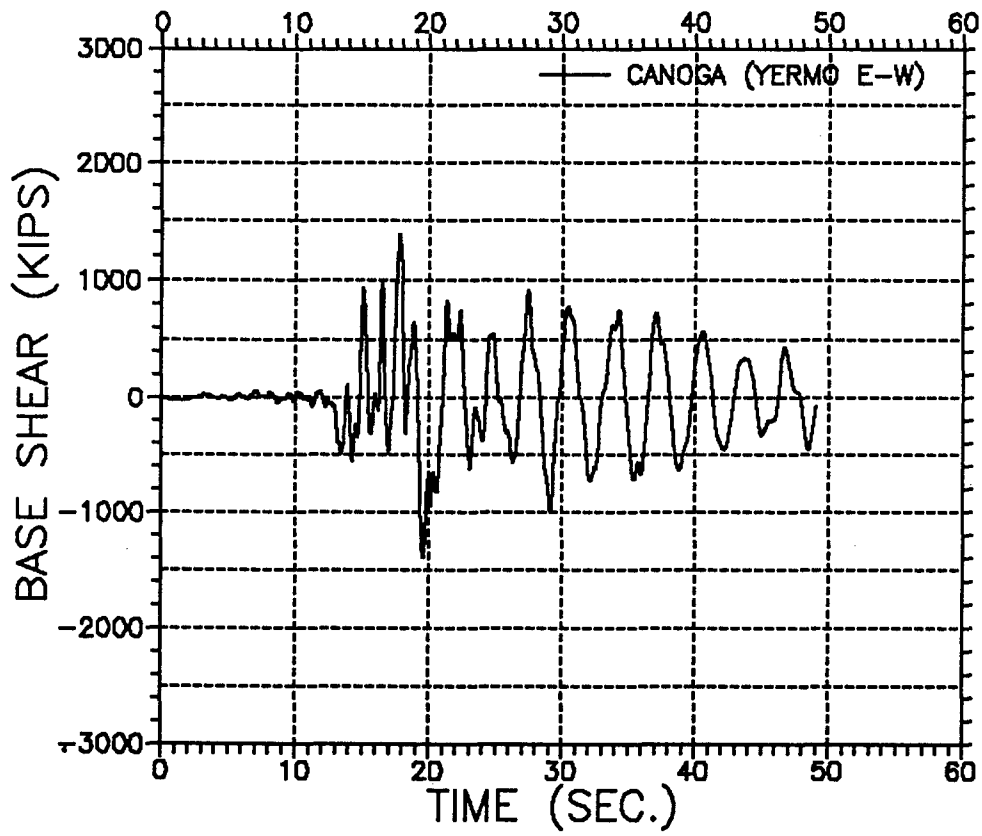


(b) Base Shear

Figure 32 Canoga Bldg. Response, Joshua Tree

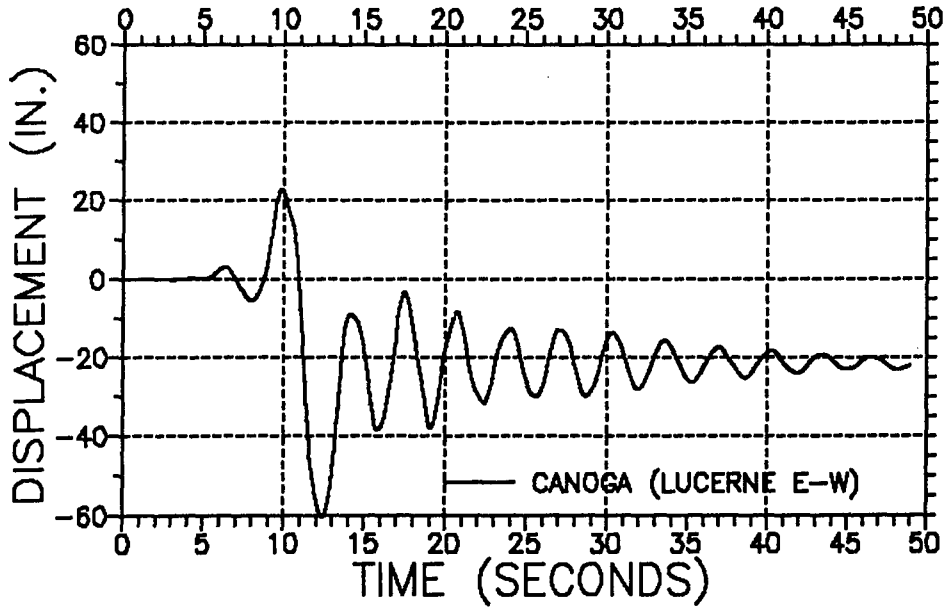


(a) Roof Displacement

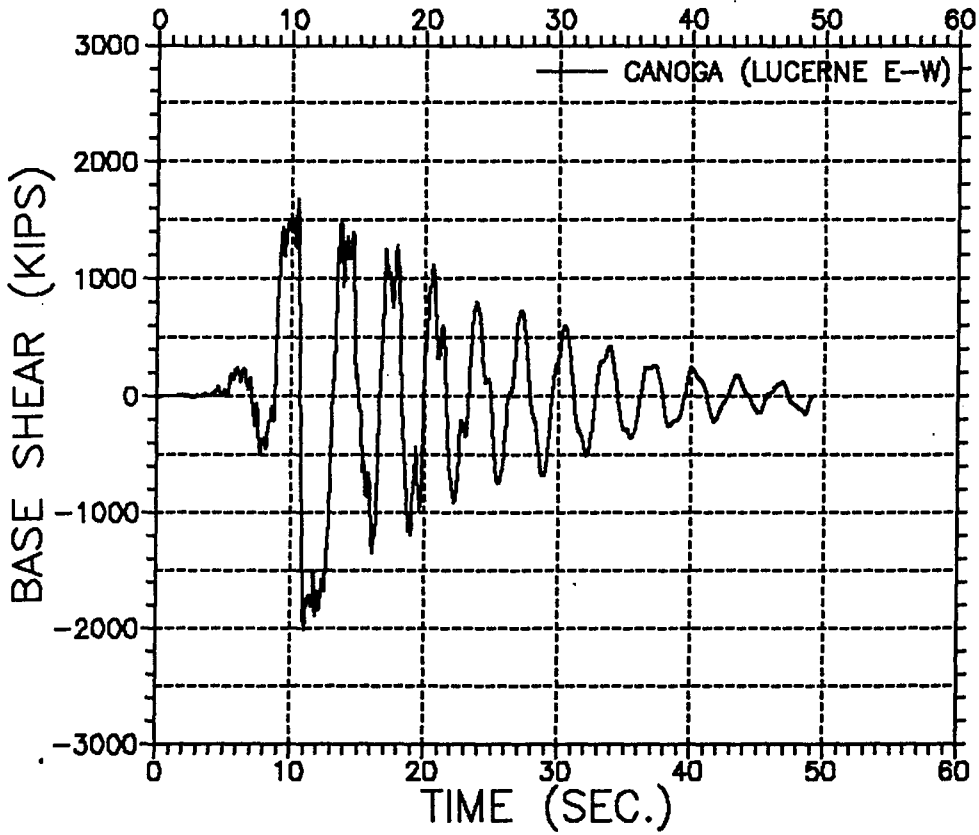


(b) Base Shear

Figure 33 Canoga Bldg. Response, Yermo



(a) Roof Displacement



(b) Base Shear

Figure 34 Canoga Bldg. Response, Lucerne

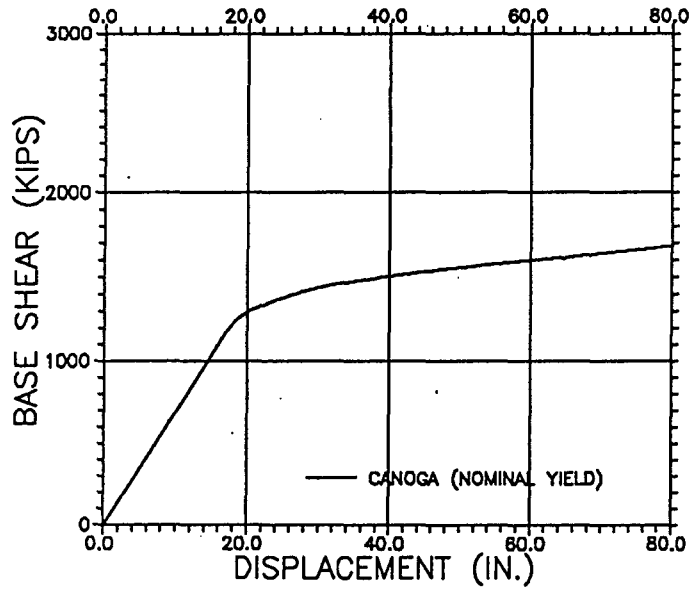


Figure 35 Pushover Analysis, Canoga Building

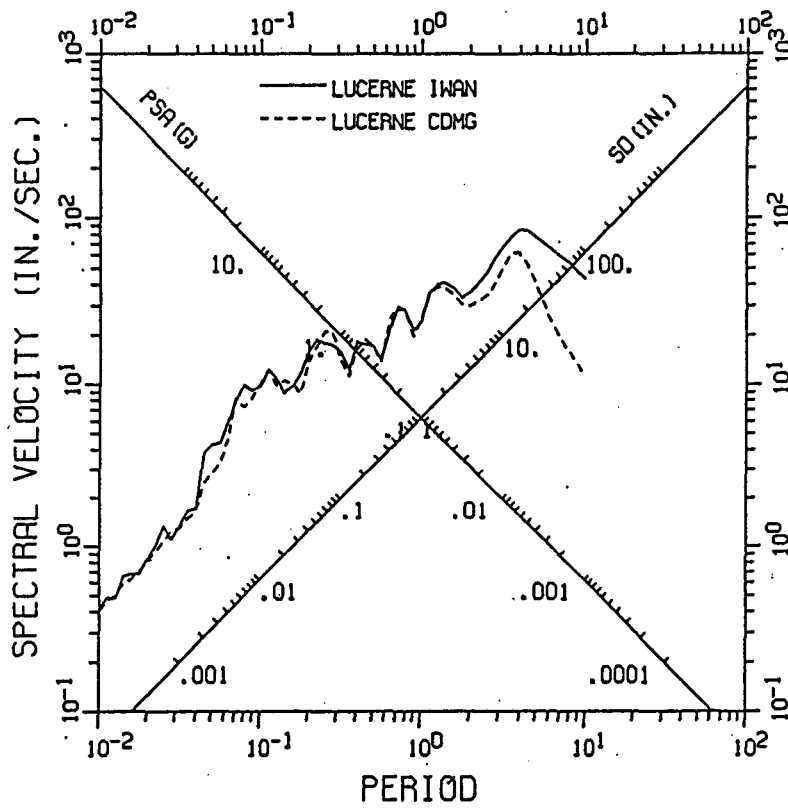


Figure 36 Comparison of Lucerne Record Processing

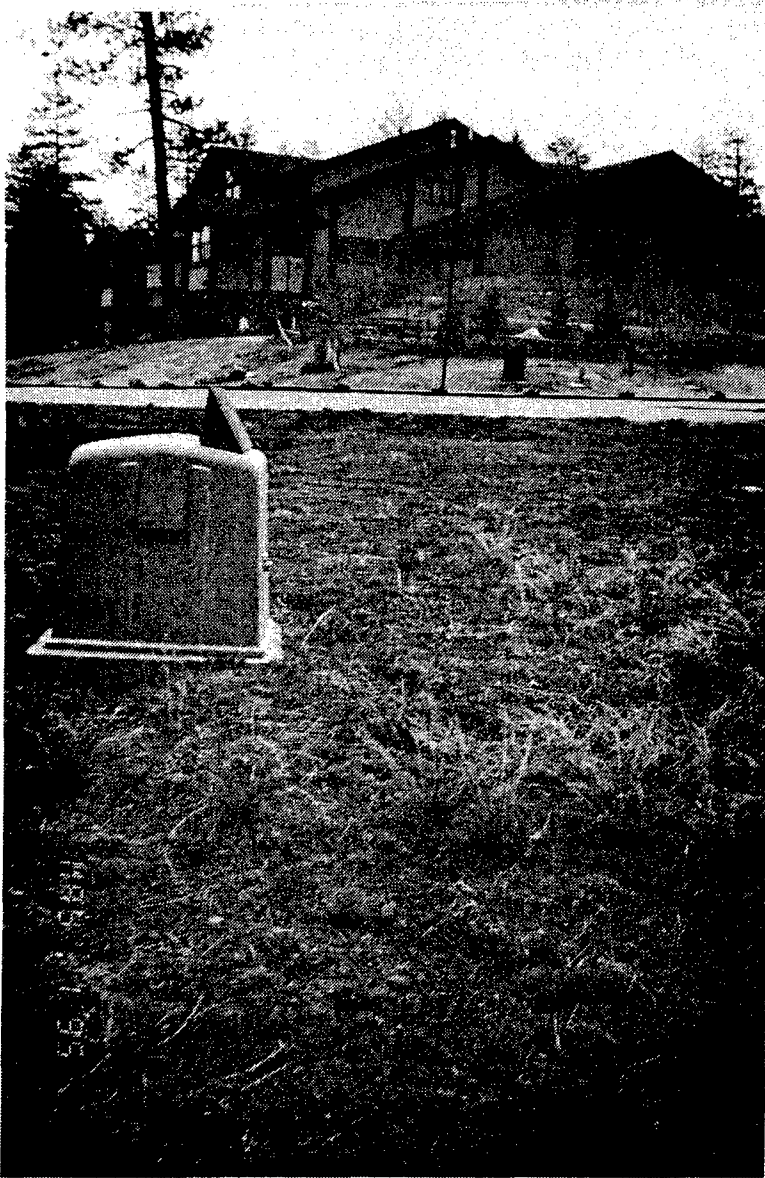


Figure 37. Big Bear Civic Center Recording Instrument

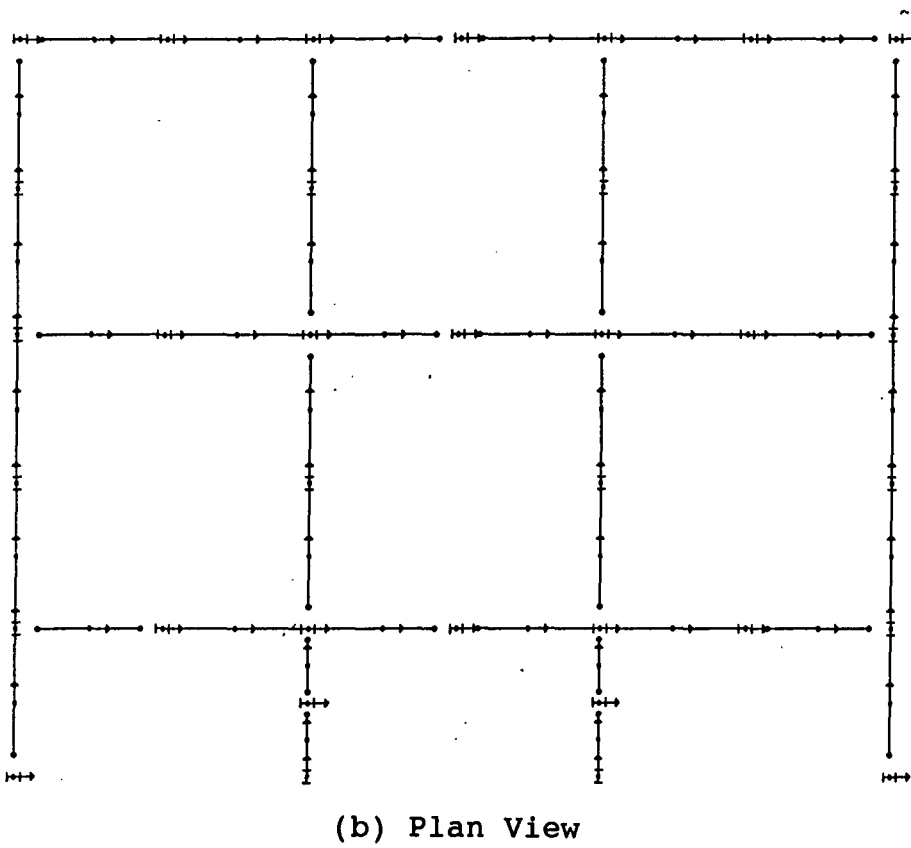
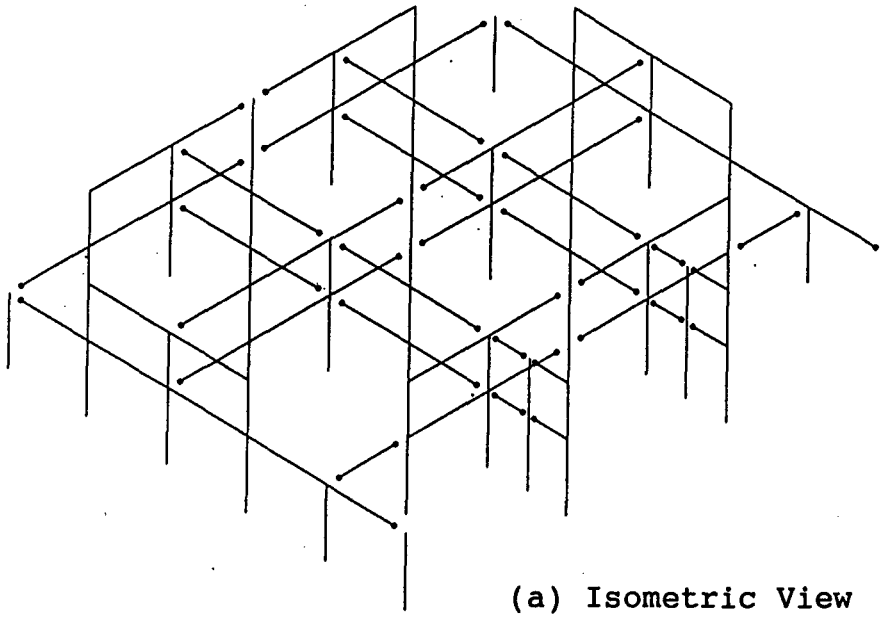
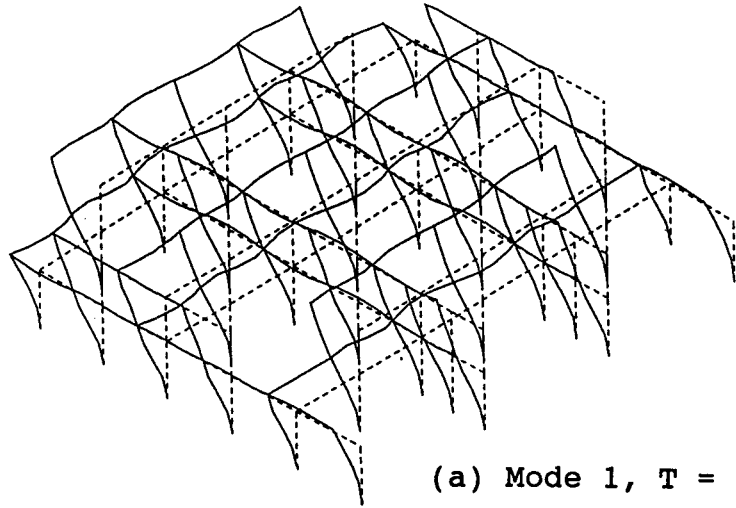
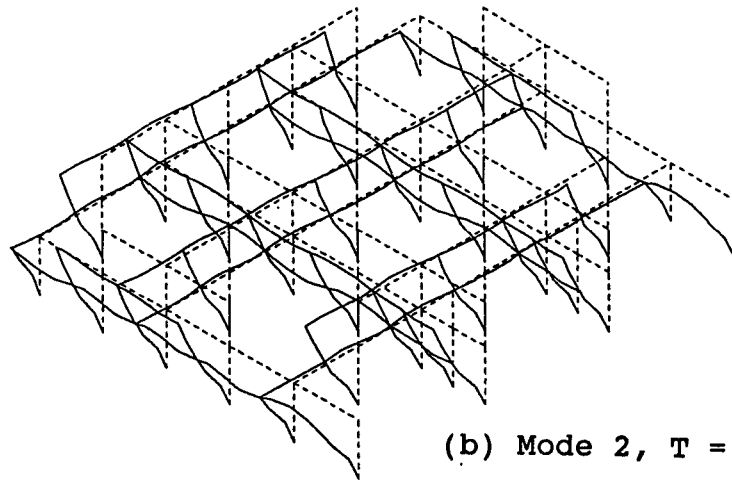


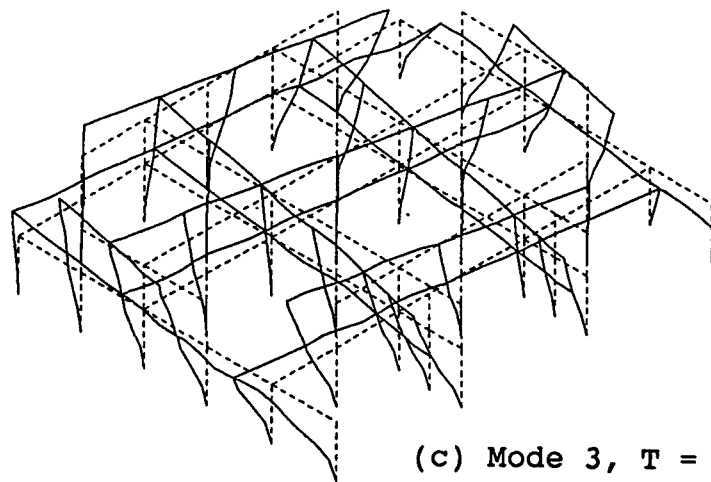
Figure 39 Elastic Response Model, Big Bear Civic Center



(a) Mode 1, $T = 0.45$ Sec

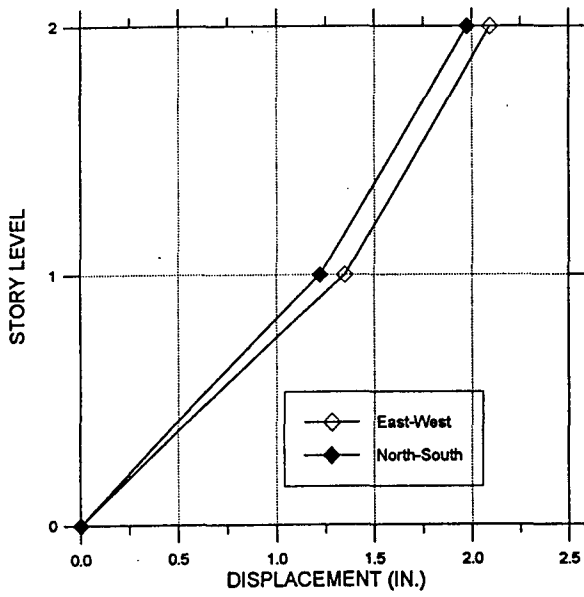


(b) Mode 2, $T = 0.40$ Sec

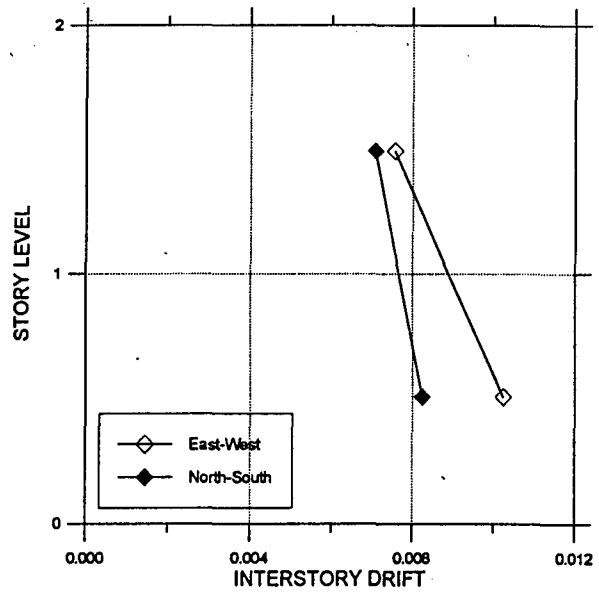


(c) Mode 3, $T = 0.34$ Sec

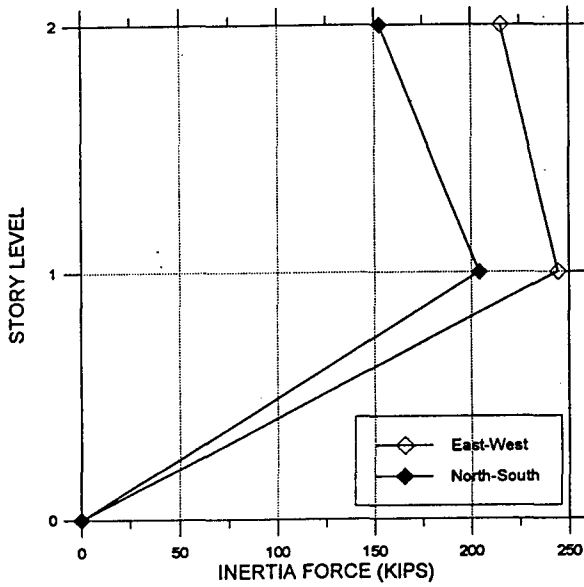
Figure 40 Calculated Mode Shapes, Big Bear Civic Center



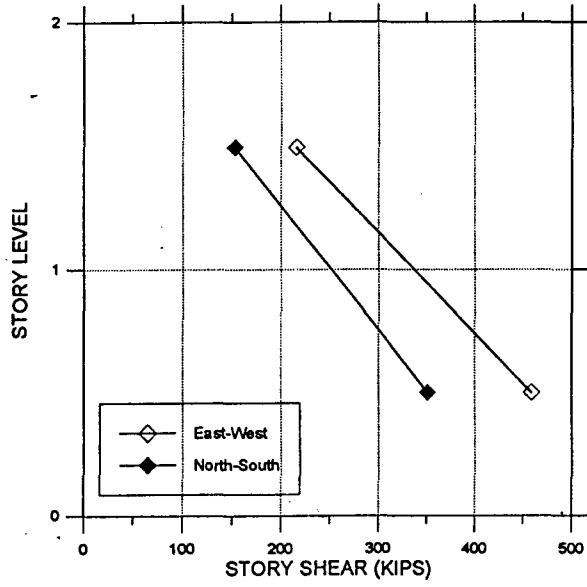
(a) Lateral Displacement



(b) Interstory Drift Index



(c) Inertia Forces



(d) Story Shears

Figure 41 Maximum Elastic Response, Big Bear Civic Center

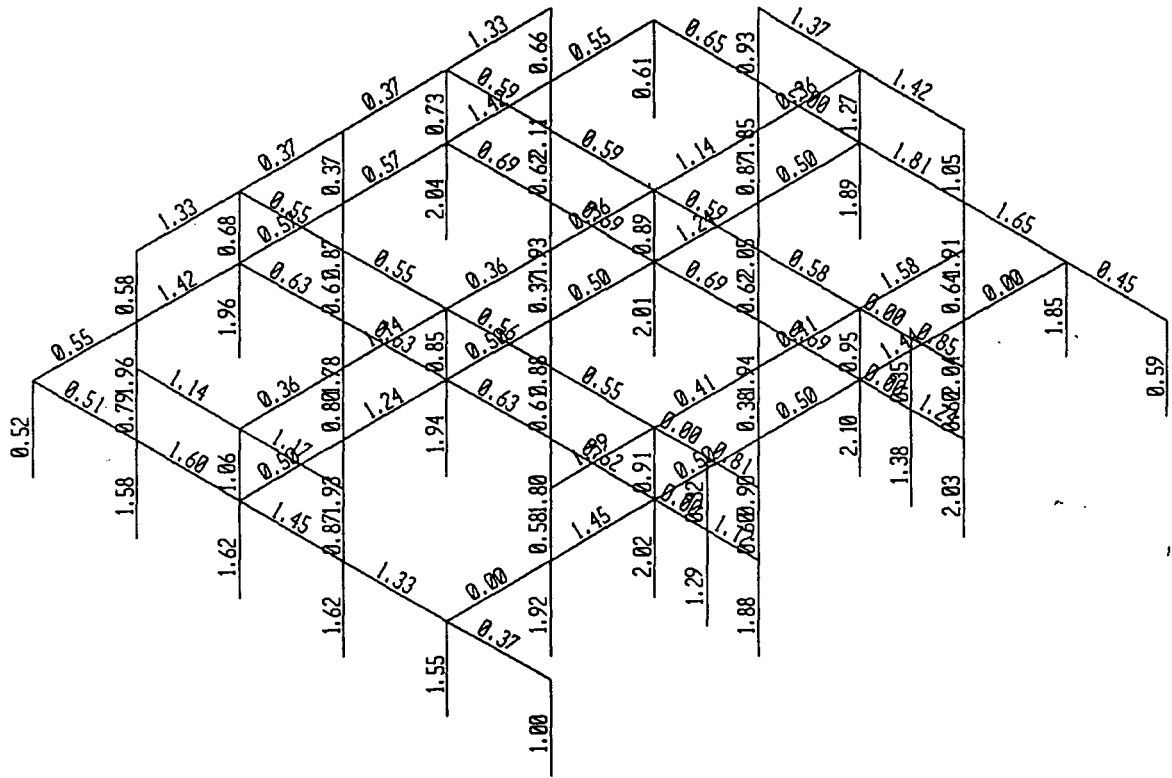
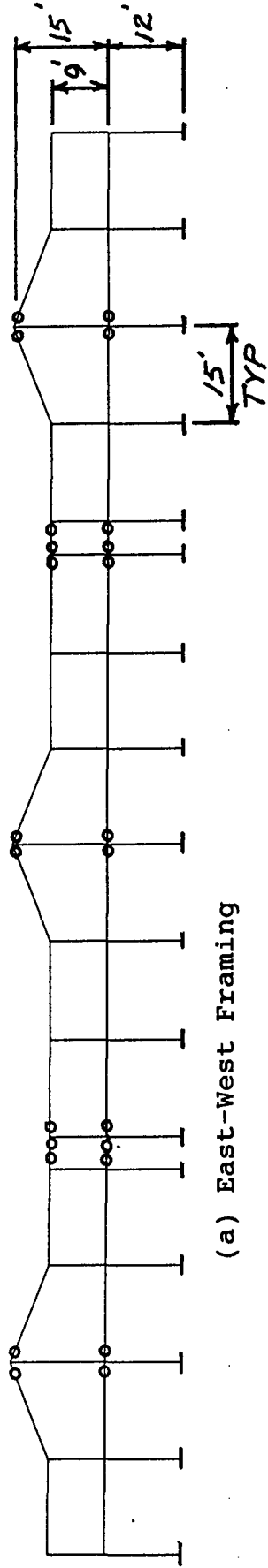
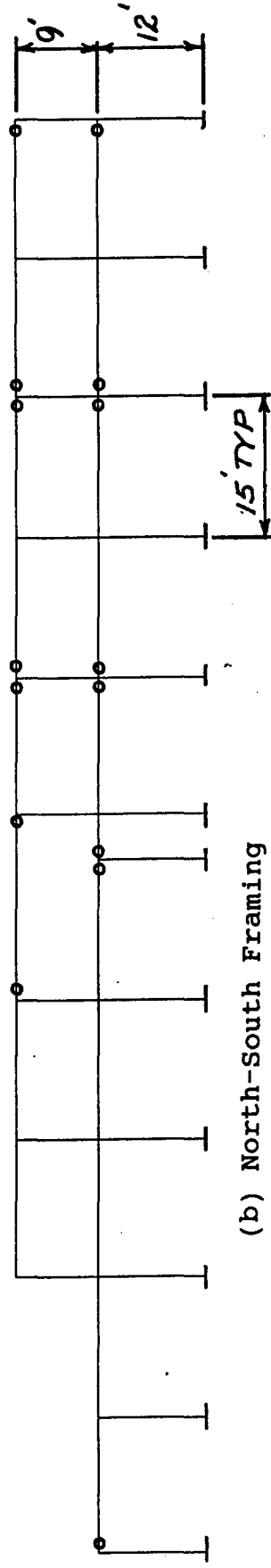


Figure 42 Stress Ratios, LRFD, Big Bear Civic Center



(a) East-West Framing



(b) North-South Framing

Figure 43 Nonlinear 2D Models, Big Bear Civic Center

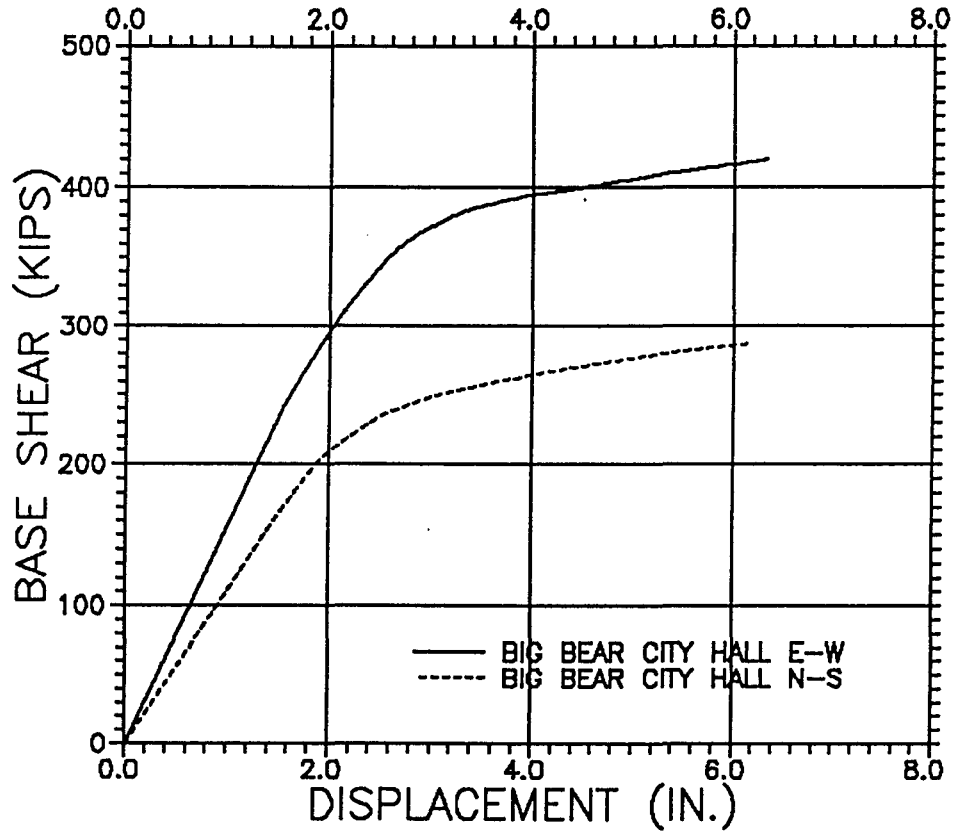
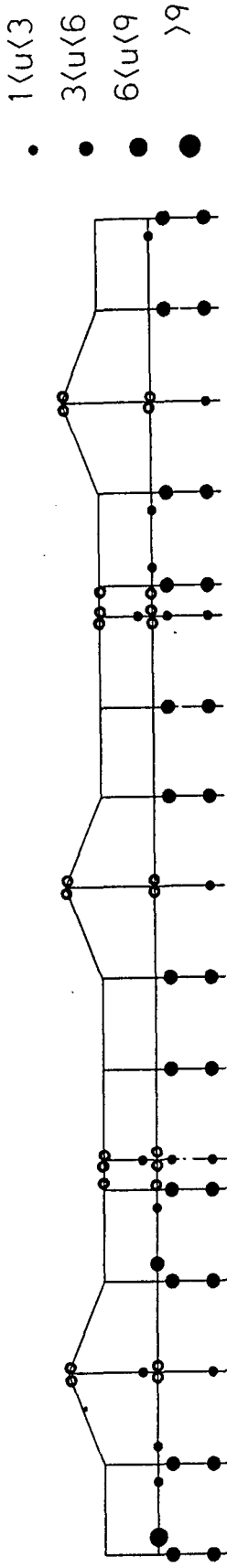
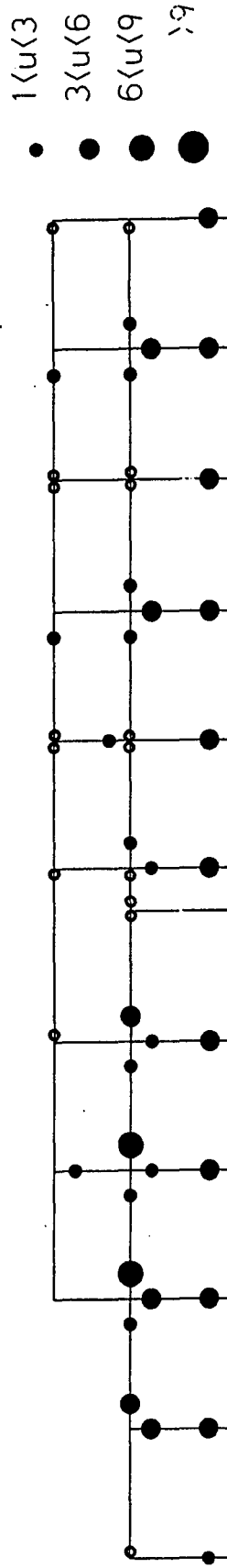


Figure 44 Pushover Analysis, Big Bear Civic Center

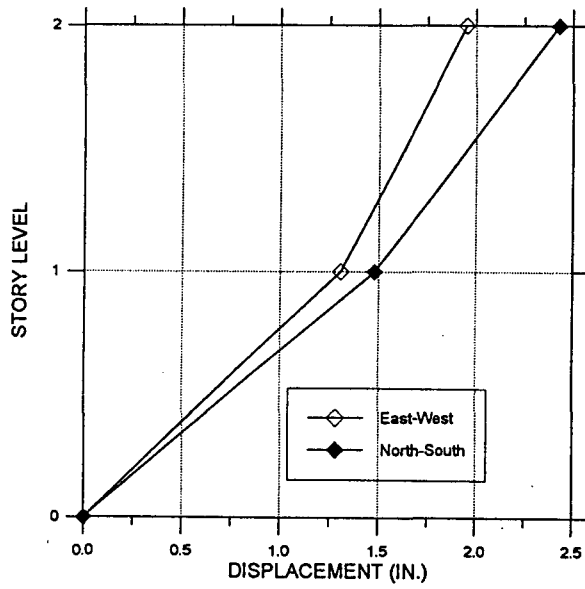


(a) E-W Frames

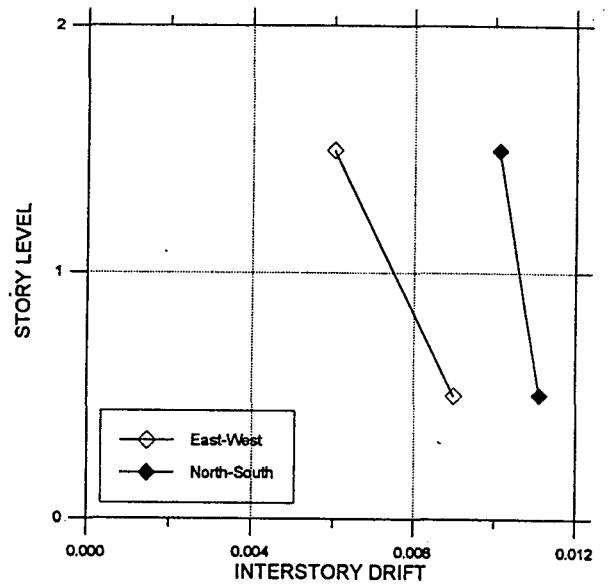


(b) N-S Frames

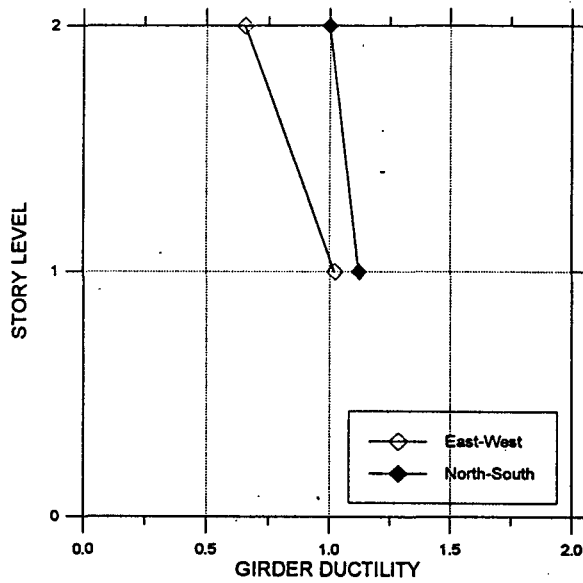
Figure 45 Plastic Hinge Locations, Pushover



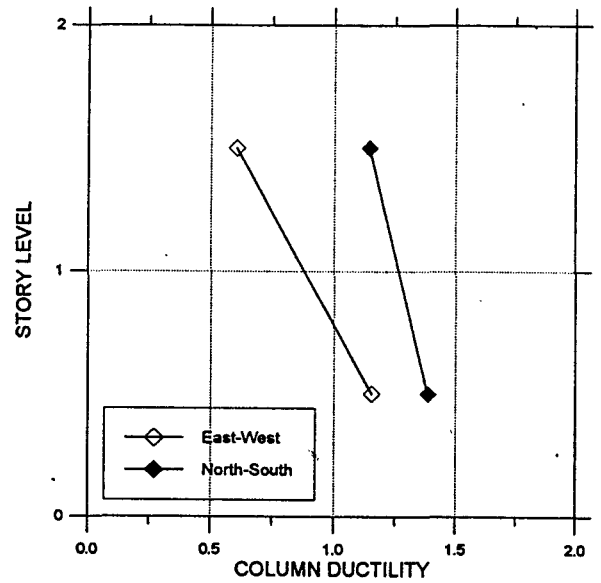
(a) Lateral Displacement



(b) Interstory Drift Index



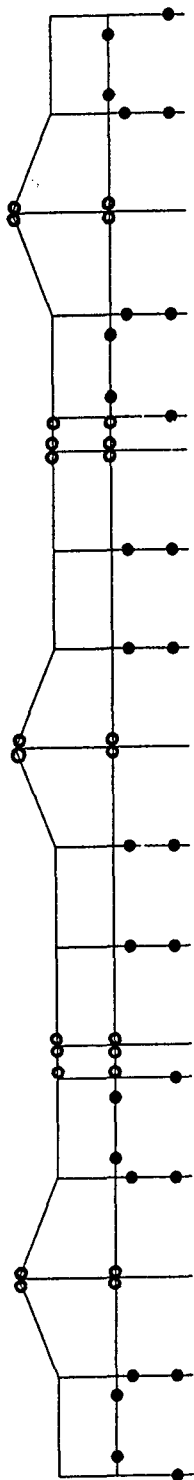
(c) Girder Ductility Demand



(d) Column Ductility Demand

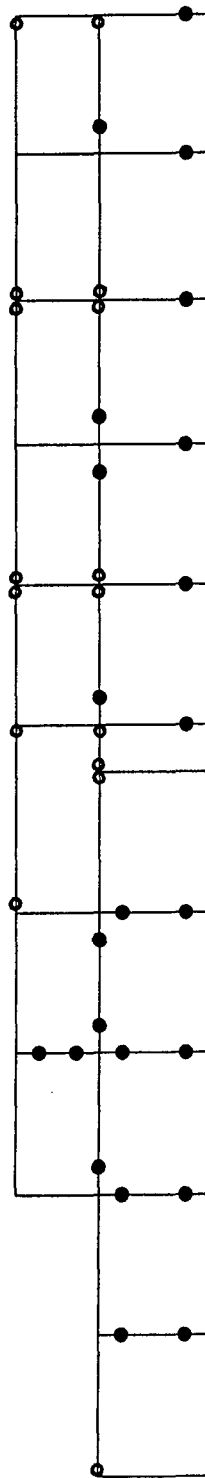
Figure 46 Maximum Inelastic Response, Big Bear Civic Center

• 1<u>3
 • 3<u>6
 • 6<u>9
 • >9



(a) East-West Framing

• 1<u>3
 • 3<u>6
 • 6<u>9
 • >9



(b) North-South Framing

Figure 47 Plastic Hinge Locations

REFERENCES

1. Jones, L., Mori, J. and Hauksson, E., "The Landers Earthquake: Preliminary Instrumental Results," *Earthquakes and Volcanoes*, Vol. 23, No. 5, 1992.
2. Shakal, A., et al., "CSMIP Strong-Motion Records From the Landers, California Earthquake of 28 June 1992, Report No. OSMS 92-09, California Dept. of Conservation, Sacramento, CA, Aug. 5, 1992.
3. Shakal, A. et al., "CSMIP Strong-Motion Records From the Big Bear, California Earthquake of 28 June 1992," Report No. OSMS 92-10, California Dept. of Conservation, Sacramento, CA, Aug. 21, 1992.
4. Somerville, P.G. and Graves R.W., "Ground Motions: Site Response and Near-Fault Effects," *Tall Building Structures, A World View*, 67th Regional Conference on Tall Building Structures, Chicago, Il, 1996.
5. Iwan, W.D. and Chen, X., "Important Near-Field Ground Motion Data From the Landers Earthquake," *Proceedings*, 10th European Conference on Earthquake Engineering, Rotterdam, 1995.
6. Anderson, J. C., and Bertero, V. V., "Seismic Performance of an Instrumented Six-Story Steel Building," Report No. UCB/EERC-91/11, Earthquake Engineering Research Center, University of California, Berkeley, CA, Nov. 1991.
7. International Conference of Building Officials, "Uniform Building Code," Whittier, CA, 1973.
8. Habibullah, A., "ETABS, Three Dimensional Analysis of Building Systems," Computers and Structures, Inc., Berkeley, CA, August, 1992.
9. Anderson, J. C. and Bertero, V. V., "Lessons Learned From Instrumented Building Response," *Proceedings*, 1993 National Earthquake Conference, Vol. 2, Memphis, Tennessee, 1993.
10. Habibullah, A., "STEELER, Stress Check of Steel Frames," Computers and Structures, Inc., Berkeley, CA, July, 1992.
11. American Institute of Steel Construction, "Manual of Steel Construction, Load & Resistance Factor Design," First Edition, Chicago, Il, 1986.
12. Anderson, J.C. and Filippou, F.C., "Dynamic Response Analyses of the 17 Story Canoga Building," *Analytical and Field Investigations of Buildings Affected by the Northridge Earthquake of January 17, 1994*, SAC 95-04 Part 2, 1995.

EERC REPORTS

EERC reports are available from the National Information Service for Earthquake Engineering (NISEE) and from the National Technical Information Service (NTIS). To order EERC Reports, please contact the Earthquake Engineering Research Center, 1301 S. 46th Street, Richmond, California 94804-4698, ph 510-231-9468.

- UCB/EERC-97/08:** Implications of the Landers and Big Bear Earthquakes on Earthquake Resistant Design of Structures, by Anderson, J.C. and Bertero, V.V., July 1997. \$20
- UCB/EERC-97/07:** Analysis of the Nonlinear Response of Structures Supported on Pile Foundations, by Badoni, D. and Makris, N., July 1997. \$26
- UCB/EERC-97/06:** Executive Summary on: Phase 3: Evaluation and Retrofitting of Multilevel and Multiple-Column Structures -- An Analytical, Experimental, and Conceptual Study of Retrofitting Needs and Methods, by Mahin, S.A., Fenves, G.L., Filippou, F.C., Moehle, J.P., Thewalt, C.R., May, 1997. \$20
- UCB/EERC-97/05:** The EERC-CUREe Symposium to Honor Vitelmo V. Bertero, February 1997. \$26
- UCB/EERC-97/04:** Design and Evaluation of Reinforced Concrete Bridges for Seismic Resistance, by Aschheim, M., Moehle, J.P. and Mahin, S.A., March 1997. \$26
- UCB/EERC-97/03:** U.S.-Japan Workshop on Cooperative Research for Mitigation of Urban Earthquake Disasters: Learning from Kobe and Northridge -- Recommendations and Resolutions, by Mahin, S., Okada, T., Shinozuka, M. and Toki, K., February 1997. \$15
- UCB/EERC-97/02:** Multiple Support Response Spectrum Analysis of Bridges Including the Site-Response Effect & MSRS Code, by Der Kiureghian, A., Keshishian, P. and Hakobian, A., February 1997. \$20
- UCB/EERC-97/01:** Analysis of Soil-Structure Interaction Effects on Building Response from Earthquake Strong Motion Recordings at 58 Sites, by Stewart, J.P. and Stewart, A.F., February 1997. \$57
- UCB/EERC-96/05:** Application of Dog Bones for Improvement of Seismic Behavior of Steel Connections, by Popov, E.P., Blondet, M. and Stepanov, L., June 1996. \$13
- UCB/EERC-96/04:** Experimental and Analytical Studies of Base Isolation Applications for Low-Cost Housing, by Taniwangsa, W. and Kelly, J.M., July 1996. \$20
- UCB/EERC-96/03:** Experimental and Analytical Evaluation of a Retrofit Double-Deck Viaduct Structure: Part I of II, by Zayati, F., Mahin, S. A. and Moehle, J. P., June 1996. \$33
- UCB/EERC-96/02:** Field Testing of Bridge Design and Retrofit Concepts. Part 2 of 2: Experimental and Analytical Studies of the Mt. Diablo Blvd. Bridge, by Gilani, A.S., Chavez, J.W. and Fenves, G.L., June 1996. \$20
- UCB/EERC-96/01:** Earthquake Engineering Research at Berkeley -- 1996: Papers Presented at the 11th World Conference on Earthquake Engineering, by EERC, May 1996. \$26
- UCB/EERC-95/14:** Field Testing of Bridge Design and Retrofit Concepts. Part 1 of 2: Field Testing and Dynamic Analysis of a Four-Span Seismically Isolated Viaduct in Walnut Creek, California, by Gilani, A.S., Mahin, S.A., Fenves, G.L., Aiken, I.D. and Chavez, J.W., December 1995. \$26
- UCB/EERC-95/13:** Experimental and Analytical Studies of Steel Connections and Energy Dissipators, by Yang, T.-S. and Popov, E.P., December 1995. \$26
- UCB/EERC-95/12:** Natural Rubber Isolation Systems for Earthquake Protection of Low-Cost Buildings, by Taniwangsa, W., Clark, P. and Kelly, J.M., June 1996. \$20
- UCB/EERC-95/11:** Studies in Steel Moment Resisting Beam-to-Column Connections for Seismic-Resistant Design, by Blackman, B. and Popov, E.P., October 1995, PB96-143243. \$20
- UCB/EERC-95/10:** Seismological and Engineering Aspects of the 1995 Hyogoken-Nanbu (Kobe) Earthquake,

- by EERC, November 1995. \$26
- UCB/EERC-95/09:** Seismic Behavior and Retrofit of Older Reinforced Concrete Bridge T-Joints, by Lowes, L.N. and Moehle, J.P., September 1995, PB96-159850. \$20
- UCB/EERC-95/08:** Behavior of Pre-Northridge Moment Resisting Steel Connections, by Yang, T.-S. and Popov, E.P., August 1995, PB96-143177. \$15
- UCB/EERC-95/07:** Earthquake Analysis and Response of Concrete Arch Dams, by Tan, H. and Chopra, A.K., August 1995, PB96-143185. \$20
- UCB/EERC-95/06:** Seismic Rehabilitation of Framed Buildings Infilled with Unreinforced Masonry Walls Using Post-Tensioned Steel Braces, by Teran-Gilmore, A., Bertero, V.V. and Youssef, N., June 1995, PB96-143136. \$26
- UCB/EERC-95/05:** Final Report on the International Workshop on the Use of Rubber-Based Bearings for the Earthquake Protection of Buildings, by Kelly, J.M., May 1995. \$20
- UCB/EERC-95/04:** Earthquake Hazard Reduction in Historical Buildings Using Seismic Isolation, by Garevski, M., June 1995. \$15
- UCB/EERC-95/03:** Upgrading Bridge Outrigger Knee Joint Systems, by Stojadinovic, B. and Thewalt, C.R., June 1995, PB95-269338. \$20
- UCB/EERC-95/02:** The Attenuation of Strong Ground Motion Displacements, by Gregor, N.J., June 1995, PB95-269346. \$26
- UCB/EERC-95/01:** Geotechnical Reconnaissance of the Effects of the January 17, 1995, Hyogoken-Nambu Earthquake, Japan, August 1995, PB96-143300. \$26
- UCB/EERC-94/12:** Response of the Northwest Connector in the Landers and Big Bear Earthquakes, by Fenves, G.L. and Desroches, R., December 1994. \$20
- UCB/EERC-94/11:** Earthquake Analysis and Response of Two-Level Viaducts, by Singh, S.P. and Fenves, G.L., October 1994, PB96-133756 (A09). \$20
- UCB/EERC-94/10:** Manual for Menshin Design of Highway Bridges: Ministry of Construction, Japan, by Sugita, H. and Mahin, S., August 1994, PB95-192100(A08). \$20
- UCB/EERC-94/09:** Performance of Steel Building Structures During the Northridge Earthquake, by Bertero, V.V., Anderson, J.C. and Krawinkler, H., August 1994, PB95-112025(A10). \$26
- UCB/EERC-94/08:** Preliminary Report on the Principal Geotechnical Aspects of the January 17, 1994 Northridge Earthquake, by Stewart, J.P., Bray, J.D., Seed, R.B. and Sitar, N., June 1994, PB94203635(A12). \$26
- UCB/EERC-94/07:** Accidental and Natural Torsion in Earthquake Response and Design of Buildings, by De la Llera, J.C. and Chopra, A.K., June 1994, PB94-203627(A14). \$33
- UCB/EERC-94/05:** Seismic Response of Steep Natural Slopes, by Sitar, N. and Ashford, S.A., May 1994, PB94-203643(A10). \$26
- UCB/EERC-94/04:** Insitu Test Results from Four Loma Prieta Earthquake Liquefaction Sites: SPT, CPT, DMT and Shear Wave Velocity, by Mitchell, J.K., Lodge, A.L., Coutinho, R.Q., Kayen, R.E., Seed, R.B., Nishio, S. and Stokoe II, K.H., April 1994, PB94-190089(A09). \$20
- UCB/EERC-94/03:** The Influence of Plate Flexibility on the Buckling Load of Elastomeric Isolators, by Kelly, J.M., March 1994, PB95-192134(A04). \$15
- UCB/EERC-94/02:** Energy Dissipation with Slotted Bolted Connections, by Grigorian, C.E. and Popov, E.P., February 1994, PB94-164605. \$26
- UCB/EERC-94/01:** Preliminary Report on the Seismological and Engineering Aspects of the January 17, 1994 Northridge Earthquake, by EERC, January 1994, (PB94 157 666/AS)A05. \$15
- UCB/EERC-93/13:** On the Analysis of Structures with Energy Dissipating Restraints, by Inaudi, J.A., Nims, D.K. and Kelly, J.M., December 1993, PB94-203619(A07). \$20
- UCB/EERC-93/12:** Synthesized Strong Ground Motions for the Seismic Condition Assessment of the Eastern Portion of the San Francisco Bay Bridge, by Bolt, B.A. and Gregor, N.J., December 1993, PB94-165842(A10). \$26
- UCB/EERC-93/11:** Nonlinear Homogeneous Dynamical Systems, by Inaudi, J.A. and Kelly, J.M., October

1995. \$20
- UCB/EERC-93/09:** A Methodology for Design of Viscoelastic Dampers in Earthquake-Resistant Structures, by Abbas, H. and Kelly, J.M., November 1993, PB94-190071(A10). \$26
- UCB/EERC-93/08:** Model for Anchored Reinforcing Bars under Seismic Excitations, by Monti, G., Spacone, E. and Filippou, F.C., December 1993, PB95-192183(A05). \$15
- UCB/EERC-93/07:** Earthquake Analysis and Response of Concrete Gravity Dams Including Base Sliding, by Chavez, J.W. and Fenves, G.L., December 1993, (PB94 157 658/AS)A10. \$26
- UCB/EERC-93/06:** On the Analysis of Structures with Viscoelastic Dampers, by Inaudi, J.A., Zambrano, A. and Kelly, J.M., August 1993, PB94-165867(A06). \$20
- UCB/EERC-93/05:** Multiple-Support Response Spectrum Analysis of the Golden Gate Bridge, by Nakamura, Y., Der Kiureghian, A. and Liu, D., May 1993, (PB93 221 752)A05. \$15
- UCB/EERC-93/04:** Seismic Performance of a 30-Story Building Located on Soft Soil and Designed According to UBC 1991, by Teran-Gilmore, A. and Bertero, V.V., 1993, (PB93 221 703)A17. \$33
- UCB/EERC-93/03:** An Experimental Study of Flat-Plate Structures under Vertical and Lateral Loads, by Hwang, S.-H. and Moehle, J.P., February 1993, (PB94 157 690/AS)A13. \$26
- UCB/EERC-93/02:** Evaluation of an Active Variable-Damping-Structure, by Polak, E., Meeker, G., Yamada, K. and Kurata, N., 1993, (PB93 221 711)A05. \$15
- UCB/EERC-92/18:** Dynamic Analysis of Nonlinear Structures using State-Space Formulation and Partitioned Integration Schemes, by Inaudi, J.A. and De la Llera, J.C., December 1992, (PB94 117 702/AS/A05. \$15
- UCB/EERC-92/17:** Performance of Tall Buildings During the 1985 Mexico Earthquakes, by Teran-Gilmore, A. and Bertero, V.V., December 1992, (PB93 221 737)A11. \$26
- UCB/EERC-92/16:** Tall Reinforced Concrete Buildings: Conceptual Earthquake-Resistant Design Methodology, by Bertero, R.D. and Bertero, V.V., December 1992, (PB93 221 695)A12. \$26
- UCB/EERC-92/15:** A Friction Mass Damper for Vibration Control, by Inaudi, J.A. and Kelly, J.M., October 1992, (PB93 221 745)A04. \$15
- UCB/EERC-92/14:** Earthquake Risk and Insurance, by Brillinger, D.R., October 1992, (PB93 223 352)A03.
- UCB/EERC-92/13:** Earthquake Engineering Research at Berkeley - 1992, by EERC, October 1992, PB93-223709(A10). \$13
- UCB/EERC-92/12:** Application of a Mass Damping System to Bridge Structures, by Hasegawa, K. and Kelly, J.M., August 1992, (PB93 221 786)A06. \$26
- UCB/EERC-92/11:** Mechanical Characteristics of Neoprene Isolation Bearings, by Kelly, J.M. and Quiroz, E., August 1992, (PB93 221 729)A07. \$20
- UCB/EERC-92/10:** Slotted Bolted Connection Energy Dissipators, by Grigorian, C.E., Yang, T.-S. and Popov, E.P., July 1992, (PB92 120 285)A03. \$20
- UCB/EERC-92/09:** Evaluation of Code Accidental-Torsion Provisions Using Earthquake Records from Three Nominally Symmetric-Plan Buildings, by De la Llera, J.C. and Chopra, A.K., September 1992, (PB94 117 611)A08. \$13
- UCB/EERC-92/08:** Nonlinear Static and Dynamic Analysis of Reinforced Concrete Subassemblages, by Filippou, F.C., D'Ambrisi, A. and Issa, A., August, 1992. \$20
- UCB/EERC-92/07:** A Beam Element for Seismic Damage Analysis, by Spacone, E., Ciampi, V. and Filippou, F.C., August 1992, (PB95-192126)A06. \$20
- UCB/EERC-92/06:** Seismic Behavior and Design of Semi-Rigid Steel Frames, by Nader, M.N. and Astaneh-Asl, A., May 1992, PB93-221760(A17). \$33
- UCB/EERC-92/05:** Parameter Study of Joint Opening Effects on Earthquake Response of Arch Dams, by Fenves, G.L., Mojtahedi, S. and Reimer, R.B., April 1992, (PB93 120 301)A04. \$15
- UCB/EERC-92/04:** Shear Strength and Deformability of RC Bridge Columns Subjected to Inelastic Cyclic Displacements, by Aschheim, M. and Moehle, J.P., March 1992, (PB93 120 327)A06. \$20

- UCB/EERC-92/03:** Models for Nonlinear Earthquake Analysis of Brick Masonry Buildings, by Mengi, Y., McNiven, H.D. and Tanrikulu, A.K., March 1992, (PB93 120 293)A08. \$20
- UCB/EERC-92/02:** Response of the Dumbarton Bridge in the Loma Prieta Earthquake, by Fenves, G.L., Filippou, F.C. and Sze, D.T., January 1992, (PB93 120 319)A09. \$20
- UCB/EERC-92/01:** Studies of a 49-Story Instrumented Steel Structure Shaken During the Loma Prieta Earthquake, by Chen, C.-C., Bonowitz, D. and Astaneh-Asl, A., February 1992, (PB93 221 778)A08. \$20
- UCB/EERC-91/18:** Investigation of the Seismic Response of a Lightly-Damped Torsionally-Coupled Building, by Boroschek, R. and Mahin, S.A., December 1991, (PB93 120 335)A13. \$26
- UCB/EERC-91/17:** A Fiber Beam-Column Element for Seismic Response Analysis of Reinforced Concrete Structures, by Taucer, F., Spacone, E. and Filippou, F.C., December 1991, (PB94 117 629AS)A07. \$20
- UCB/EERC-91/16:** Evaluation of the Seismic Performance of a Thirty-Story RC Building, by Anderson, J.C., Miranda, E., Bertero, V.V. and The Kajima Project Research Team, July 1991, (PB93 114 841)A12. \$26
- UCB/EERC-91/15:** Design Guidelines for Ductility and Drift Limits: Review of State-of-the-Practice and State-of-the-Art in Ductility and Drift-Based Earthquake-Resistant Design of Buildings, by Bertero, V.V., Anderson, J.C., Krawinkler, H., Miranda, E. and The CUREe and The Kajima Research Teams, July 1991, (PB93 120 269)A08. \$20
- UCB/EERC-91/14:** Cyclic Response of RC Beam-Column Knee Joints: Test and Retrofit, by Mazzoni, S., Moehle, J.P. and Thewalt, C.R., October 1991, (PB93 120 277)A03. \$13
- UCB/EERC-91/13:** Shaking Table - Structure Interaction, by Rinawi, A.M. and Clough, R.W., October 1991, (PB93 114 917)A13. \$26
- UCB/EERC-91/12:** Performance of Improved Ground During the Loma Prieta Earthquake, by Mitchell, J.K. and Wentz, Jr., F.J., October 1991, (PB93 114 791)A06. \$20
- UCB/EERC-91/11:** Seismic Performance of an Instrumented Six-Story Steel Building, by Anderson, J.C. and Bertero, V.V., November 1991, (PB93 114 809)A07. \$20
- UCB/EERC-91/10:** Evaluation of Seismic Performance of a Ten-Story RC Building During the Whittier Narrows Earthquake, by Miranda, E. and Bertero, V.V., October 1991, (PB93 114 783)A06. \$20
- UCB/EERC-91/09:** A Preliminary Study on Energy Dissipating Cladding-to-Frame Connections, by Cohen, J.M. and Powell, G.H., September 1991, (PB93 114 510)A05. \$15
- UCB/EERC-91/08:** A Response Spectrum Method for Multiple-Support Seismic Excitations, by Der Kiureghian, A. and Neuenhofer, A., August 1991, (PB93 114 536)A04. \$15
- UCB/EERC-91/07:** Estimation of Seismic Source Processes Using Strong Motion Array Data, by Chiou, S.-J., July 1991, (PB93 114 551/AS)A08. \$20
- UCB/EERC-91/06:** Computation of Spatially Varying Ground Motion and Foundation-Rock Impedance Matrices for Seismic Analysis of Arch Dams, by Zhang, L. and Chopra, A.K., May 1991, (PB93 114 825)A07. \$20
- UCB/EERC-91/05:** Base Sliding Response of Concrete Gravity Dams to Earthquakes, by Chopra, A.K. and Zhang, L., May 1991, (PB93 114 544/AS)A05. \$15
- UCB/EERC-91/04:** Dynamic and Failure Characteristics of Bridgestone Isolation Bearings, by Kelly, J.M., April 1991, (PB93 114 528)A05. \$15
- UCB/EERC-91/03:** A Long-Period Isolation System Using Low-Modulus High-Damping Isolators for Nuclear Facilities at Soft-Soil Sites, by Kelly, J.M., March 1991, (PB93 114 577/AS)A10. \$26
- UCB/EERC-91/02:** Displacement Design Approach for Reinforced Concrete Structures Subjected to Earthquakes, by Qi, X. and Moehle, J.P., January 1991, (PB93 114 569/AS)A09. \$20
- UCB/EERC-90/21:** Observations and Implications of Tests on the Cypress Street Viaduct Test Structure, by Bollo, M., Mahin, S.A., Moehle, J.P., Stephen, R.M. and Qi, X., December 1990, (PB93 114 775)A13. \$26

- UCB/EERC-90/20:** Seismic Response Evaluation of an Instrumented Six Story Steel Building, by Shen, J.-H. and Astaneh-Asl, A., December 1990, (PB91 229 294/AS)A04. \$15
- UCB/EERC-90/19:** Cyclic Behavior of Steel Top-and-Bottom Plate Moment Connections, by Harriott, J.D. and Astaneh-Asl, A., August 1990, (PB91 229 260/AS)A05. \$15
- UCB/EERC-90/18:** Material Characterization of Elastomers used in Earthquake Base Isolation, by Papoulia, K.D. and Kelly, J.M., 1990, PB94-190063(A08). \$15
- UCB/EERC-90/17:** Behavior of Peak Values and Spectral Ordinates of Near-Source Strong Ground-Motion over a Dense Array, by Niazi, M., June 1990, (PB93 114 833)A07. \$20
- UCB/EERC-90/14:** Inelastic Seismic Response of One-Story, Asymmetric-Plan Systems, by Goel, R.K. and Chopra, A.K., October 1990, (PB93 114 767)A11. \$26
- UCB/EERC-90/13:** The Effects of Tectonic Movements on Stresses and Deformations in Earth Embankments, by Bray, J. D., Seed, R. B. and Seed, H. B., September 1989, PB92-192996(A18). \$39
- UCB/EERC-90/12:** Effects of Torsion on the Linear and Nonlinear Seismic Response of Structures, by Sedarat, H. and Bertero, V.V., September 1989, (PB92 193 002/AS)A15. \$33
- UCB/EERC-90/11:** Seismic Hazard Analysis: Improved Models, Uncertainties and Sensitivities, by Araya, R. and Der Kiureghian, A., March 1988, PB92-193010(A08). \$20
- UCB/EERC-90/10:** Experimental Testing of the Resilient-Friction Base Isolation System, by Clark, P.W. and Kelly, J.M., July 1990, (PB92 143 072)A08. \$20
- UCB/EERC-90/09:** Influence of the Earthquake Ground Motion Process and Structural Properties on Response Characteristics of Simple Structures, by Conte, J.P., Pister, K.S. and Mahin, S.A., July 1990, (PB92 143 064)A15. \$33
- UCB/EERC-90/08:** Soil Conditions and Earthquake Hazard Mitigation in the Marina District of San Francisco, by Mitchell, J.K., Masood, T., Kayen, R.E. and Seed, R.B., May 1990, (PB 193 267/AS)A04. \$15
- UCB/EERC-90/07:** A Unified Earthquake-Resistant Design Method for Steel Frames Using ARMA Models, by Takewaki, I., Conte, J.P., Mahin, S.A. and Pister, K.S., June 1990, PB92-192947(A06). \$15
- UCB/EERC-90/05:** Preliminary Report on the Principal Geotechnical Aspects of the October 17, 1989 Loma Prieta Earthquake, by Seed, R.B., Dickenson, S.E., Riemer, M.F., Bray, J.D., Sitar, N., Mitchell, J.K., Idriss, I.M., Kayen, R.E., Kropp, A., Harder, L.F., Jr. and Power, M.S., April 1990, (PB 192 970)A08. \$20
- UCB/EERC-90/03:** Earthquake Simulator Testing and Analytical Studies of Two Energy-Absorbing Systems for Multistory Structures, by Aiken, I.D. and Kelly, J.M., October 1990, (PB92 192 988)A13. \$26
- UCB/EERC-90/02:** Javid's Paradox: The Influence of Preform on the Modes of Vibrating Beams, by Kelly, J.M., Sackman, J.L. and Javid, A., May 1990, (PB91 217 943/AS)A03. \$13
- UCB/EERC-89/16:** Collapse of the Cypress Street Viaduct as a Result of the Loma Prieta Earthquake, by Nims, D.K., Miranda, E., Aiken, I.D., Whittaker, A.S. and Bertero, V.V., November 1989, (PB91 217 935/AS)A05. \$15
- UCB/EERC-89/15:** Experimental Studies of a Single Story Steel Structure Tested with Fixed, Semi-Rigid and Flexible Connections, by Nader, M.N. and Astaneh-Asl, A., August 1989, (PB91 229 211/AS)A10. \$26
- UCB/EERC-89/14:** Preliminary Report on the Seismological and Engineering Aspects of the October 17, 1989 Santa Cruz (Loma Prieta) Earthquake, by EERC, October 1989, (PB92 139 682/AS)A04. \$15
- UCB/EERC-89/13:** Mechanics of Low Shape Factor Elastomeric Seismic Isolation Bearings, by Aiken, I.D., Kelly, J.M. and Tajirian, F.F., November 1989, (PB92 139 732/AS)A09. \$20
- UCB/EERC-89/12:** ADAP-88: A Computer Program for Nonlinear Earthquake Analysis of Concrete Arch Dams, by Fenves, G.L., Mojtahedi, S. and Reimer, R.B., September 1989, (PB92 139 674/AS)A07. \$20

- UCB/EERC-89/11:** Static Tilt Behavior of Unanchored Cylindrical Tanks, by Lau, D.T. and Clough, R.W., September 1989, (PB92 143 049)A10. \$26
- UCB/EERC-89/10:** Measurement and Elimination of Membrane Compliance Effects in Undrained Triaxial Testing, by Nicholson, P.G., Seed, R.B. and Anwar, H., September 1989, (PB92 139 641/AS)A13. \$26
- UCB/EERC-89/09:** Feasibility and Performance Studies on Improving the Earthquake Resistance of New and Existing Buildings Using the Friction Pendulum System, by Zayas, V., Low, S., Mahin, S.A. and Bozzo, L., July 1989, (PB92 143 064)A14. \$33
- UCB/EERC-89/08:** Seismic Performance of Steel Moment Frames Plastically Designed by Least Squares Stress Fields, by Ohi, K. and Mahin, S.A., August 1989, (PB91 212 597)A05. \$15
- UCB/EERC-89/07:** EADAP - Enhanced Arch Dam Analysis Program: Users's Manual, by Ghanaat, Y. and Clough, R.W., August 1989, (PB91 212 522)A06. \$20
- UCB/EERC-89/06:** Effects of Spatial Variation of Ground Motions on Large Multiply-Supported Structures, by Hao, H., July 1989, (PB91 229 161/AS)A08. \$20
- UCB/EERC-89/05:** The 1985 Chile Earthquake: An Evaluation of Structural Requirements for Bearing Wall Buildings, by Wallace, J.W. and Moehle, J.P., July 1989, (PB91 218 008/AS)A13. \$26
- UCB/EERC-89/04:** Earthquake Analysis and Response of Intake-Outlet Towers, by Goyal, A. and Chopra, A.K., July 1989, (PB91 229 286/AS)A19. \$39
- UCB/EERC-89/03:** Implications of Site Effects in the Mexico City Earthquake of Sept. 19, 1985 for Earthquake-Resistant Design Criteria in the San Francisco Bay Area of California, by Seed, H.B. and Sun, J.I., March 1989, (PB91 229 369/AS)A07. \$20
- UCB/EERC-89/02:** Earthquake Simulator Testing of Steel Plate Added Damping and Stiffness Elements, by Whittaker, A., Bertero, V.V., Alonso, J. and Thompson, C., January 1989, (PB91 229 252/AS)A10. \$26
- UCB/EERC-89/01:** Behavior of Long Links in Eccentrically Braced Frames, by Engelhardt, M.D. and Popov, E.P., January 1989, (PB92 143 056)A18. \$39
- UCB/EERC-88/20:** Base Isolation in Japan, 1988, by Kelly, J.M., December 1988, (PB91 212 449)A05. \$15
- UCB/EERC-88/19:** Steel Beam-Column Joints in Seismic Moment Resisting Frames, by Tsai, K.-C. and Popov, E.P., November 1988, (PB91 217 984/AS)A20. \$39
- UCB/EERC-88/18:** Use of Energy as a Design Criterion in Earthquake-Resistant Design, by Uang, C.-M. and Bertero, V.V., November 1988, (PB91 210 906/AS)A04. \$15
- UCB/EERC-88/17:** Earthquake Engineering Research at Berkeley - 1988, by EERC, November 1988, (PB91 210 864)A10. \$26
- UCB/EERC-88/16:** Reinforced Concrete Flat Plates Under Lateral Load: An Experimental Study Including Biaxial Effects, by Pan, A. and Moehle, J.P., October 1988, (PB91 210 856)A13. \$26
- UCB/EERC-88/15:** Dynamic Moduli and Damping Ratios for Cohesive Soils, by Sun, J.I., Golesorkhi, R. and Seed, H.B., August 1988, (PB91 210 922)A04. \$15
- UCB/EERC-88/14:** An Experimental Study of the Behavior of Dual Steel Systems, by Whittaker, A.S., Uang, C.-M. and Bertero, V.V., September 1988, (PB91 212 712)A16. \$33
- UCB/EERC-88/13:** Implications of Recorded Earthquake Ground Motions on Seismic Design of Building Structures, by Uang, C.-M. and Bertero, V.V., November 1988, (PB91 212 548)A06. \$20
- UCB/EERC-88/12:** Nonlinear Analysis of Reinforced Concrete Frames Under Cyclic Load Reversals, by Filippou, F.C. and Issa, A., September 1988, (PB91 212 589)A07. \$20
- UCB/EERC-88/11:** Liquefaction Potential of Sand Deposits Under Low Levels of Excitation, by Carter, D.P. and Seed, H.B., August 1988, (PB91 210 880)A15. \$33
- UCB/EERC-88/10:** The Landslide at the Port of Nice on October 16, 1979, by Seed, H.B., Seed, R.B., Schlosser, F., Blondeau, F. and Juran, I., June 1988, (PB91 210 914)A05. \$15
- UCB/EERC-88/09:** Alternatives to Standard Mode Superposition for Analysis of Non-Classically Damped Systems, by Kusainov, A.A. and Clough, R.W., June 1988, (PB91 217 992/AS)A04. \$15

- UCB/EERC-88/08:** Analysis of Near-Source Waves: Separation of Wave Types Using Strong Motion Array Recordings, by Darragh, R.B., June 1988, (PB91 212 621)A08. \$20
- UCB/EERC-88/07:** Theoretical and Experimental Studies of Cylindrical Water Tanks in Base-Isolated Structures, by Chalhoub, M.S. and Kelly, J.M., April 1988, (PB91 217 976/AS)A05. \$15
- UCB/EERC-88/06:** DRAIN-2DX User Guide, by Allahabadi, R. and Powell, G.H., March 1988, (PB91 212 530)A12. \$26
- UCB/EERC-88/05:** Experimental Evaluation of Seismic Isolation of a Nine-Story Braced Steel Frame Subject to Uplift, by Griffith, M.C., Kelly, J.M. and Aiken, I.D., May 1988, (PB91 217 968/AS)A07. \$20
- UCB/EERC-88/04:** Re-evaluation of the Slide in the Lower San Fernando Dam in the Earthquake of Feb. 9, 1971, by Seed, H.B., Seed, R.B., Harder, L.F. and Jong, H.-L., April 1988, (PB91 212 456/AS)A07. \$20
- UCB/EERC-88/03:** Cyclic Behavior of Steel Double Angle Connections, by Astaneh-Asl, A. and Nader, M.N., January 1988, (PB91 210 872)A05. \$15
- UCB/EERC-88/02:** Experimental Evaluation of Seismic Isolation of Medium-Rise Structures Subject to Uplift, by Griffith, M.C., Kelly, J.M., Coveney, V.A. and Koh, C.G., January 1988, (PB91 217 950/AS)A09. \$20
- UCB/EERC-88/01:** Seismic Behavior of Concentrically Braced Steel Frames, by Khatib, I., Mahin, S.A. and Pister, K.S., January 1988, (PB91 210 898/AS)A11. \$26

